

POLITECNICO DI TORINO  
Department of Mechanical and Aerospace Engineering

M. Sc. MECHANICAL ENGINEERING

Master Thesis



INVESTIGATION OF THE POTENTIAL OF HYDROGEN  
TO IMPROVE THE POWERTRAIN EFFICIENCY USING  
1D-CFD SOFTWARE



SUPERVISORS

Prof. Federico Millo  
Dipl. -Ing Vincenzo Bevilacqua  
M.Sc. Alessandro Gallo

CANDIDATE

Oliviero Agnelli

July 2021

*A Nonna Clara .*

## SPERRVERMERK



Der vorliegende Bericht enthält zum Teil Informationen, die nicht für die Öffentlichkeit bestimmt sind. Alle Rechte an der Masterarbeit einschließlich der Verbreitung auf elektronischen Medien liegen bei der Porsche Engineering Services GmbH. Abweichend hiervon darf der Inhalt der Masterarbeit während einer Sperrzeit von 5 Jahren ab dem Abgabedatum mit der ausdrücklichen schriftlichen Genehmigung der Porsche Engineering Services GmbH an Dritte weitergegeben werden. Nach Ablauf der Sperrzeit ist diese Genehmigung nicht mehr erforderlich.



**PORSCHE**

## CONFIDENTIALITY AGREEMENT



This report contains some information which is not intended for publication. All the rights on the thesis, including the distribution through electronic media, are held by Porsche Engineering Services GmbH. The content of this work cannot be published or transmitted to third parties without an explicit written authorization from Porsche Engineering Services GmbH, for 5 years from the date of submission. After this period, the authorization is no longer compulsory.



**PORSCHE**

## Abstract

The continuous tightening of emissions limits is pushing the automotive world towards "green" alternatives to fossil fuels. In this context, hydrogen is a promising solution for the future of mobility, both with Fuel Cell vehicles and Hydrogen internal combustion engines.

The goal of the work is to design a hydrogen powertrain that meets the requirements of: High Performances, High Efficiency and zero emissions without after-treatment systems. In a first phase, after a detailed analysis of the different solutions, the hydrogen internal combustion engine has been selected as the most promising solution to meet both emissions and performance targets. Therefore a V8 turbocharged gasoline engine, currently used on a production car, has been converted into an hydrogen version capable to provide the same performances with negligible emissions. Consequently, through the use of a 1D-CFD software, an hydrogen engine concept with 600HP and high efficiency with almost zero NOx emissions, has been designed. In order to correctly reproduce the behavior of the engine under different loads and speeds, different new methodologies to take into account the hydrogen properties have been developed, like the one to predict the hydrogen knock occurrence. This last one has been developed using OD-CFD chemistry simulations and it has been validated against experimental results.

Then, after a complete redesign of the existing supercharging system using innovative technologies such as eTurbo and Back-to-Back compressors, full load and part load conditions were simulated. The resulting engine maps were then used in a vehicle model to perform driving cycle simulations in order to calculate NOx emissions and fuel consumption data. In conclusion, the engine and vehicle data were fed into the simulator to run lap time simulations at the Nürburgring and analyze the telemetry data.

## Sommario

Il continuo inasprimento dei limiti riguardo le emissioni sta spingendo il mondo automotive verso alternative "verdi" ai combustibili fossili. In questo contesto l'idrogeno è una soluzione promettente per il futuro della mobilità, sia in veicoli Fuel Cell che con motori a combustione interna di Idrogeno.

L'obiettivo del lavoro progettare un powertrain ad idrogeno che soddisfi i requisiti di : Elevate Prestazioni, Elevata Efficienza e zero emissioni senza l'ausilio di sistemi after-treatment. In una prima fase, dopo un'attenta analisi delle diverse soluzioni, il motore a combustione interna H<sub>2</sub> è stato selezionato come il più promettente per soddisfare sia gli obiettivi di emissioni che quelli di prestazioni. Quindi si è deciso di riconvertire un motore benzina, sovralimentato, V8, attualmente utilizzato su una vettura di serie, in una versione ad idrogeno in grado di fornire le stesse prestazioni con emissioni praticamente trascurabili. Di conseguenza, attraverso l'utilizzo di un software 1D-CFD, è stato sviluppato un concept di motore a combustione interna di idrogeno, con 600HP e alta efficienza con emissioni di NO<sub>x</sub> quasi nulle. Al fine di riprodurre correttamente il comportamento del motore sotto diversi carichi e regimi, sono state sviluppate, da foglio bianco, differenti nuove metodologie basate sulle proprietà del nuovo combustibile, come quella per predire l'insorgere della detonazione nel caso di utilizzo dell'idrogeno come combustibile. Quest'ultima è basata su simulazioni chimiche OD-CFD ed è stata validata sulla base di risultati sperimentali.

A questo punto, dopo una completa riprogettazione del sistema di sovralimentazione esistente utilizzando tecnologie innovative come eTurbo e compressori Back-to-Back, sono state simulate le condizioni di pieno carico e carico parziale. Successivamente le mappe motore ottenute, sono state utilizzate in un modello veicolo per eseguire simulazioni di cicli di guida al fine di calcolare le emissioni di NO<sub>x</sub> e i dati sul consumo di carburante. In conclusione, i dati del motore e del veicolo sono stati inseriti nel simulatore per eseguire simulazioni di tempo sul giro al Nürburgring ed analizzare i dati di telemetria.

# Acknowledgments

I'm immensely grateful to the whole Porsche Engineering for giving me the opportunity to work among them in the last year and for making this work possible. Despite the challenging period, I have always been supported from beautiful human beings and talented engineers, I will never thank you enough.

Un ringraziamento speciale va al mio tutor, ma soprattutto amico, Alessandro, per non essersi mai risparmiato un secondo nel trasmettermi la sua esperienza e il suo talento. Se oggi mi sento una persona più matura e sicura di sé, gran parte è merito suo.

Allo zio Vincenzo, maestro, fonte di ispirazione e punto di riferimento costante. Dal cuore grande almeno quanto la sua esperienza e il suo talento, porterò per sempre con me i suoi insegnamenti.

I would like to thank my Team in Porsche Engineering: Drago Matthias, Michal and David. They always made me feel like home and I will always bring them in my heart. Thank you.

Al professor Millo, instancabile e meravigliosa persona che ha avuto il coraggio di credere in me sin dall'inizio e che mi ha dato gli strumenti ed il supporto necessario per inseguire i miei sogni. Non riuscirò mai a trovare le parole giuste per esprimergli la mia riconoscenza. Un giorno mi sdebiterò, prometto.

Alla mia famiglia per tutto quello che hanno sempre fatto per me, lasciandomi sempre lo spazio per crescere prendendomi le mie responsabilità. Da sempre fine ultimo di ogni mio sforzo ed ambizione, spero di renderli fieri ed orgogliosi di me fin quando potrò.

Agli amici di sempre che hanno sempre dovuto sopportare me e le mie, a volte folli, ambizioni, ma che non hanno mai smesso di essermi vicino nonostante la mia lontananza. Saranno sempre un tassello fondamentale della mia vita e indipendentemente da cosa mi riserverà il futuro, li porterò sempre con me.

Ai miei compagni di università, è difficile anche solo credere che sia possibile creare dei legami così forti in così poco tempo. Senza di loro non sarebbe mai stato lo stesso.

E infine grazie a Mara, per il suo instancabile supporto e la sua dolce complicità. Non potevo desiderare una compagna di viaggio migliore di te.

# Table of Contents

1.	<b>Introduction</b>	- 1 -
2.	<b>Hydrogen and the Future of the Energy Production</b>	- 3 -
2.1	Energy Storages	- 7 -
2.2	Hydrogen	- 8 -
3.	<b>Fuel Cells</b>	- 9 -
3.1	PEM Fuel Cells	- 11 -
3.2	Efficiency of a Fuel Cell	- 11 -
4.	<b>Hydrogen Internal Combustion Engines</b>	- 14 -
4.1	Properties of Hydrogen	- 14 -
4.2	H <sub>2</sub> -ICE Emissions	- 16 -
4.2.1	NOx Emissions	- 16 -
5.	<b>Powertrain Solution Selection</b>	- 18 -
5.1	Reference Engine	- 21 -
5.2	Reference Performances	- 24 -
6.	<b>Methodologies</b>	- 25 -
6.1	Ignition Delay and Autoignition	- 26 -
6.2	Abnormal Combustion and Engine Knock	- 29 -
6.3	Engine Knock Prediction	- 32 -
6.4	Knock prediction methodology	- 33 -
6.4	Maximum In-Cylinder pressure control	- 37 -
6.5	Hydrogen Flame Speed Prediction Methodology	- 38 -
7.	<b>Turbocharger solution</b>	- 40 -
7.1	Single Stage Compression : Bi-Turbo and Inlet Guided Vanes	- 42 -
7.2	Two Stage Compression : Lancia Delta S4 Twincharger Inspired	- 44 -
7.3	Parallel Compression : Bugatti Chiron Inspired	- 45 -
7.4	Two Stage Intercooled Compression with Back-to-Back Compressors	- 47 -
8.	<b>Performances</b>	- 50 -
8.1	Full Load Performances	- 50 -
8.2	Part Load Performances	- 53 -

9.	<b>Driving Cycles</b>	- 57 -
9.1	Driving Cycle simulation methodology	- 59 -
9.2	Kinematic Model	- 61 -
9.3	Emissions and Fuel Consumption Calculation	- 63 -
9.4	Calculation of the mechanical energy required and recoverable	- 65 -
9.5	Start & Stop and Cut-Off Technologies Implementation	- 66 -
10.	<b>Results</b>	- 68 -
10.1	Comparison With European Union Limits	- 70 -
10.2	Emissions vs Air Quality	- 71 -
11.	<b>Nürburgring Nordschleife Lap Time Simulation</b>	- 72 -
12.	<b>Conclusions</b>	- 75 -

# List of Figures

Figure 1 - Trend of the CO <sub>2</sub> Concentration in the atmosphere	- 3 -
Figure 2 - Temperature Anomaly Scenario Comparison - Top: 1918 vs Bottom: 2018	- 4 -
Figure 3 - Energy Production in Germany - Week 4 - Year 2020	- 5 -
Figure 4 - Energy Production divided by production sources - Week 4 - Year 2020	- 5 -
Figure 5 - Energy Production divided by production sources - Week Comparison	- 6 -
Figure 6 - Energy Storages and how to use the energy in the Transportation Sector	- 7 -
Figure 7 - Fuel Cell Scheme [CITA]	- 9 -
Figure 8 - High-Level Comparison of 5 typical Fuel Cell Types [CITA]	- 10 -
Figure 9 - Fuel Cell vs H <sub>2</sub> -ICE vs Gasoline ICE Efficiency Comparison	- 13 -
Figure 10 - NO <sub>x</sub> Production in Internal Combustion Engines	- 17 -
Figure 11 - Current FCEV on the market	- 19 -
Figure 12 - Mercedes GLC Fuel Cell Powertrain Architecture	- 20 -
Figure 13 - a) Exhaust Manifold Design b) twisted Camshaft	- 22 -
Figure 14 - Hybrid Architecture	- 22 -
Figure 15 - Reference Gasoline Engines Performances	- 24 -
Figure 16- Rapid Compression Machine	- 27 -
Figure 17 - Rapid Compression Machine p-t	- 27 -
Figure 18 - Ignition Delay vs Temperature - Example	- 28 -
Figure 19 - Ignition Delay for Gasoline and Hydrogen	- 28 -
Figure 20 - Example of Knock Occurrence [10]	- 30 -
Figure 21 - Comparison between Normal Combustion (up) and Abnormal Combustion (down)	- 31 -
Figure 22 - Ignition Delay from CONVERGE - Top: Constant Pressure - Low: Constant Lambda	- 34 -
Figure 23 - Dataset from ignition delay calculation	- 35 -
Figure 24 - In-Cylinder Pressure Comparison	- 37 -
Figure 25 - Combustion Speed Comparison	- 38 -
Figure 26 - Burn Duration Estimation Methodology	- 39 -
Figure 27 - Air Flow Rate Comparison	- 40 -
Figure 28 - Compressor Pressure Ratio Comparison	- 40 -
Figure 29 - Turbine Inlet Temperature Comparison	- 41 -
Figure 30 - Bi-Turbo and IGV Engine Scheme	- 42 -
Figure 31 - Inlet Guided Vanes - IGV	- 42 -
Figure 32 - IGV Compressor Map Scaling	- 43 -
Figure 33- Lancia Delta S4 Engine Scheme	- 44 -
Figure 34 - Lancia Delta S4 Inspired Engine Scheme	- 44 -
Figure 35 - Bugatti Chiron Turbo Engine	- 45 -
Figure 36 - Bugatti Chiron Inspired Engine Scheme	- 45 -
Figure 37 - SC-VNT Garrett Turbo	- 47 -
Figure 38 - Back-To-Back Turbo Engine Scheme	- 47 -
Figure 39 - Boost Pressure Comparison	- 48 -
Figure 40 - Intake Manifold Temperature Comparison	- 48 -
Figure 41 - Full Load Performances Comparison - Power, Torque, Efficiency and P2 Power	- 50 -
Figure 42 - Full Load Performances Comparison - P22, T22, PMax and T3	- 51 -

Figure 43 - Full Load Performances - Engine-Out Emission Comparison	- 52 -
Figure 44 - Power from P2 eMachine to eTurbo	- 53 -
Figure 45 - Throttle Position	- 53 -
Figure 46 - Ignition Limits: Hydrogen vs Gasoline	- 54 -
Figure 47 - Full Engine Map Average Lambda	- 54 -
Figure 48 - H64 Engine - Full Map Data: NO <sub>x</sub> , Fuel Consumption, Efficiency and Power from P2	- 55 -
Figure 49 - H64 Engine - Full Map Data: Max In-Cylinder Pressure, P22, T22 and T3	- 56 -
Figure 50 - WLTC Speed Profile	- 58 -
Figure 51 - WLTC Gear Shift Profile	- 58 -
Figure 52 - Aurus Senat	- 59 -
Figure 53 - Fuel Consumption Map from Stationary Simulations	- 63 -
Figure 54 - NO <sub>x</sub> Emission Map from Stationary Simulations	- 63 -
Figure 55 - Cumulative NO <sub>x</sub> Emissions and H <sub>2</sub> Consumption	- 68 -
Figure 56 - NO <sub>x</sub> European Union's Limits between Euro3 and Euro 6	- 70 -
Figure 57 - NO <sub>x</sub> European Union's Limits between Euro3 and Euro 7	- 70 -
Figure 58 - Example of Air Quality Index for NO <sub>x</sub> in Europe	- 71 -
Figure 59 - European Air Quality Index Scale based on NO <sub>x</sub> Concentration	- 71 -
Figure 60 - Nürburgring Nordschleife Circuit Map	- 72 -
Figure 61 - Aurus Senat on the HotLap at Nordschleife	- 73 -
Figure 62 - Nordschleife Selected Sectors	- 73 -

# List of Tables

Table 1 - Hydrogen Properties	- 14 -
Table 2 - Fuel Cell vs H <sub>2</sub> -ICE Comparison	- 19 -
Table 3 - Reference Stock Engine	- 21 -
Table 4 - Lambda 1.0 Version Reference Engine	- 23 -
Table 5 - Stock Engine, Lambda 1 Version and H64 Specs	- 49 -
Table 6 - WLTC Test Cycles	- 57 -
Table 7 - Aurus Senat Vehicle Data	- 59 -
Table 8 - Aurus Senat Transmission Parameters	- 59 -
Table 9 - Aurus Senat - Engine and Wheels Data	- 60 -
Table 10 - WLTC Simulation Results	- 69 -
Table 11 - Nordschleife Sectors Data Summary	- 74 -

# List of Symbols

$\alpha$	Air-fuel ratio
$\alpha_{st}$	Stoichiometric air-fuel ratio
$\beta$	Connecting rod angle
$\beta_c$	Compression ratio of the compressor
$\epsilon_t$	Expansion ratio of the turbine
$\eta_{TC}$	Turbocharger efficiency
$\eta_f$	Fuel conversion efficiency
$\eta_{id}$	Ideal efficiency
$\eta_m$	Mechanical efficiency
$\lambda$	Air equivalence ratio
$\lambda_v$	Volumetric efficiency
$\omega$	Angular velocity
$\varphi$	Equivalence ratio
$\rho$	Density
$\tau$	Time ignition delay
$\theta$	Crank-angle
$a$	Acceleration
BDC	Bottom dead center
bmep	brake mean effective pressure
bsfc	Brake specific fuel consumption
B	Bore
CADeg	Crank-angle degree
CFD	Computational fluido-dynamics
CI	Compression-ignition
CR	Compression ratio
$C_{Spec}$	Specific Fuel Consumption
EVO	Exhaust valve opening
$E_a$	Activation energy
$f_c$	Fuel Consumption
G	Gibbs Free Energy
GHG	Green House Gasses
HI	Lower heating value
$h$	Enthalpy
$h_i$	Heat transfer coefficient
$h_t$	Total enthalpy
imep	Indicated mean effective pressure
$i$	Cylinder number
$l_c$	Work
KI	Knock index
MFB	Mass fraction burned

$\dot{m}$	Mass-flow rate
m	Mass
NO <sub>x</sub>	Nitric Oxides
ON	Octane number
SA	Spark Advance
SI	Spark-ignition
TDC	Top dead center
VVT	Variable valve train
$J_w$	Wheel Inertia
$J_{eng}$	Engine Inertia
k	Isentropic coefficient
$k_r$	Reaction rate
T	Engine torque
n	Engine speed
$p_{max}$	Max In-Cylinder Pressure
p	Pressure
$P_m$	Brake power
$p_{tr}$	Motored engine pressure
Q	Heat
R	Gas constant
SF	Scaling Factor
$S_L$	Laminar flame speed
$S_T$	Turbulent flame speed
T	Temperature
$T_g$	Gas temperature
$T_w$	Wall temperature
V	Volume
v	Velocity
$V_c$	Clearance volume
$V_d$	Displacement volume

# 1. Introduction

In the recent years the attention of the world governments and media has been shifted towards the necessity of a clean, safe and renewable future. The energy sector is playing a major role in this scenario and the development of long-term energy supply solution is nowadays crucial.

The actual world's energy supply system is mainly based on fossil fuel thanks to their abundance and low costs but they are not neither clean, nor infinitely available.

The greenhouse gases emitted in a business-as-usual scenario would lead to an increase of the average global temperature of about 4°C. This, in turn, would raise sea levels, shift climate zones, and make extreme weather and droughts more frequent, as well as causing other changes, all impacting biological, social, and economic systems [6]. Transportation sector is facing a challenging period of transition. Most of the vehicles are fuelled by fossil fuels and their combustion contributes to GHG emissions (Carbon Dioxide) and pollutants emissions (Carbon monoxide, Nitrogen Oxides and Unburned Hydrocarbons. Their number increased from 47 million in 1939 to 800 million in 2006 and will continue to increase with the growth of the world population and the fact that the developing and threshold countries wish to reach the same level of comfort as in industrialised countries [2].

Renewable electricity is also considered nowadays as the future of mobility but the battery technology developed in the last years are still far away from fulfilling all requirements of suitable energy storage for automotive applications. The stored energy density and the maximum possible driving range are still too low. In this context, Hydrogen has the potential to be a powerful enabler of this energy transition, as it offers a clean, sustainable, and flexible option for overcoming multiple obstacles that stand in the way of a resilient and low-carbon economy. Hydrogen is the simplest and most abundant element in the universe, it can be produced from renewable sources and it is a Carbon Free energy carrier that can be stored in different ways for long periods of time, overcoming the electricity storage problems. It has also great potential for CO<sub>2</sub> emissions reduction because it can be used in Fuel Cells to produce electricity on board, and it's combustion with oxygen produces only water and air, making possible the development of clean Hydrogen Internal Combustion Engines. Both Fuel Cell and Hydrogen Internal Combustion Engines can represent a mid- and long- term alternative to gasoline and diesel towards CO<sub>2</sub> emission-free vehicles.

The aim of this work is to investigate the potential of hydrogen in the automotive sector and in which way this fuel, or energy vector, can be used to design more efficient and clean high performances propulsions systems that can move the future.

In the first part different power-train architectures has been analysed and an H<sub>2</sub> Internal Combustion engine concept has been considered the most promising solution for an High Performance application. One of the key feature of Hydrogen Internal combustion engine is the possibility to use the same hardware of a gasoline or diesel engine. For this reason a 1D-CFD GT-Suite engine model of an existent 600HP V8 S.I. Turbocharged Engine has been selected as a reference and converted to an Hydrogen-Powered version, targeting the same performances but with no emission without after treatment systems.

The main part of the work will be focused on the development of new Artificial Intelligence based Methodologies and innovative turbocharger layouts to manage the challenging aspects of Hydrogen used as a fuel. Both Full Load and Part Load simulations have been performed to have a complete engine model. This one has been implemented in a vehicle model built in Matlab, capable to reproduce the vehicle behaviour on WLTC Driving cycle to calculate Fuel Consumption and Emissions Data.

In the final chapter, the complete vehicle model has been implemented at the simulator to perform an Hot Lap at Nürburgring-Nordschleife Circuit to test the effective performances of the engine by a lap data analysis using a developed tool on Matlab.

## 2. Hydrogen and the Future of the Energy Production

Decarbonization is the key to shape a green and sustainable future. The greenhouse gasses emissions, especially CO<sub>2</sub>, related to the fossil fuels burning have led to an increase of the CO<sub>2</sub> concentration in the atmosphere of about the 40% over the last century, as shown in Figure 1.

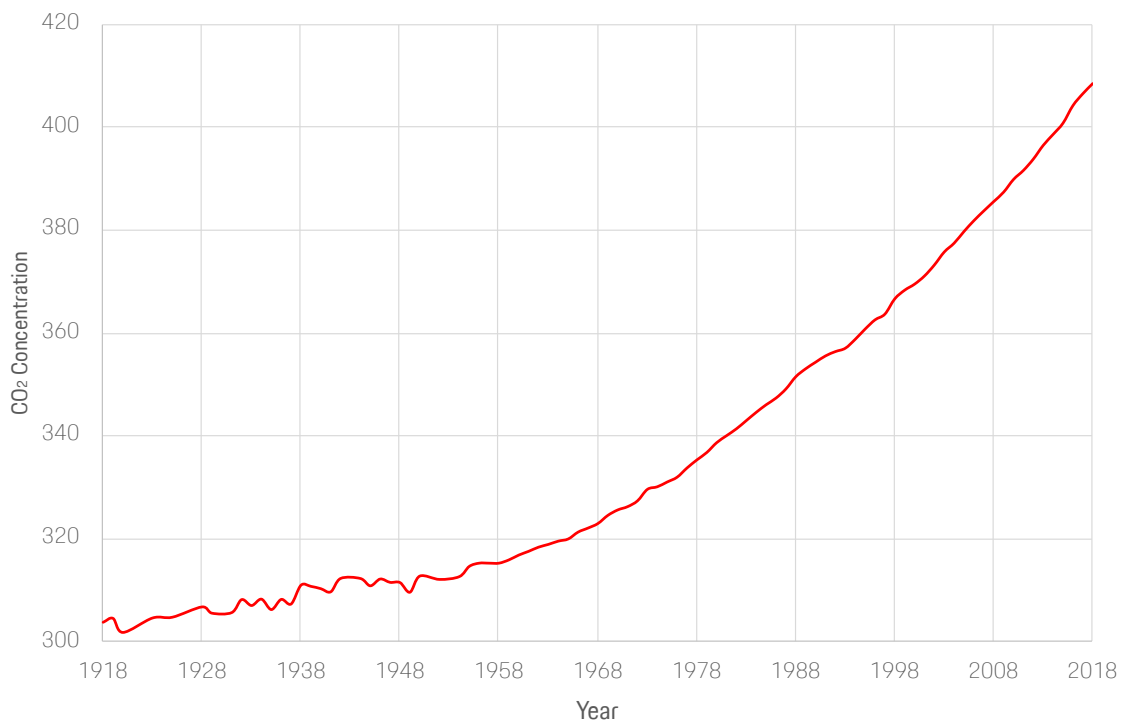


Figure 1 - Trend of the CO<sub>2</sub> Concentration in the atmosphere

It is clear that a drastic reduction of the GHG emissions must be achieved. However it must be pointed out that even if the world achieves a stabilization in CO<sub>2</sub> emissions, this would not translate into the same for atmospheric concentrations. This is because CO<sub>2</sub> accumulates in the atmosphere based on what it is called a 'residence time'. Residence time is the time required for emitted CO<sub>2</sub> to be removed from the atmosphere through natural processes in Earth's carbon cycle. The length of this time can vary, some CO<sub>2</sub> is removed in less than 5 years through fast cycling processes, meanwhile other processes, such as absorption through land vegetation, soils and cycling into the deep ocean can take hundreds to thousands of years. If we stopped emitting CO<sub>2</sub> today, it would take several hundred years before the majority of human emissions were removed from the atmosphere [15].

When CO<sub>2</sub> and other air pollutants collect in the atmosphere and absorb sunlight and solar radiation that have bounced off the earth's surface, a phenomenon called "Global Warming" occurs. Normally this radiation would escape into space, but these pollutants, which can last for years to centuries in the atmosphere, trap the heat and cause the planet to get hotter. These heat-trapping pollutants, specifically carbon dioxide, methane, nitrous oxide, water vapor, and synthetic fluorinated gases, are known as "Greenhouse Gases" (GHG), and their impact is called the "Greenhouse Effect" which leads to a worldwide increase of the average temperature.

In Figure 2 [16] a comparison of the temperature anomaly scenario over the last century is reported. It is clear how the global average temperature is increased worldwide, more than 2°C in Europe and up to 4°C in the North Pole. This situation has led to important climate changes that are posing severe risks for our future.

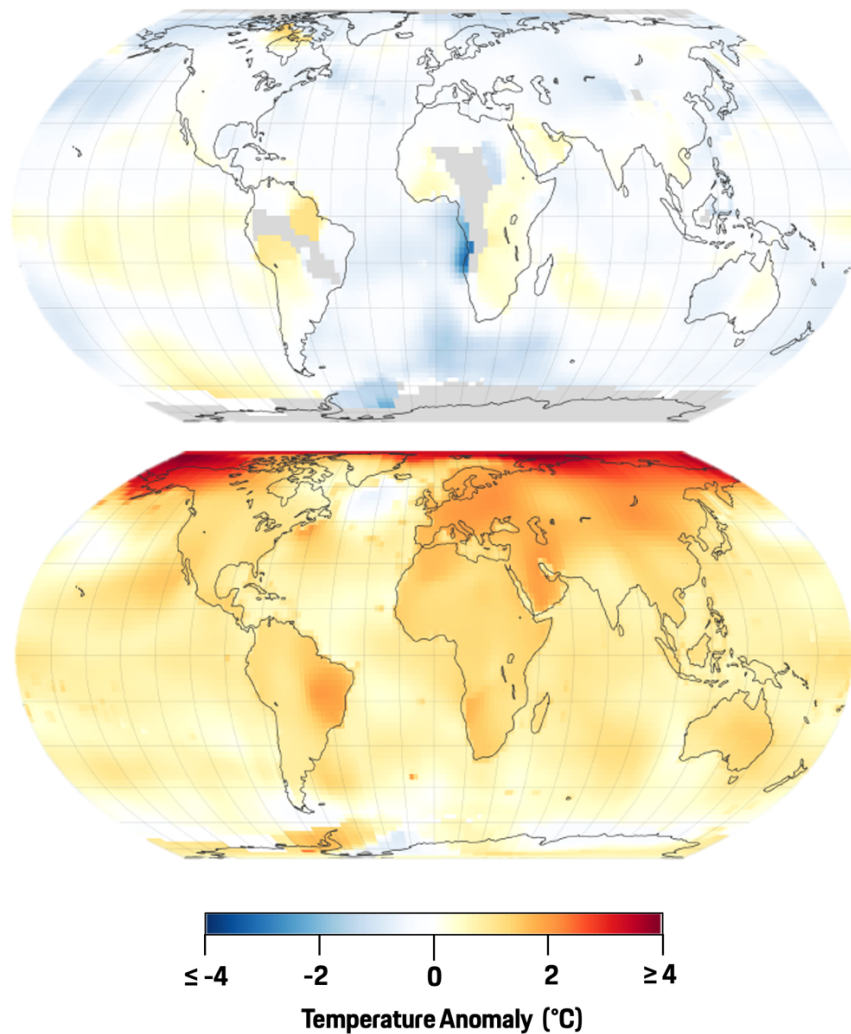


Figure 2 - Temperature Anomaly Scenario Comparison - Top: 1918 vs Bottom: 2018

In the 2015 Paris Agreement, the European Union has set the goal to limit the global warming to 1.5 °C compared to preindustrial levels, and to do that, global net human-caused emissions of CO<sub>2</sub> should be brought to “net zero” within three decades. One of the main topics related to the CO<sub>2</sub> emission reduction is the complete decarbonization of the energy supply sector by adopting clean and renewable energy.

Renewable energy sources like wind, solar, geothermal, hydroelectric (...) can be the long term solution towards the complete decarbonization but there are some critical aspects that must be taken into account. In Figure 3 is reported, for example, the energy produced in Germany in one week in 2020. In the X axis are reported the days of the week and in the Y axis the instantaneous GW of produced power.



Figure 3 – Energy Production in Germany – Week 4 - Year 2020

In Figure 4 the same power production of Figure 3 has been divided taking into account the different energy production sources like Hydroelectric, Wind, Coal, etc...

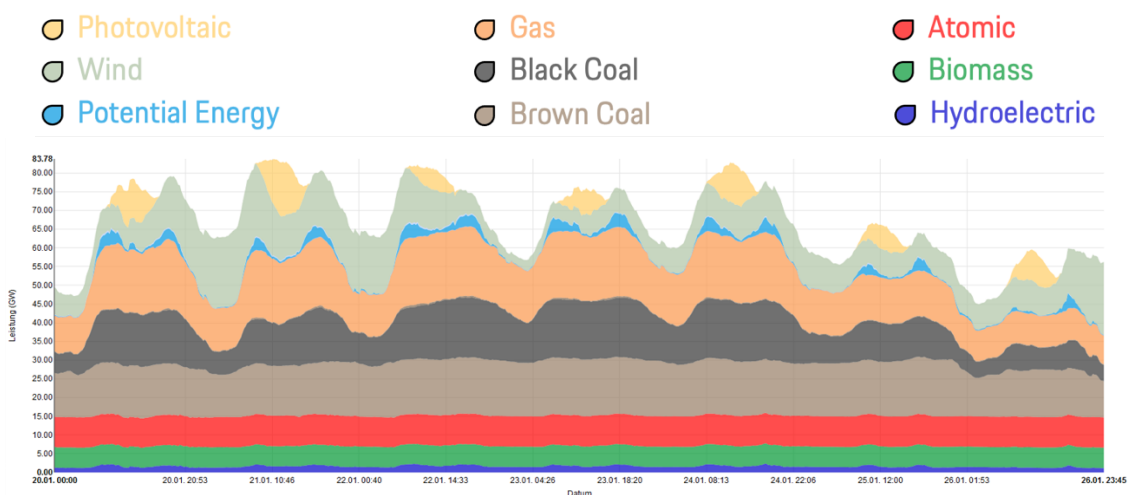


Figure 4 - Energy Production divided by production sources – Week 4 - Year 2020

In Figure 5, instead, is reported a comparison between the diagram in figure 4 and one referred to another week of the same year. It can be noticed how the power produced from wind is increased of more than 100%.

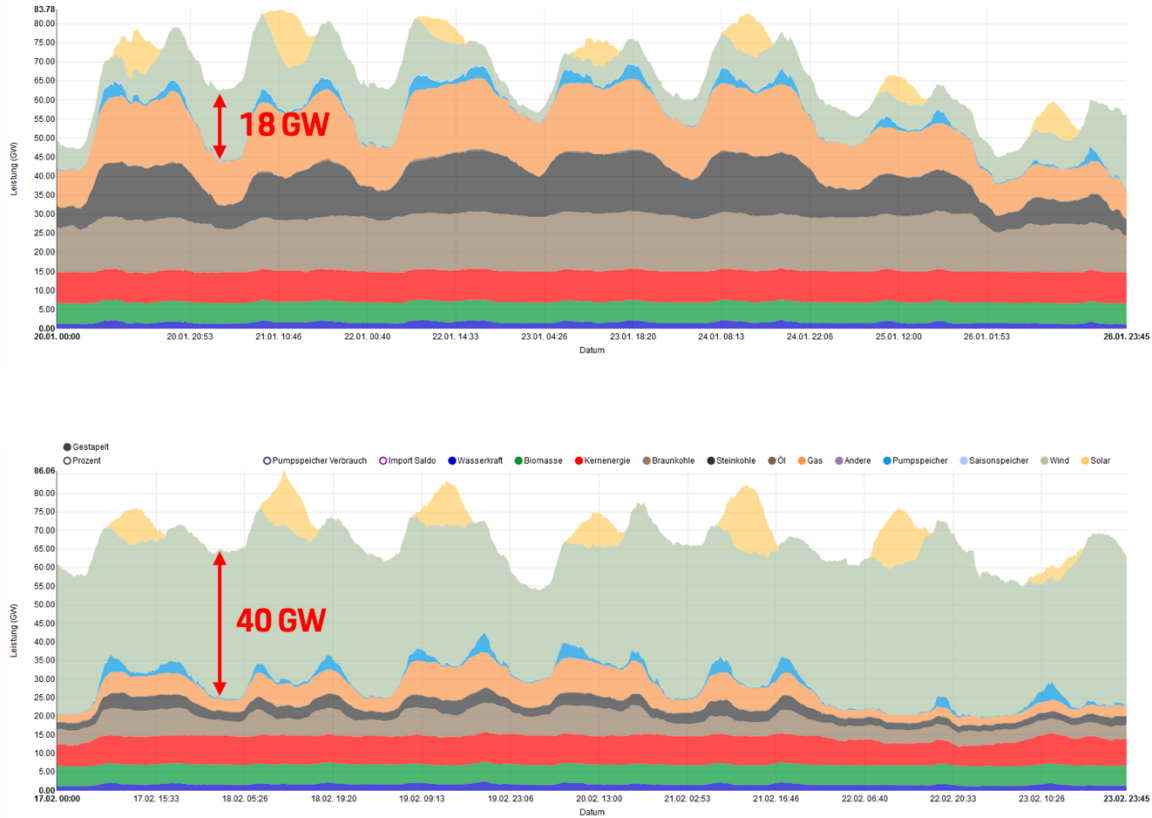


Figure 5 - Energy Production divided by production sources – Week Comparison

This excess of energy has been compensated by reducing the non-renewable part of the energy production, but let's imagine a future with a 100% Renewable energy production. Also in that ideal scenario, it has to be considered that renewable sources, due to the behaviour of the natural phenomena, are intermittent. For this reason, a reliable energy storage will be needed to store, for example, this eventual excess of energy to have it available when the generated power is not enough to fulfil the energy requests.

## 2.1 Energy Storages

But how to store the energy?

There are different ways to store the energy like: batteries, potential energy, eMethane, eFuels and, of course, also Hydrogen. Hydrogen represents a valuable and promising alternative for the energy storage in terms of Transportability, Ease of Storage and Efficiency in the energy conversion process.

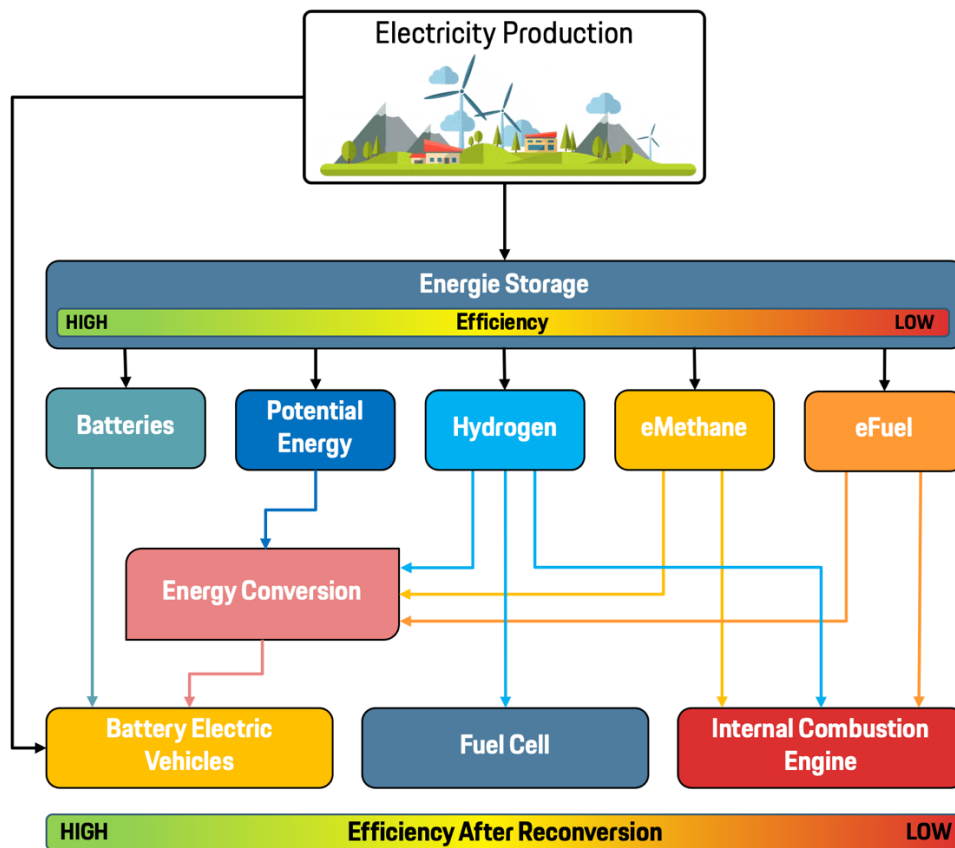


Figure 6 - Energy Storages and how to use the energy in the Transportation Sector

This stored energy can be used as a buffer for the energy supply sector but can be also used by the transportation sector or, before an energy conversion, for Battery Electric Vehicles, or directly, still in Battery Electric Vehicles, but also with Fuel Cell and H<sub>2</sub> Internal Combustion Engine.

These last two solutions will be the focus of this work, whose goal is to develop an Hydrogen Powertrain concept able to meet the requirement of:

- High Performances
- High Efficiency
- No Emissions without after-treatment systems

But before to proceed, let's have a brief overview regarding Hydrogen.

## 2.2 Hydrogen

Hydrogen is the simplest and most abundant element in the universe. On earth, however, hydrogen is not available in pure form as primary energy source, but always chemically bound and has to be released by the introduction of energy. Thanks to his carbon-free structure it has, like electricity, great potential of reducing CO<sub>2</sub> emissions, assuming that it is produced from renewable sources. Nowadays, hydrogen is part of the European Union's decarbonization strategy that consider a gradual transition with a phased approach:

- **From 2020 to 2024:** EU will support the installation of at least 6 gigawatts of renewable hydrogen electrolyzers in the EU zone, and the production of up to one million tonnes of renewable hydrogen.
- **From 2025 to 2030:** hydrogen needs to become an intrinsic part of EU integrated energy system, with at least 40 gigawatts of renewable hydrogen electrolyzers and the production of up to ten million tonnes of renewable hydrogen in the EU.
- **From 2030 to 2050:** renewable hydrogen technologies should reach maturity and be deployed at large scale across all hard-to-decarbonise sectors [17].

Compared to all other alternatives to gasoline and diesel, the technical fuel substitution potential of hydrogen virtually has no limit, but it needs to be stated that economic considerations will shape the introduction of hydrogen, too.

Thanks to his carbon free structure it can be used by the automotive sector in two ways:

- **Fuel Cell Vehicles:** in which H<sub>2</sub> is used to generate electricity on board to power electric motors
- **H<sub>2</sub> Internal Combustion Engine:** exploiting the GHG-free products of Hydrogen Combustion

In the following paragraphs Fuel Cell and H<sub>2</sub>-ICE Technology will be discussed.

### 3. Fuel Cells

A Fuel Cell is an electrochemical reactor that converts the chemical energy of a fuel and an oxidant directly to electricity. In modern fuel cell, hydrogen is a carrier of energy, by reacting with oxygen to form electricity.

Hydrogen and oxygen are introduced separately with hydrogen supplied to one electrode of the fuel cell and oxygen to the other.

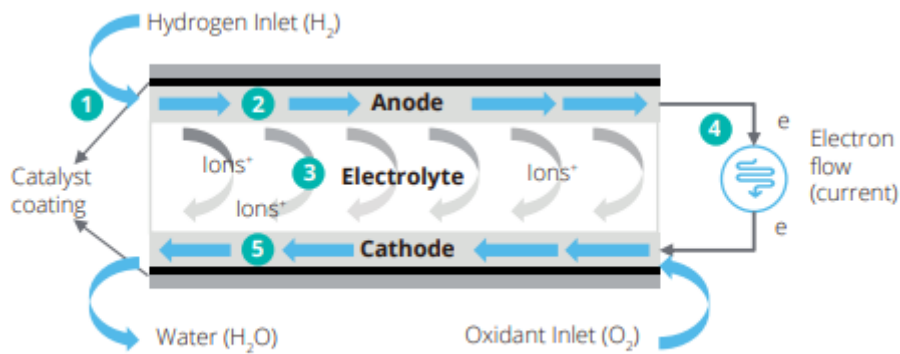
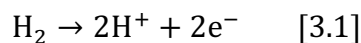


Figure 7 - Fuel Cell Scheme [CITA]

The two electrodes are separated by a material called the electrolyte, which acts as a filter to both stop the cell reactants mixing directly with one another and to control how the charged ions created during the partial cell reactions are allowed to reach each other [5]. The process of generating electricity with H<sub>2</sub> in a fuel cell can be easily described in 5 steps:

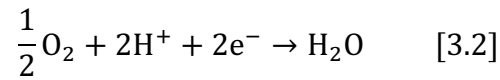
- **Step 1:** Hydrogen molecules are delivered to the anode side of the fuel cell (hydrogen electrode)
- **Step 2:** The hydrogen molecules then react with the catalyst coating the anode following the following reaction:



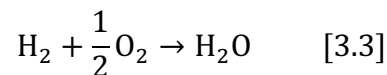
Electrons are released to form a positively charged hydrogen ion.

- **Step 3:** Hydrogen ions pass through the electrolyte towards the oxygen at the cathode
- **Step 4:** The electrons, which cannot pass the electrolyte, travel along an external load circuit thus generating the current output of the fuel cell system.

- **Step 5:** At the cathode, the catalyst causes the hydrogen ions and electrons arriving through the external circuit to bond with oxygen from the air to form water vapor, which is the only by-product of the process. The cathode reaction is the following:



The overall reaction inside the fuel cell can be expressed as:



Different Fuel cell solution are available on the market and typically they are categorized by the type of electrolyte used like : Proton Exchange Membrane ("PEM"), Alkaline fuel cell ("AFC"), Phosphoric Acid Fuel cell ("PAFC"), Solid Oxide Fuel Cells ("SOFC") and Molten Carbonate Fuel cell ("MCFC"). In Figure 8 some main characteristics of each type of fuel cell are summarized.

Fuel cell type	Electrolyte type	Operating temperature (°C)	Catalyst type	Key advantages	Key weaknesses	Areas of application
<b>PEM</b>	Proton Exchange Membrane	50-100	Platinum	<ul style="list-style-type: none"> <li>• Quick start</li> <li>• Work at room temperature</li> <li>• Air as oxidant</li> </ul>	<ul style="list-style-type: none"> <li>• Sensitive to CO</li> <li>• Reactants need to be humidified</li> </ul>	<ul style="list-style-type: none"> <li>• Vehicle power</li> <li>• Portable power</li> </ul>
<b>AFC</b>	Alkaline	90-100	Nickel /Silver	<ul style="list-style-type: none"> <li>• Quick start</li> <li>• Work at room temperature</li> </ul>	<ul style="list-style-type: none"> <li>• Need pure oxygen as oxidant</li> </ul>	<ul style="list-style-type: none"> <li>• Aerospace</li> <li>• Military</li> </ul>
<b>PAFC</b>	Phosphoric Acid	150-200	Platinum	<ul style="list-style-type: none"> <li>• Insensitive to CO<sub>2</sub></li> </ul>	<ul style="list-style-type: none"> <li>• Sensitive to CO</li> <li>• Slow start</li> </ul>	<ul style="list-style-type: none"> <li>• Distributed generation<sup>1</sup></li> </ul>
<b>SOFC</b>	Solid Oxide	650-1,000	LaMnO3/LaCoO3	<ul style="list-style-type: none"> <li>• Air as oxidant</li> <li>• High energy efficiency<sup>2</sup></li> </ul>	<ul style="list-style-type: none"> <li>• High operating temperature</li> </ul>	<ul style="list-style-type: none"> <li>• Large distributed generation</li> <li>• Portable power</li> </ul>
<b>MCFC</b>	Molten Carbonate	600-700	Nickel	<ul style="list-style-type: none"> <li>• Air as oxidant</li> <li>• High energy efficiency<sup>2</sup></li> </ul>	<ul style="list-style-type: none"> <li>• High operating temperature</li> </ul>	<ul style="list-style-type: none"> <li>• Large distributed generation</li> </ul>

Figure 8 - High-Level Comparison of 5 typical Fuel Cell Types [CITA]

### 3.1 PEM Fuel Cells

Proton Exchange Membrane Fuel Cell (PEMFC) are the most employed for vehicle applications. PEMFC are built out of membrane electrode assemblies (MEA) which include the electrodes, electrolyte, catalyst, and gas diffusion layers. An ink of catalyst, carbon, and electrode are sprayed or painted onto the solid electrolyte and carbon paper is hot pressed on either side to protect the inside of the cell and also act as electrodes. The pivotal part of the cell is the triple phase boundary (TPB) where the electrolyte, catalyst, and reactants mix and thus where the cell reactions actually occur. Importantly, the membrane must not be electrically conductive so the half reactions do not mix. Operating temperatures above 100 °C are desired so the water byproduct becomes steam and water management becomes less critical in cell design. [1]

### 3.2 Efficiency of a Fuel Cell

Fuel Cells have an inherently high conversion efficiency, higher than an internal combustion engine where the maximum efficiency is related to the Carnot's cycle. Indeed, the efficiency of an internal combustion engine is given by:

$$\eta_{th} = \frac{l_{mech}}{\Delta H} = \frac{T_2 - T_1}{T_2} \quad [3.2.1]$$

where:

- $l_{mech}$  represents the mechanical work;
- $\Delta H$  the enthalpy of the reaction;
- $T_2$  the highest temperature;
- $T_1$  the lowest temperature;

In other words the maximum efficiency depends simply on a large temperature difference between two reservoirs and represents the theoretical upper limit of a thermodynamic machine operating between a high temperature, typically achieved by burning fuel in the combustion chamber, and a low temperature which is somewhere between exhaust gas and feed gas temperature. For this reason a value of efficiency greater than about 55% are not possible even in a perfect-world scenario. Nowadays the current Hybrid Power Unit used in Formula 1 have as a maximum total efficiency, considering also the hybrid potential, of about 50%. In the case of a fuel cell, two gases – hydrogen and oxygen – are converted into water, and the difference in their chemical potentials is transformed into electrical work. Since a fuel cell does not a priori represent a thermal engine, no temperature difference between two reservoirs is needed for energy generation. Relevant are the internal energies of the chemical compounds involved and only the usable free energy is converted into electrical work [2].

The theoretical efficiency of a fuel cell system is defined by the following equation:

$$\eta_{th} = \frac{l_{el}}{\Delta H} = \frac{\Delta G}{\Delta H} \quad [3.2.2]$$

where:

- $W_{el}$  represents the electrical work;
- $\Delta G$  the Gibbs free energy;
- $\Delta H$  the enthalpy of the reaction;

The thermodynamic efficiency of fuel cells is thus defined as the ratio of the Gibbs free energy  $\Delta G$  and the enthalpy  $\Delta H$  which is equal to  $\Delta G + T\Delta S$ . The work of the cell consists in driving the electrons through the external electric circuit. In this case,  $\Delta G$  and  $\Delta H$  in Eq. (3.2.2) can be expressed as cell voltage. Hence, the efficiency of a fuel cell is the ratio of the usable cell voltage  $U_{rev}$  and the thermoneutral voltage value  $U_{th}$ .

$$\eta_{FC} = \frac{\Delta G}{\Delta H} = \frac{\Delta G}{\Delta G + T\Delta S} = \frac{U_{rev}}{U_{th}} \quad [3.2.3]$$

where:

- $U_{rev}$  is the reversible cell voltage;
- $U_{th}$  is how large the cell voltage would be, if the entire chemical energy could be transformed into electricity;

However, thermodynamic losses are always present due to the entropy release. In the case of hydrogen and oxygen, a certain amount of entropy is released in the form of heat during the formation of water molecules. The water molecule represents a state of higher order, and its entropy is reduced by heat emission. For this reason nowadays the predicted maximum efficiency of the last generation of fuel cells is about 60-65%.

In the Figure [7] we can see a predicted efficiency of a fuel cell vehicle in comparison to an hydrogen internal combustion engine. Despite the fact that the new generation of H<sub>2</sub>-Ice with Direct Injection and Multi-Stage Turbochargers are expected to have higher efficiencies as the one in the picture, Fuel Cell vehicle are generally more efficient with a peak efficiency at about the 25% of the load.

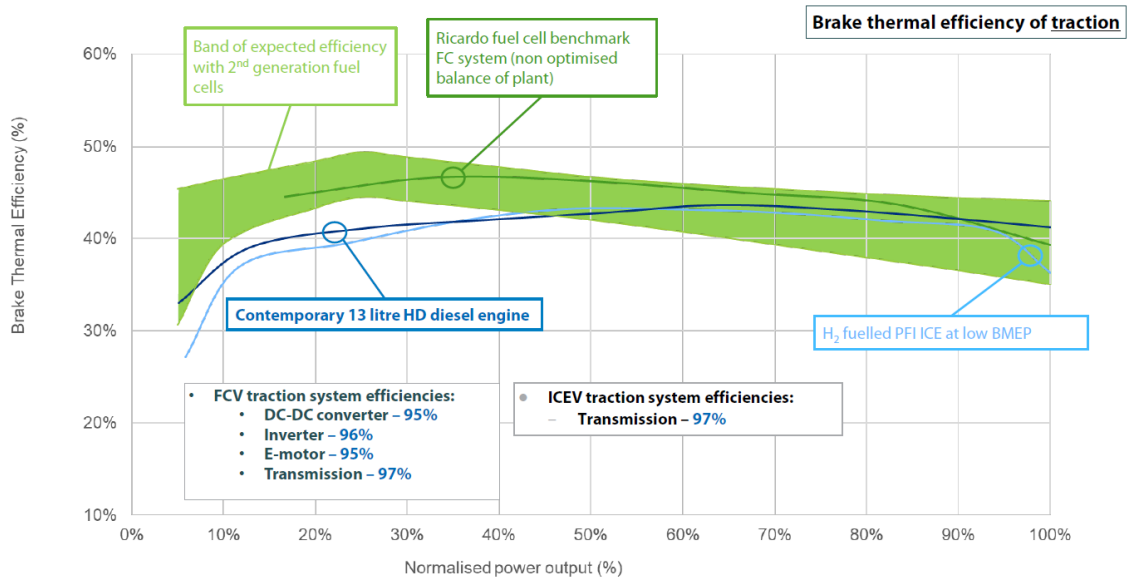


Figure 9 - Fuel Cell vs H<sub>2</sub>-ICE vs Gasoline ICE Efficiency Comparison

## 4. Hydrogen Internal Combustion Engines

Hydrogen can be a promising a valuable solution also with Internal Combustion Engines. It is the most abundant element in the universe and it can replace fossil fuels thanks to his GHG-Free combustion that offers little or no harmful pollutant emissions. However, H<sub>2</sub> properties have some important differences compared to gasoline that influences the design of the engine. In the next chapters, the main properties of hydrogen and how they influences the engine design will be described.

### 4.1 Properties of Hydrogen

The properties of hydrogen that play an important role in the combustion process are the wide range of flammability, the low ignition energy, the high auto-ignition temperature, the small quenching distance, the low density, and the high flame velocity. In the table a comparison of these properties between diesel, Gasoline, Methane and Hydrogen are reported [8].

Parameter	Symbol	Unit	Diesel	Gasoline	Methane	H <sub>2</sub>
Density	$\rho$	kg/m <sup>3</sup>	830 <sup>I</sup>	730-780 <sup>I</sup>	0,72 <sup>I</sup>	0,089 <sup>I</sup> 71 <sup>II,III</sup>
Stoichiometric air demand	L <sub>St</sub>	kg <sub>air</sub> /kg <sub>fuel</sub>	14,5	14,7	17,2	34,3
Lower heating value	H <sub>u</sub>	MJ/kg <sub>Kst</sub>	42,5	43,5	50	120
Mixture calorific value <sup>V</sup>	H <sub>G</sub> H <sub>G</sub>	MJ/m <sup>3</sup>	3,83 3,83	3,82 3,82	3,4 3,76	3,2 4,53
Boiling temperature <sup>III</sup>	T <sub>Boiling</sub>	°C	180-360	25-215	-162	-253
Ignition limits <sup>IV</sup>		Vol-% $\lambda$	0,6-5,5 0,5-1,3	1,0-7,6 0,4-1,4	5,3-15 0,7-2,1	4-76 0,2-10
Minimum ignition energy <sup>III,IV,V</sup>	E <sub>Ignition</sub>	mJ	0,24	0,24	0,29	0,02
Self-ignition temperature	T <sub>Ignition</sub>	°C	approx. 250	approx. 350	595	585
Diffusion coefficient <sup>I,IV</sup>	D	m <sup>2</sup> /s	-	-	1,9x10 <sup>-6</sup>	8,5x10 <sup>-6</sup>
Quenching distance <sup>III,IV,VI</sup>		mm		2	2,03	0,64
Laminar flame speed <sup>IV,V</sup>	v <sub>lam</sub>	cm/s	40-80	40-80	40	200
Carbon content	C	Mass-%	86	86	75	0

<sup>I</sup> at 1,013 bar und 0 °C   <sup>II</sup> at -253°C   <sup>III</sup> at 1,013 bar   <sup>IV</sup> in air   <sup>V</sup>  $\lambda=1$    <sup>VI</sup> at 20°C

Table 1 - Hydrogen Properties

In order to analyze how these different properties influences the engine design they will be analyzed singularly:

1. **Wide range of flammability:** Hydrogen can be burnt over a wide range Lambda values. This important property give another degree of freedom for the combustion management of the engine, it makes possible to adopt lean mixtures having a more complete combustion and fuel economy. The lean mixture helps also to reduce the

peak temperature during the combustion and, thus, reduce the nitrous oxide emissions. However, an advanced turbo configuration for the high level of boost will be necessary.

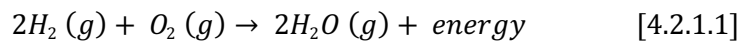
2. **High Octane Number** : Hydrogen octane number is around 135 and so much higher than the standard gasoline with about 100. This leads to and high knock resistance that allows the exploitation of high compression ratios, increasing the overall efficiency of the engine.
3. **High flame velocity**: at unitary lambda, Hydrogen laminar flame speed is about 220 cm/s that compared with the 33 cm/s of gasoline results in a 5/6 times faster combustion. This leads to tighter ignition timing and to precisely control of the spark timing.
4. **Low ignition energy**: Compared to the other common fuels, H<sub>2</sub> needs about one order of magnitude less energy to ignite than gasoline. This may lead to problems like premature ignition caused by hot sources and hot spots in the cylinder that must be managed. Cold-rated Spark Plugs must be adopted and they should not be platinum-tipped, because Pt is a catalyst-promoting ignition. Cold-rated plugs are designed to cool quickly and therefore avoid the possibility of acting like a "glow plug" and causing pre-ignition.
5. **High diffusivity**: The high diffusivity of hydrogen in air ensures that if a leak develops it disperses rapidly thus improving the safety of H<sub>2</sub>-fuelled vehicles. From a combustion point of view, an high diffusivity produces a more uniform air-fuel mixture. This is important because hydrogen has a very low density compared to gasoline and this results to longer injections with same injected mass. To have an improved mixing helps to reach an uniform mixture before the spark, also with a late end of injection, improving NOx emissions and knock behaviour.
6. **Small quenching distance**: H<sub>2</sub> will burn closer to a given surface than gasoline increasing the heat exchange that must be taken into account.
7. **Low density**: as discussed, the low density of hydrogen leads to a more difficult fuel injection timing management but it is also a great disadvantage for H<sub>2</sub> storage . It necessitates a larger volume for storage and normally, to store a decent amount of fuel (i.e. 6kg like the actual FCEV on the market) a 700 bar tank is needed. Moreover the low density of the fuel is a concern because of the amount of volume it occupies in the cylinder prior to ignition. This is a problem for naturally aspirated PFI engines but it has been solved with Turbocharged DI engines.

## 4.2 H<sub>2</sub>-ICE Emissions

Hydrogen Internal combustion engines do not have any GHG emissions and therefore they have no impact to the global warming. Regarding pollutants, emissions the most important ones that must be taken into are nitrous oxide emissions (NO<sub>x</sub>). HC emissions can be caused only by particles of oil that from the cylinder walls goes through the exhaust and therefore are negligible [2].

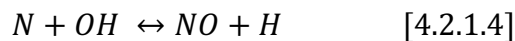
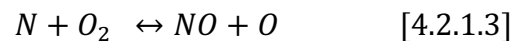
### 4.2.1 NO<sub>x</sub> Emissions

NO<sub>x</sub> emissions in hydrogen internal combustion engines are related to the presence of Nitrogen in the ambient air. Theoretically, the combustion of Hydrogen and Oxygen produces only Water vapor and releases energy:



However, the ambient air contains about the 20% of Nitrogen that at high temperatures can react with oxygen to form NO<sub>x</sub>. Generally, the nitric oxides formation stems from three principal sources: Thermal NO<sub>x</sub>, Prompt NO<sub>x</sub> and Fuel NO<sub>x</sub>. Regarding internal combustion engines, the only one that must be taken into account is the **Thermal NO<sub>x</sub> formation**.

The reaction mechanism can be expressed in terms of the *Extended Zeldovich Mechanism*:



The first reaction (eq. 4.2.1.2) represents the rate-limiting step in comparison to the other reactions. A very high activation energy (and so temperature) is necessary to decompose the stable triple bond of the molecular air-nitrogen so this reaction is significantly fast at high temperatures and it is the main reason why NO<sub>x</sub> are a concern for Hydrogen Internal Combustion engines. In order to limit the maximum temperature reached during the combustion, very lean mixtures must be adopted.

In Figure 10 [8] is reported how the NO<sub>x</sub> production varies with the average lambda and the maximum temperature in the combustion chamber, assuming an homogeneous mixture:

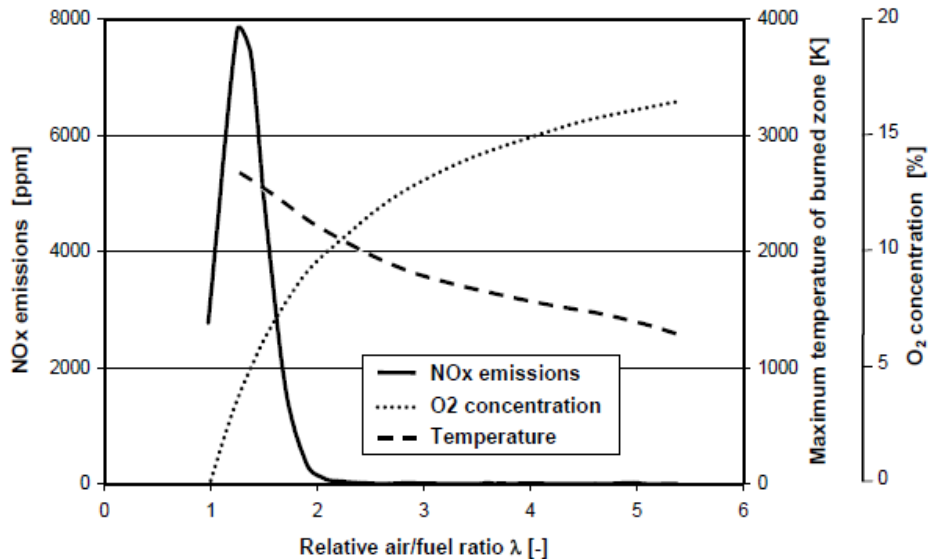


Figure 10 - NO<sub>x</sub> Production in Internal Combustion Engines

It is clear how emissions are at maximum in slightly lean mixtures, near stoichiometric conditions, and then decrease, as the engine's equivalence ratio becomes leaner. This means that, in order to have a NO<sub>x</sub>-Free engine, for the whole engine map the lambda value must be 2.3/2.4 at minimum.

However this leads to several concerns which are listed below:

1. **Leaner-burning engines need more air.** In this case, about 2.5 times more air. That means that the gasoline engine's throttle body, intake manifold, and intake valves are not large enough and, as a result, restrict the amount of air that the engine can get into the cylinder. This reduces the amount of power that can be produced. This means that that a turbo charger is needed, and to have high performances a traditional turbo system layout is not enough, as we will discuss in chapter 7.
2. **Leaner-burning engines are harder to control** and need both a good engine control and a good set of sensors, often referred to as the sensor suite. The oxygen sensor is critical, because the only feedback the controller has is from the exhaust gas stream and only the amount of oxygen in that stream is reliable enough for good control. The amount of oxygen in the exhaust gas increases, as the engine is run leaner. [2]
3. **Leaner-burning engines normally run at higher cylinder pressures.** Care must be taken to keep the maximum cylinder pressure within specifications. [2]

## 5. Powertrain Solution Selection

As previously mentioned, the aim of the work is to develop an hydrogen powertrain concept with :

- **High Performances**
- **High Efficiency**
- **No-Emissions without Aftertreatment system**

Fuel Cell and H<sub>2</sub>-ICE are valuable solutions to achieve these objectives but only the most promising one will be further analyzed in this work. It is possible to compare the two solutions in terms of:

- Performances
- Efficiency
- Greenhouse Gasses Emissions
- Sound
- Costs

Efficiency and GHG emissions have already been analyzed in the previous chapters. Fuel Cells Efficiency is slightly higher than the current H<sub>2</sub>-ICE technology but both the solutions have no local GHG emissions. Regarding sound, it is clear that, for a high performance solution, the sounds represents an advantage in terms of appealing of the solution. Costs are also an important part of the analysis that will not be deeply analyzed in this work. However, it is easy to note how Hydrogen internal combustion engines have different advantages in terms of cost. First, nowadays the price of the current technology of fuel cells is order of magnitude higher than a traditional engine, then it must be also considered that it is possible to convert existent gasoline/diesel engines to Hydrogen versions. Moreover, the high level of knowledge and the various methodologies currently used for gasoline/diesel engines can be adapted with few changes to the hydrogen versions.

	Fuel Cell	H2-ICE
Performances	✗	✓
Efficiency	✓	✗
CO <sub>2</sub> Emissions	⊖	⊖
Sound	✗	✓
Costs	✗	✓

Table 2 - Fuel Cell vs H<sub>2</sub>-ICE Comparison

The Table 2 summarizes the main advantages and disadvantages of both the solutions. However, the most limiting one for the purposes of the current work, is the impossibility to reach high performances with a fuel cell powertrain.

Nowadays on the market, different fuel cell vehicles are available like:

— **2021 Toyota Mirai**

> Power: **128 kW**



— **2021 Honda Clarity Fuel Cell**

> Power: **103 kW**



— **Hyundai NEXO Blue**

> Power: **120 kW**



— **Mercedes Benz GLC Fuel Cell**

> Power: **147 kW**



Figure 11 - Current FCEV on the market

As it can be noticed, the order of magnitude of the power output is **100kW-150kW**, not comparable with a high performance application where at least 2-3 times this power must be achieved. Moreover also with this relatively low power output, there is no more space available in the car thus it is not possible to increase this values by increasing the fuel cell stack dimension.

In the Fig. 7 it is reported the Mercedes GLC Fuel Cell Powertrain architecture, although the car is a SUV, the powertrain and the H<sub>2</sub> tanks fill all the available space in the car. The current technology of fuel cell, in fact, has still a low energy density and volume to power ratio, and for this reason, the hydrogen internal combustion engine has been selected as the powertrain concept to develop in this work.



Figure 12 - Mercedes GLC Fuel Cell Powertrain Architecture

It has been decided not to start from a scratch, but to convert an existent turbocharged gasoline engine to a hydrogen version whose technical specifications are reported in the next paragraph.

## 5.1 Reference Engine

The first engine that will be used as a reference is a 90° V8 Twin-Turbocharged S.I Direct Injection (GDI) engine. The main specifications are reported in the Table 3, below:

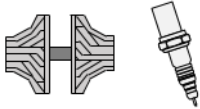
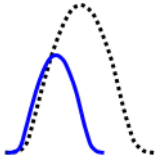
<b>Engine Block</b> 	Cylinders	V8 90°
	Displacement	4.4 L
	Bore x Stroke	88 mm x 90 mm
	Firing Order	1 - 3 - 7 - 2 - 6 - 5 - 4 - 8
	Compression Ratio	9.5 : 1
	Crankshaft	Cross - Plane
	<hr/>	
<b>Mixture Preparation &amp; Combustion</b> 	Fuel Supply	Direct Injection
	Turbocharger	Bi-Turbo Single Stage
	Compressor Size	56 mm
	Turbine Size	50 mm
	Boost Control	WasteGate
<hr/>		
<b>Gas Exchange</b> 	Camshaft	Twisted Camshaft
	Valve Train	Double VVT
	Intake Valve Opening Duration	190 CA deg
	Intake Valve Maximum Lift	10.5 mm
	Exhaust Valve Opening Duration	210 CAdeg
	Exhaust Valve Maximum Duration	10 mm

Table 3 - Reference Stock Engine

The engine has a cross-plane crankshaft that, despite its characteristic smooth running due to the intrinsic balancing, it causes a series of gas exchange problems determined by the uneven firing distance on each bank [11]. This translates in a series of blowdown interferences among cylinders on the same bank, which causes an uneven filling and mixture composition in the cylinders (different residual content), which is detrimental for final performance optimization of the engine. With this regard, the 4-2-1 exhaust manifold in Figure 8 (a) and the Twisted Camshaft [12] in Figure 8 (b) were adopted on the engine, so that to overcome the issues related to the blowdown pulses interferences of subsequent firing cylinders.

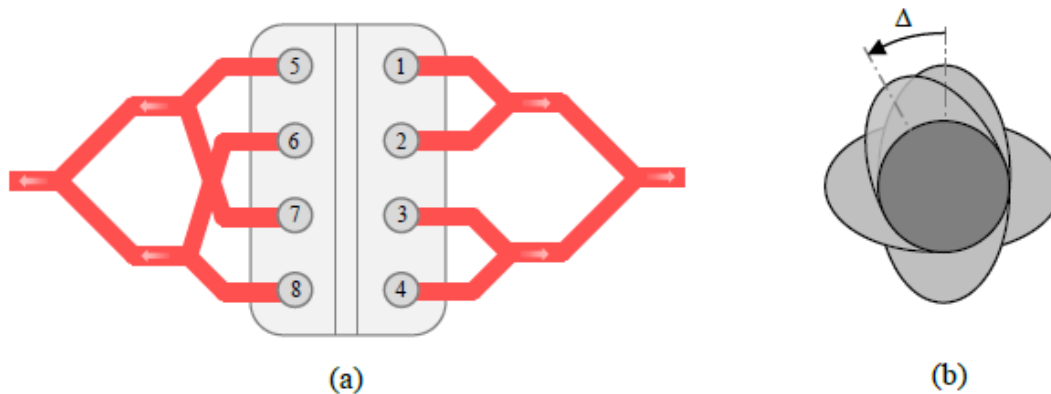


Figure 13 - a) Exhaust Manifold Design b) twisted Camshaft

The stock engine has also an hybrid configuration with an electric motor in P2 position, between gearbox and clutch, as shown in Figure 9. Indeed, being the P2 eMachine connected to the gearbox input shaft, it is possible to run the vehicle in pure electric mode and to have a good kinetic energy recovery in braking. The P2 electric motor (P2 EM) will be widely used in the hydrogen configuration.

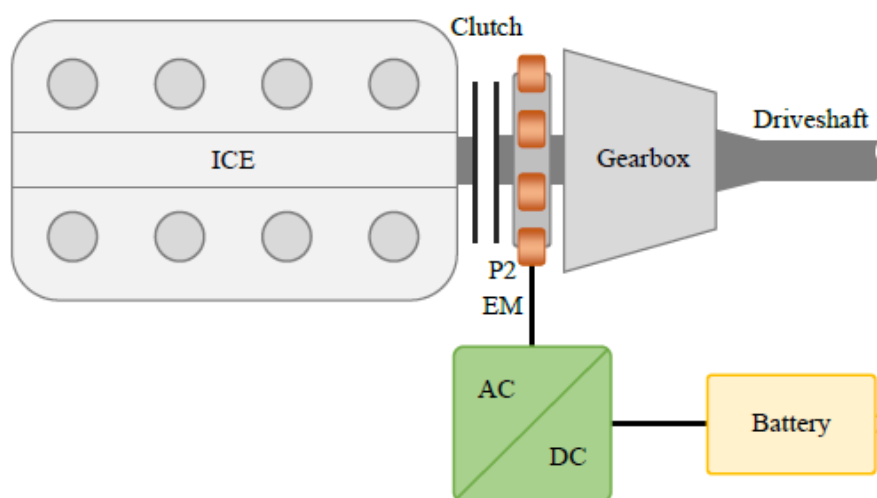


Figure 14 - Hybrid Architecture

The stock engine is Euro 6D compliant but there is also a concept of Euro 7 version based on that, with the exploitation of eTurbo and Turbulent Jet Ignition (TJI) in order to have lambda 1.0 on the whole engine map.

This version will be also used as a reference for the H<sub>2</sub> concept and the its main specifications are reported in Table 4.

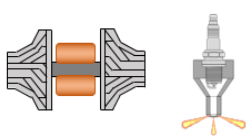
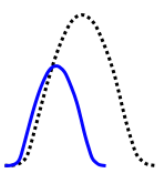
<b>Engine Block</b> 	Cylinders	V8 90°
	Displacement	4.4 L
	Bore x Stroke	88 mm x 90 mm
	Firing Order	1 - 3 - 7 - 2 - 6 - 5 - 4 - 8
	Compression Ratio	10.5 : 1
	Crankshaft	Cross - Plane
	<b>Mixture Preparation &amp; Combustion</b>	
	Fuel Supply	Direct Injection + Turbulent Jet Ignition
	Turbocharger	Bi-Turbo Single Stage
	Compressor Size	58 mm
	Turbine Size	60 mm
	Boost Control	eTurbo – 10kW
<b>Gas Exchange</b>		
	Camshaft	Twisted Camshaft
	Valve Train	Double VVT
	Intake Valve Opening Duration	140 CAdeg (Miller Cycle)
	Intake Valve Maximum Lift	10.5 mm
	Exhaust Valve Opening Duration	210 CAdeg
Exhaust Valve Maximum Duration	10 mm	

Table 4 - Lambda 1.0 Version Reference Engine

It must be pointed out that both the lambda 1 and hydrogen versions feature an eTurbo solution powered with the energy from the P2 Machine. In this case the efficiency of the energy exchange process has been estimated as 80%.

## 5.2 Reference Performances

The Stock and the Lambda 1.0 versions will be used as a reference in terms of performances. As discussed in chapter 5, the aim of the work is to reach the same level of Peak Power and Peak Torque of these two versions while being emissions free and reaching high Brake Thermal Efficiency. In Figure 15, Power, Torque, Efficiency and electrical power from P2 to eTurbo are reported for the two versions. Please remember that the stock version has not an eTurbo and therefore no data have been reported.

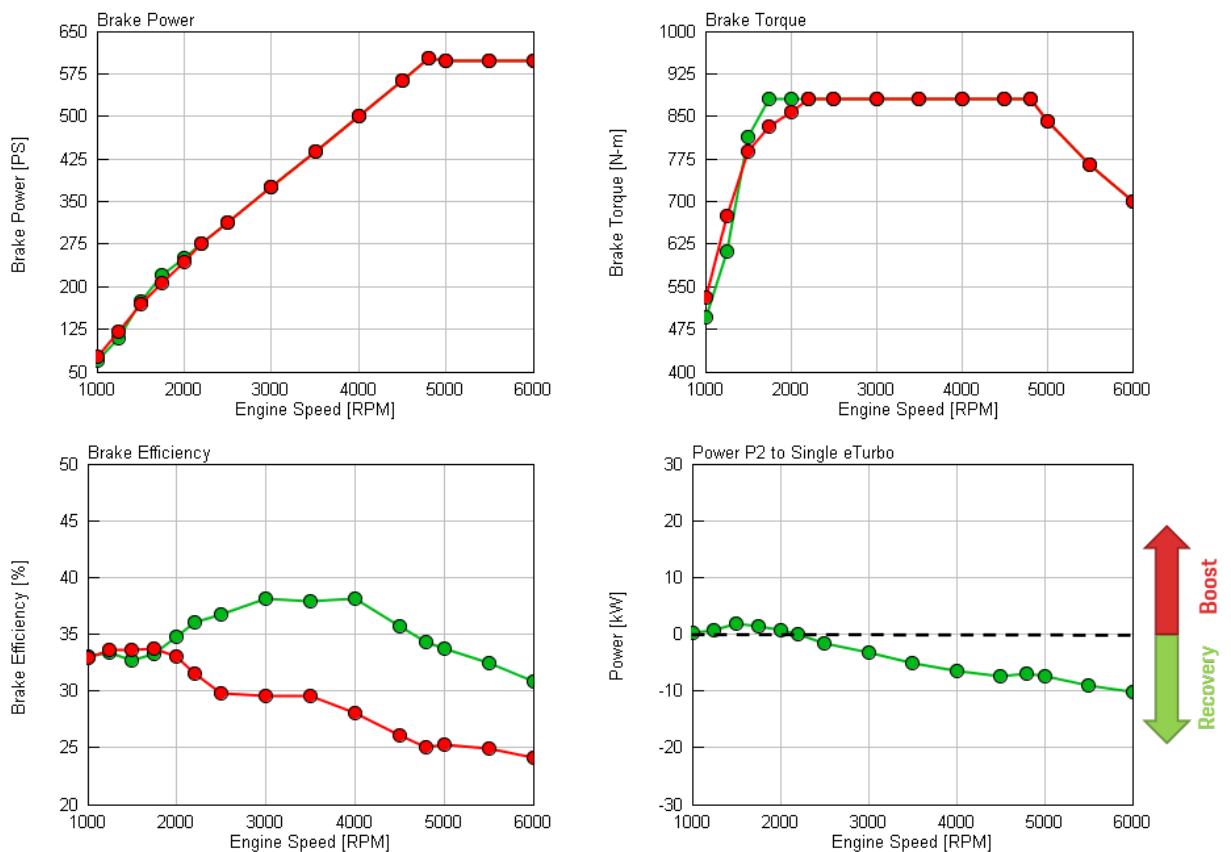


Figure 15 - Reference Gasoline Engines Performances

## 6. Methodologies

Most of the current methodologies for Internal combustion engines are related to common used fuels like gasoline, diesel or methane, especially regarding knock prediction and combustion modelling. Hydrogen has a complete different behavior compared to the traditional fuels and there is a poor literature regarding H<sub>2</sub>-CFD simulations. This lead to the big challenge to design the hydrogen engine concept and, at the same time, to develop precise and reliable methodologies to take into account the H<sub>2</sub> properties in the CFD simulations.

Thereby, to convert the gasoline reference engine to an the hydrogen version , different new methodologies have been studied, regarding Hydrogen Knock Prediction, Hydrogen Combustion Simulation and Control. In particular three new interesting methodologies have been developed :

1. **Knock Prediction Methodology:** the 1D-CFD software used for this work (GT Suite by Gamma technologies) do not have available knock models for hydrogen, for this reason, a controller based on a new methodology has been implemented
2. **Maximum In-Cylinder Pressure Control:** hydrogen fast combustion and high knock resistance, combined with the high value of lambda, leads to really high in cylinder pressures that must be controlled to avoid damages
3. **Combustion Speed Prediction:** at same lambda hydrogen has a laminar flame speed 5-6 times faster than gasoline and in order to use an imposed combustion model (like Wiebe) to have a correct combustion speed prediction is crucial

Before going into details of the methodology that has been developed it is important to have an overview regarding ignition delay, abnormal combustion phenomena and Wiebe combustion models on 1D-CFD software.

These topic will be discussed in the next chapters.

## 6.1 Ignition Delay and Autoignition

Ignition delay  $\tau$  is defined as the time needed for the combustion's start of a certain mixture under certain conditions (temperature, pressure, lambda, etc..) .. During this lapse of time a pool of radicals large enough, which consumes a small fraction of fuel necessary to trigger the combustion process, is generated and a low heat released is identified. The ignition delay time can be linked to the fuel properties and the local temperature and pressure of the mixture by the following relation :

$$\tau = C_1 \cdot p^{-n} \cdot e^{\left(\frac{C_2}{T}\right)} \quad [6.1.1]$$

where  $C_1$ ,  $C_2$  and  $n$  are parameters characteristic of the fuel and are related to the Octane Number, the higher is the octane number and the higher is the time required from the autoignition to occur. A clear similarity with the Arrhenius equation (eq. 6.1.2) which gives the dependence of the rate constant of a chemical reaction on the absolute temperature as:

$$k = A \cdot e^{-\frac{E_a}{RT}} \quad [6.1.2]$$

where:

- $A$  is a constant linked to the characteristics of the fuel ;
- $E_a$  is called activation energy and it is a reaction constant. It represents the energy barrier that has to be overcome in order to obtain a successful reaction.
- $T$  is the temperature
- $R$  is the gas constant

It can be noticed how the ignition delay time is dependent on the reaction speed of the system as the constant  $k$  in the Arrhenius equation.

The ignition delay time can be evaluated with the so-called rapid compression machine (Figure 16) where the charge is highly compressed in a very short time to a predefined pressure level, which is then kept constant.



Figure 16- Rapid Compression Machine

The ignition delay time is then evaluated from the compression to the self-ignition of the charge. The typical pressure behavior of a rapid compression machine is schematically represented in Figure 16.

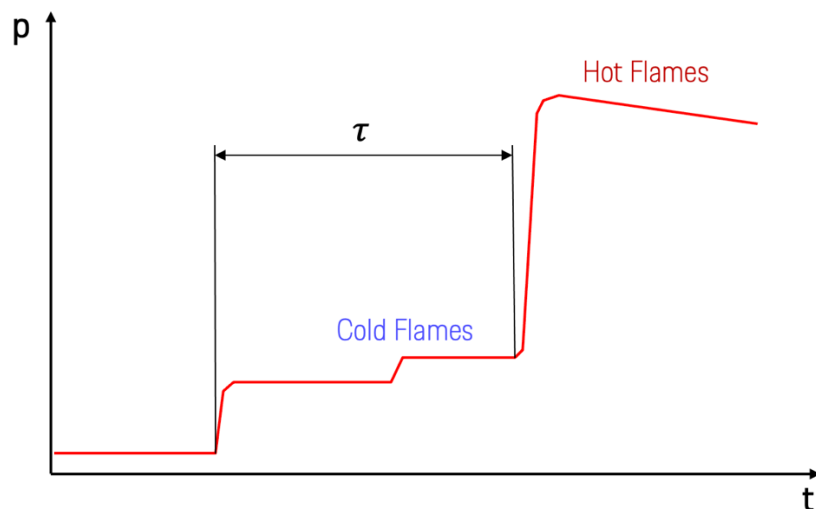


Figure 17 - Rapid Compression Machine p-t

What happens in a rapid compression machine can be summarized as follows : the charge is first compressed very rapidly to the required pressure level, ideally the charge must be compressed instantaneously in order to avoid the occurrence of any pre-reaction during the compression phase, however in a real world application the compression is done as fast as possible. Then the charge is kept to the reached pressure and temperature level, and some first reactions occur, leading to the generation of cold flames, which are usually characterized by a light blue color. This flames leads to a further increase of pressure and temperature and when a sufficiently large number of radicals is formed during the first

step, the main high exothermic reaction occurs and the pressure shows an abrupt increase. In this phase hotter flames, characterized by a red color, are generated. The ignition delay time  $\tau$ , as reported in Figure 17, is the time between the end of the compression phase and the start of the combustion. Ignition delay time shows a high dependency on the temperature and for this reason, it is usually represented, at constant pressure, with respect to the inverse of the initial temperature, as shown in Figure 18.

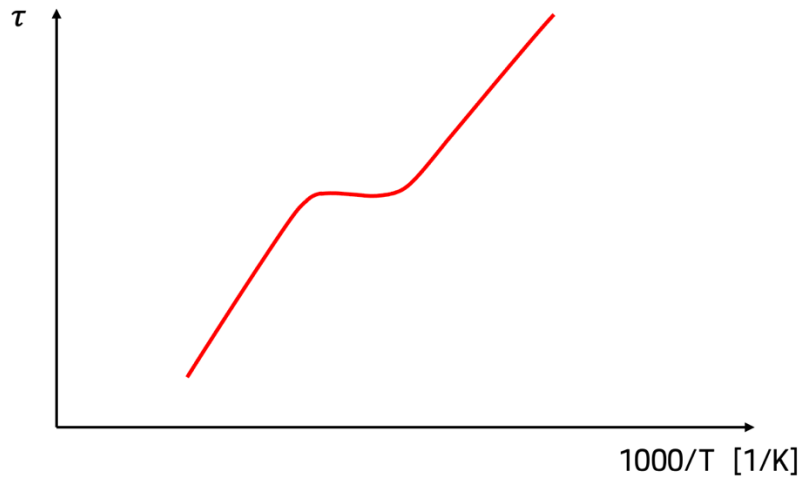


Figure 18 - Ignition Delay vs Temperature - Example

Hydrogen and gasoline show a different trend with respect of the temperature. Hydrogen has a different molecular structure compared to gasoline and its octane number is about 135, as discussed in chapter 4. In Figure 19, below, it is reported a comparison between an ignition delay map at 40 bar of pressure and lambda 1.0 for Hydrogen and a 100 RON gasoline.

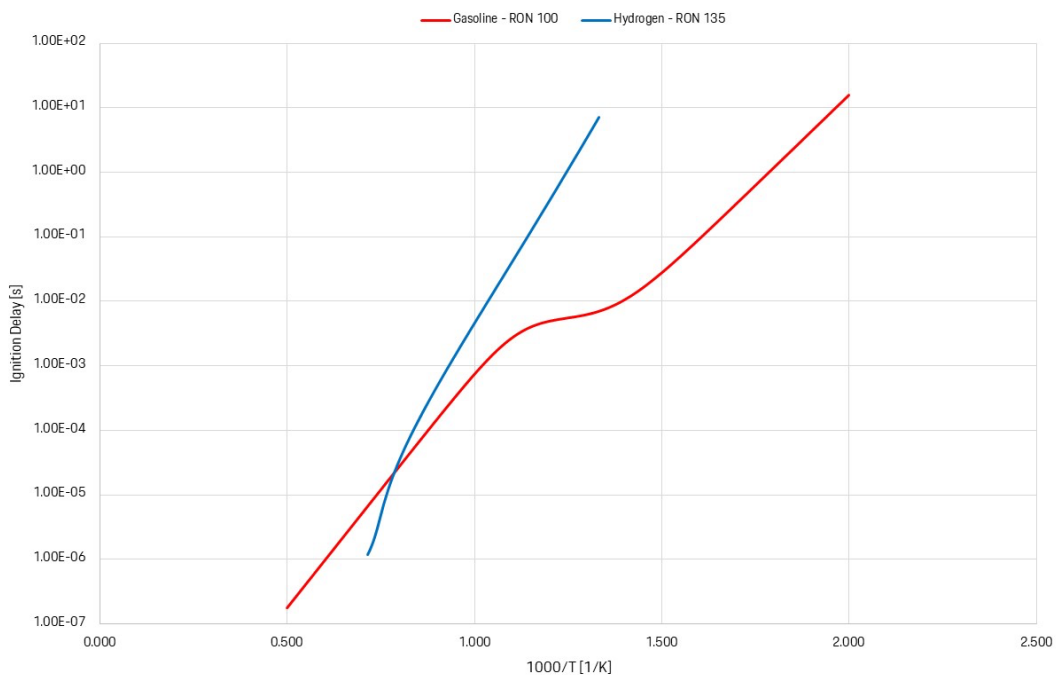


Figure 19 - Ignition Delay for Gasoline and Hydrogen

Gasoline-Air mixtures show an exponential dependency at very low temperature (below 650K) and at high temperature (above 1000K), while at different behaviour is shown in the middle range. Hydrogen has a completely different trend, the exponential dependency starts at higher temperatures and leads, for internal combustion engines relevant temperatures, to higher values of ignition delay and so lower tendency to preignition. By adopting high values of lambda the charge dilution leads to higher ignition delay and at the same time the maximum temperature of the unburned gas in the combustion chamber is decreased thus contributing to reduce the autoignition tendency.

## 6.2 Abnormal Combustion and Engine Knock

Regarding the ignition type, Hydrogen combustion engines are similar to the gasoline engines. There is a spark plug that is used to ignite the mixture and the spark advance is a crucial calibration parameter. However, in some unwanted situation, an abnormal ignition may occur, leading to a so called abnormal combustion. Abnormal combustion reveals itself in many ways but the two major phenomena are [4]:

- Surface ignition
- Engine knock

Surface ignition is ignition of the fuel-air mixture by an hot spot on the combustion chamber walls such as an overheated valve or spark plug, or, for example, glowing combustion chamber deposit: hydrogen, as discussed in chapter 4, has a very little ignition energy and this kind of abnormal ignition must be seriously taken into account. This abnormal ignition generates a turbulent flame that propagate in the combustion chamber as if it was produced by the spark and it can also eventually evolve into knock, which may be dangerous since it usually cannot be controlled with the spark timing. It is potentially critical, because it usually results in an uncontrolled increase of temperature, which can cause the generation of other hot spots that may eventually lead to even more severe surface ignition phenomena. However this phenomenon does not represent usually a critical situation, because it can be avoided with a proper design of the combustion chamber and of the cylinder cooling system. Engine knock, instead, is a most dangerous phenomenon of abnormal combustion in a SI-engine. Knock is the name given to the noise which is transmitted through the engine structure when essentially spontaneous ignition of a portion of the end-gas-the fuel, air, residual gas, mixture ahead of the propagating flame occurs. When this abnormal combustion process takes place, there is an extremely rapid release of much of the chemical energy in the end-gas, causing very high local pressures and the propagation of pressure waves of substantial amplitude across the combustion chamber. [4]

The actual origin of engine knock is not yet completely known, but many experiments observed that it is caused by the autoignition of the fresh charge ahead of the flame front, called end gas. During the development of the flame front caused by the spark, the end gas is compressed and heated up, so that, according to equation [6.1.1], the ignition delay time  $\tau$  is reduced and the charge self-ignites. [10]

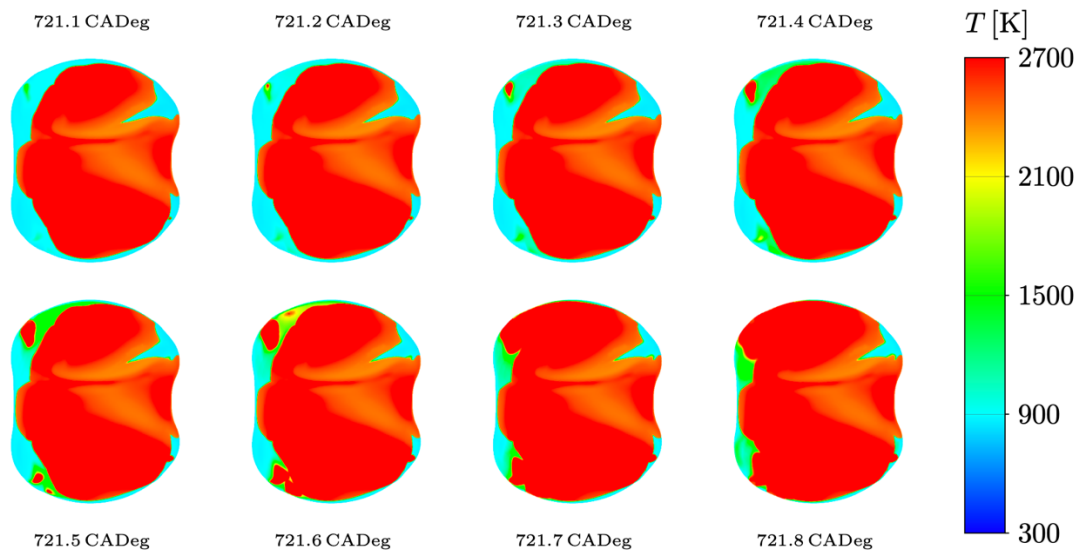


Figure 20 - Example of Knock Occurrence [10]

An evidence of the different reaction rate of a detonating flame can be clearly seen in Figure 20 taken from [10]. In this sequence of images, the evolution of the flame between 721.1 and 721.8 CADeg is represented, considering a step between each image of 0.1 CADeg. In particular, the temperature is here shown in a section plane from a top view of the combustion chamber, so that the red area shows the temperatures above 2500 K, i.e. the presence of the flame. By looking at the image on the right top, two areas can be identified: the flame inside the flame front, in red, which is moving towards the end gases, in light blue. It can be noticed that, due to the relatively low laminar flame speed the flame front looks almost still in the successive images. On the other hand, in the second image a new ignition position can be identified: this is the location where the knock is generated and, from this position, it propagates with a considerably higher velocity towards the region of the combustion chamber which has not burned yet, consuming it in less than 1 CADeg. During the occurrence of knock, the flame propagates in the combustion chamber, generating pressure oscillations typical of the knocking behaviour.

These can be noticed in Figure 21, where a normal combustion is compared with a knocking combustion as a function of the crank-angle.

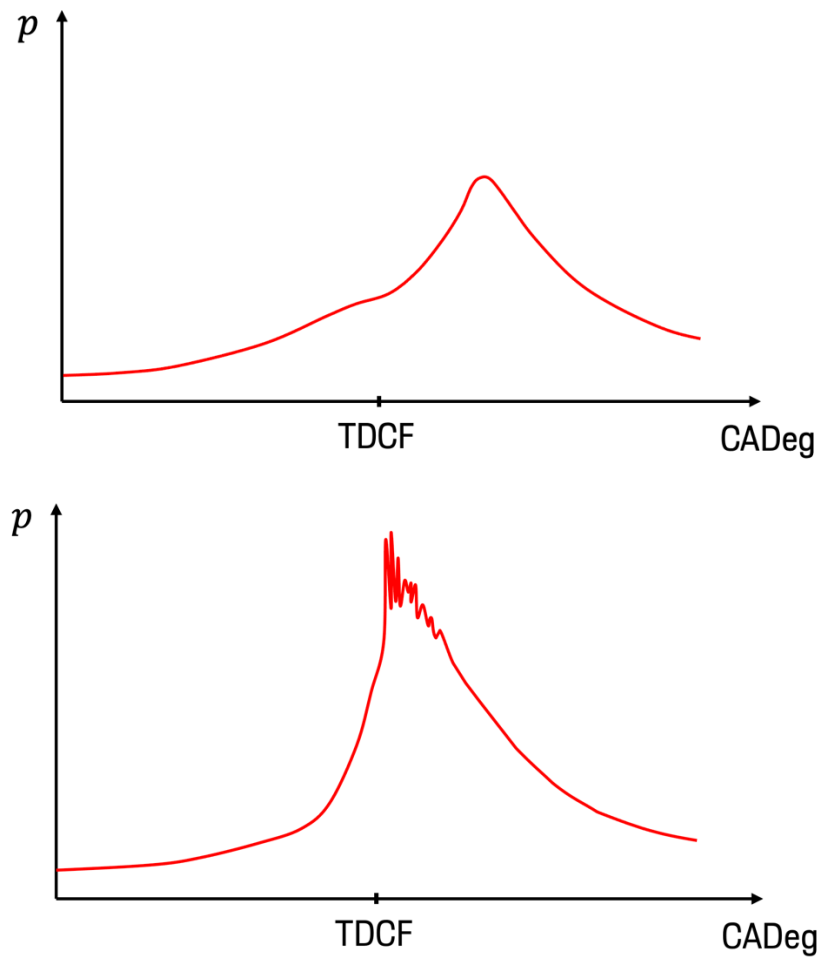


Figure 21 - Comparison between Normal Combustion (up) and Abnormal Combustion (down)

### 6.3 Engine Knock Prediction

To predict the knock occurrence is crucial both in real applications and in simulations. For 1D-CFD models it is crucial to have a sophisticated knock controller to be sure that the model is able to reproduce the performances of the real engine.

However the engine knock is a local phenomenon and depends on many factors, and it is not easy to predict. In particular, the tendency to the knocking behaviour increases with:

- Higher pressure and temperature of the mixture, also due to supercharging;
- Mixture near to stoichiometric;
- Earlier spark timing;
- Slow combustion process;
- Higher compression ratio;
- Lower octane number of the fuel.

Although ignition can be reasonably predicted by using advanced CFD codes with detailed chemistry, the required computing time is too long to be solved in real time. Thus, simple numerical methods with very short computing time are the only ones that can be implemented in an engine control unit. Methods accurate enough allow improving the control of the engine by making it possible to take decisions in real time. The Livengood & Wu hypothesis [9], also known as the Livengood & Wu integral or, simply, the integral method, allows to obtain ignition delays of processes under variable conditions of temperature and pressure by using the ignition characteristics under constant thermodynamic conditions, which are much easier to obtain. The theory is also called "conservation of delay", it is possible to consider the ignition delay in every timestep separately, summing up the contributions coming from each of them. In particular, the following equation holds:

$$KI = KITI = \int_{t_0}^{t_b} \frac{dt}{\tau_i} \quad [6.2.1]$$

where

- **KI** stands for knock index;
- **t<sub>0</sub>** is the initial timestep considered;
- **t<sub>b</sub>** is the timestep at which the mixture is burned;
- **dt** is the timestep;
- **τ<sub>i</sub>** is the ignition time delay at the timestep **dt**, evaluated as in equation 6.1.1.

It must be noted that the Livengood & Wu integral assumes that the oxidation process during the ignition delay can be described by a single zero-order global reaction and, therefore, the reaction rate does not depend on time under constant thermodynamic

conditions. Moreover, the authors assumed that the autoignition happens when a critical concentration of chain carriers is reached, being this critical concentration constant for a given air-fuel mixture

Based on the equation 6.2.1, the knocking condition should occur when the knock index is equal to 1, no autoignition should occur for values below 1 and the equation loses its meaning for values of the integral above 1. This has been the idea behind the knock prediction methodology that has been developed for the hydrogen engine and that is reported in the next paragraph.

#### 6.4 Knock prediction methodology

The main problem with hydrogen is that there is no empirical model that is available to calculate the ignition delay based on the mixture condition in the combustion chamber. The proposed methodology can be divided in:

1. **Ignition Delay Calculation** of the Air-Hydrogen Mixture under different conditions in terms of Pressure, Temperature and Lambda.
2. **Neural Network Training based on the Ignition Delay data.** The neural network will have unburned gas temperature, in cylinder pressure, lambda and EGR Ratio as an input each crank angle during the combustion simulation giving as an output the value of ignition delay
3. **1D-CFD controller building to** integrate the ignition delay over a user defined window during combustion, and, based on the Livengood and Wu hypothesis, calculate the value of KI each Cycle
4. **Checking of KI value,** if  $KI > 1$  the controller moves the MFB50 to reduce the knock tendency of the engine

To calculate the ignition delay of the mixture an ignition delay map at different temperature, pressure and Lambda (it is also possible to add an EGR Ratio) has been obtained using OD Simulations with CONVERGE. The software is capable to reproduce what ideally has to happen in a rapid compression machine. A constant volume chamber is filled with a Hydrogen-Air mixture at a certain lambda, when the simulation starts the conditions in the chamber are directly initialized to a user imposed value of temperature and pressure [16].

The simulation stops when:

- Autoignition Occurs
- Maximum simulation time (user-defined) is reached if no autoignition occurs

In other words the mixture is kept at a certain value of lambda, pressure and temperature. If the conditions are such that the development of the first pre-reactions starts, the mixture, after a certain time (ignition delay time), ignite spontaneously, otherwise, if the conditions will not lead to ignition, the simulation will finish after a user defined time, in this case 10 seconds. In Figure 22 two examples of the ignition delay extracted from this simulations are reported.

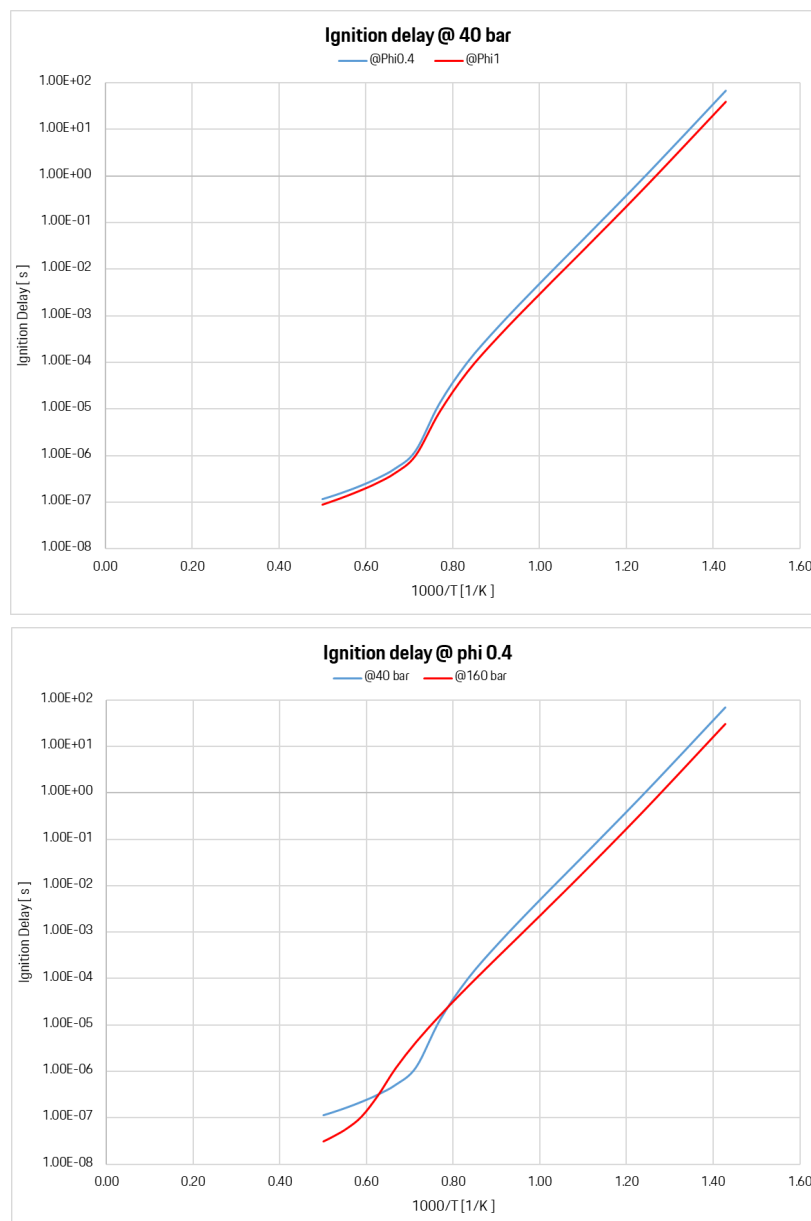


Figure 22 - Example of Ignition Delay from CONVERGE - Top: Constant Pressure - Low: Constant Lambda

Then a DoE approach has been used, calculating the value of ignition delay for a mixture with:

- Temperature between 500K and 1700 K
- Pressure between 40bar and 150 bar
- Lambda between 1 and 5

Obtaining the values of ignition delay for each possible combinations of the temperature, pressure and lambda value. A dataset with about **14849 different combinations** has been extracted and part of this is reported in Figure 23.

#NUM	Pressure	Temperature	Phi fuel oxid	EGR ratio	Phi elem	Time1
0	4.000000e+01	5.000000e+02	3.000000e-01	0.000000e+00	3.000000e-01	9.900000e+01
1	4.000000e+01	6.000000e+02	3.000000e-01	0.000000e+00	3.000000e-01	1.000000e+02
2	4.000000e+01	7.000000e+02	3.000000e-01	0.000000e+00	3.000000e-01	8.305715e+01
3	4.000000e+01	8.000000e+02	3.000000e-01	0.000000e+00	3.000000e-01	1.423459e+00
4	4.000000e+01	9.000000e+02	3.000000e-01	0.000000e+00	3.000000e-01	6.672809e-02
5	4.000000e+01	1.000000e+03	3.000000e-01	0.000000e+00	3.000000e-01	5.924862e-03
6	4.000000e+01	1.100000e+03	3.000000e-01	0.000000e+00	3.000000e-01	7.634797e-04
7	4.000000e+01	1.200000e+03	3.000000e-01	0.000000e+00	3.000000e-01	1.170208e-04
8	4.000000e+01	1.300000e+03	3.000000e-01	0.000000e+00	3.000000e-01	1.526418e-05
9	4.000000e+01	1.400000e+03	3.000000e-01	0.000000e+00	3.000000e-01	1.445505e-06
10	4.000000e+01	1.500000e+03	3.000000e-01	0.000000e+00	3.000000e-01	5.937818e-07
11	4.000000e+01	1.600000e+03	3.000000e-01	0.000000e+00	3.000000e-01	3.625787e-07
12	4.000000e+01	1.700000e+03	3.000000e-01	0.000000e+00	3.000000e-01	2.563725e-07
13	4.000000e+01	1.800000e+03	3.000000e-01	0.000000e+00	3.000000e-01	1.979056e-07
14	4.000000e+01	1.900000e+03	3.000000e-01	0.000000e+00	3.000000e-01	1.612294e-07
15	4.000000e+01	2.000000e+03	3.000000e-01	0.000000e+00	3.000000e-01	1.377150e-07
16	4.500000e+01	5.000000e+02	3.000000e-01	0.000000e+00	3.000000e-01	1.000000e+02
17	4.500000e+01	6.000000e+02	3.000000e-01	0.000000e+00	3.000000e-01	1.000000e+02
18	4.500000e+01	7.000000e+02	3.000000e-01	0.000000e+00	3.000000e-01	7.746197e+01
19	4.500000e+01	8.000000e+02	3.000000e-01	0.000000e+00	3.000000e-01	1.326541e+00
20	4.500000e+01	9.000000e+02	3.000000e-01	0.000000e+00	3.000000e-01	6.232178e-02
21	4.500000e+01	1.000000e+03	3.000000e-01	0.000000e+00	3.000000e-01	5.582144e-03
22	4.500000e+01	1.100000e+03	3.000000e-01	0.000000e+00	3.000000e-01	7.336052e-04
23	4.500000e+01	1.200000e+03	3.000000e-01	0.000000e+00	3.000000e-01	1.170453e-04
24	4.500000e+01	1.300000e+03	3.000000e-01	0.000000e+00	3.000000e-01	1.753126e-05
25	4.500000e+01	1.400000e+03	3.000000e-01	0.000000e+00	3.000000e-01	1.625081e-06
26	4.500000e+01	1.500000e+03	3.000000e-01	0.000000e+00	3.000000e-01	5.709735e-07
27	4.500000e+01	1.600000e+03	3.000000e-01	0.000000e+00	3.000000e-01	3.347646e-07
28	4.500000e+01	1.700000e+03	3.000000e-01	0.000000e+00	3.000000e-01	2.321485e-07
29	4.500000e+01	1.800000e+03	3.000000e-01	0.000000e+00	3.000000e-01	1.766384e-07
30	4.500000e+01	1.900000e+03	3.000000e-01	0.000000e+00	3.000000e-01	1.427132e-07
31	4.500000e+01	2.000000e+03	3.000000e-01	0.000000e+00	3.000000e-01	1.208926e-07
32	5.000000e+01	5.000000e+02	3.000000e-01	0.000000e+00	3.000000e-01	1.000000e+02
33	5.000000e+01	6.000000e+02	3.000000e-01	0.000000e+00	3.000000e-01	1.000000e+02
34	5.000000e+01	7.000000e+02	3.000000e-01	0.000000e+00	3.000000e-01	7.267592e+01
35	5.000000e+01	8.000000e+02	3.000000e-01	0.000000e+00	3.000000e-01	1.245404e+00
36	5.000000e+01	9.000000e+02	3.000000e-01	0.000000e+00	3.000000e-01	5.861223e-02
37	5.000000e+01	1.000000e+03	3.000000e-01	0.000000e+00	3.000000e-01	5.286793e-03
38	5.000000e+01	1.100000e+03	3.000000e-01	0.000000e+00	3.000000e-01	7.059038e-04
39	5.000000e+01	1.200000e+03	3.000000e-01	0.000000e+00	3.000000e-01	1.161713e-04
40	5.000000e+01	1.300000e+03	3.000000e-01	0.000000e+00	3.000000e-01	1.806363e-05
41	5.000000e+01	1.400000e+03	3.000000e-01	0.000000e+00	3.000000e-01	1.920921e-06
42	5.000000e+01	1.500000e+03	3.000000e-01	0.000000e+00	3.000000e-01	5.591134e-07
43	5.000000e+01	1.600000e+03	3.000000e-01	0.000000e+00	3.000000e-01	3.134470e-07
44	5.000000e+01	1.700000e+03	3.000000e-01	0.000000e+00	3.000000e-01	2.134130e-07

Figure 23 - Dataset from ignition delay calculation

At this point this dataset has been used as a training dataset of a Neural Network. Different training algorithm has been tested but the one which leads to a minimum error is a 30 Neurons Feed Forward Algorithm. The training has been performed in GT-Power which gives the possibility to generate a .nno file to be used in a Neural Network Object. By giving to this object the value of temperature, pressure and lambda of the mixture as inputs, the corresponding value of ignition delay will be calculated very fast.

Now the idea was to give to the neural network in the 1D model the value of unburned gas temperature, In-Cylinder pressure and mixture's lambda each crank angle in order to calculate the corresponding ignition delay. Then the ignition delay will be used in an integrator in order to calculate the KI, according to the Livengood and Wu hypothesis. The integration has been performed on a user defined window that starts 70 CADeg before

the TDC firing and end as soon as the 98% of mass fuel burned is reached, considering that in this case a knock occurrence will not be dangerous.

In this way if, during a cycle, the value of the calculated  $KI > 1$  (knock occurrence) the controller moves the combustion MFB50 until the value of becomes less or equal to 1.

In conclusion it must be pointed out that in this particular case the engine has the so called "Twisted Camshaft" that is used to solve the issue related to the blowdown interference of a V8 Crossplane Crankshaft (see [12]). Unfortunately this solution lead to big cylinder-to-cylinder variations in terms of volumetric efficiency and knock tendency must be evaluated for each single cylinder. For this reason a 1D-CFD controller has been developed, evaluating the Knock Index (KI) for each cylinder and then moving the MFB50 of all the 8 cylinders considering only the worst KI within them.

## 6.4 Maximum In-Cylinder pressure control

As previously discussed, hydrogen engines can reach very high In-Cylinder pressures, mainly because of the H<sub>2</sub> fast combustion, high knock resistance and the high lambda value adopted. Therefore it is possible that under certain conditions the limiting factor for the combustion it is not the knock occurrence but a too high In-Cylinder pressure that can damage the piston assembly. For this reason, the knock controller has been combined with a maximum In-Cylinder pressure control. A PID controller moves the MFB50 taking into account not only the value of KI but the more dangerous condition between knock occurrence and maximum In-Cylinder pressure. If the value of KI < 1 and the In-Cylinder pressure overcomes the imposed limit of 210 bar, the MFB50 will be shifted forward to reduce the pressure under that limit.

In Figure 24 it is reported a comparison between an In-Cylinder pressure trace of the stock gasoline engine and the Hydrogen version which is, as discussed, limited to 210 bar.

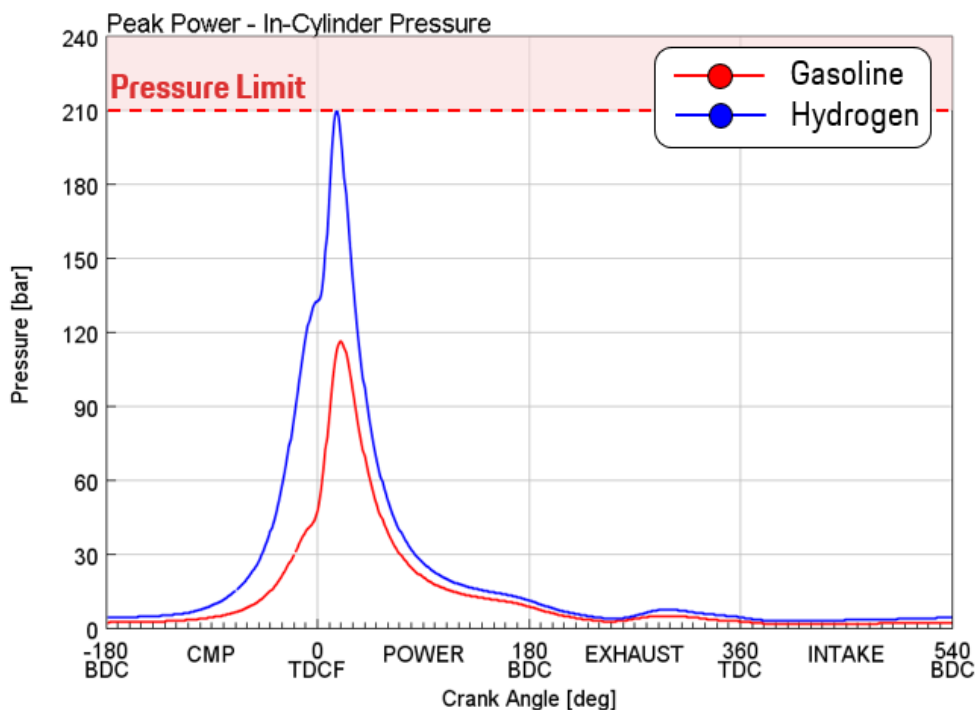


Figure 24 - In-Cylinder Pressure Comparison

## 6.5 Hydrogen Flame Speed Prediction Methodology

The last methodology that has been developed is to calculate the hydrogen flame speed that has to be used in order to estimate the combustion duration under different conditions. The combustion is simulated with a Wiebe model where the burn rate profile is calculated by imposing the MFB50 and the combustion duration.

However hydrogen has a laminar flame speed much higher than gasoline, about 5–6 times faster at same lambda, as reported in the comparison below (Figure 25), and for this reason a correct estimation of the combustion duration it is crucial to have realistic results from the model.

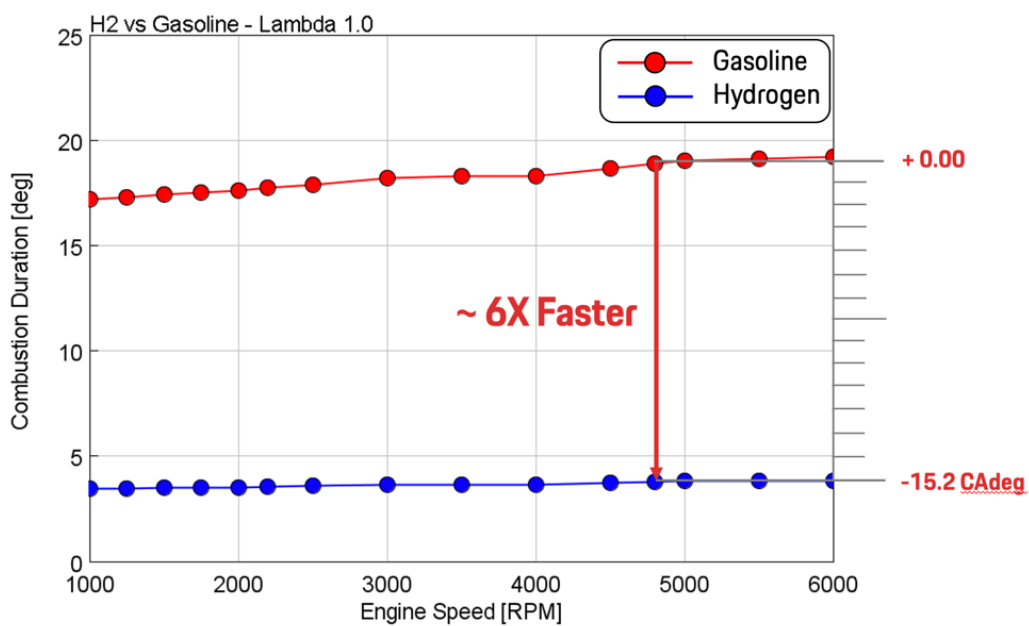


Figure 25 - Combustion Speed Comparison

Thus, the burn duration has been estimated in the following way. First, the burn duration of the gasoline reference engine was available and also the value of lambda of each engine operative point. Then, during the simulation, a correction factor has been calculated dividing the laminar flame speed of hydrogen, at the desired lambda, with the laminar flame speed of gasoline at the value of lambda (stored in a look-up table) of the considered engine operative point. In conclusion this correction factor has been used to scale the burn duration of the gasoline engine, in that specific operative point, obtaining the corresponding value of Hydrogen Burn Duration.

The methodology is summarized in Figure 26 below:

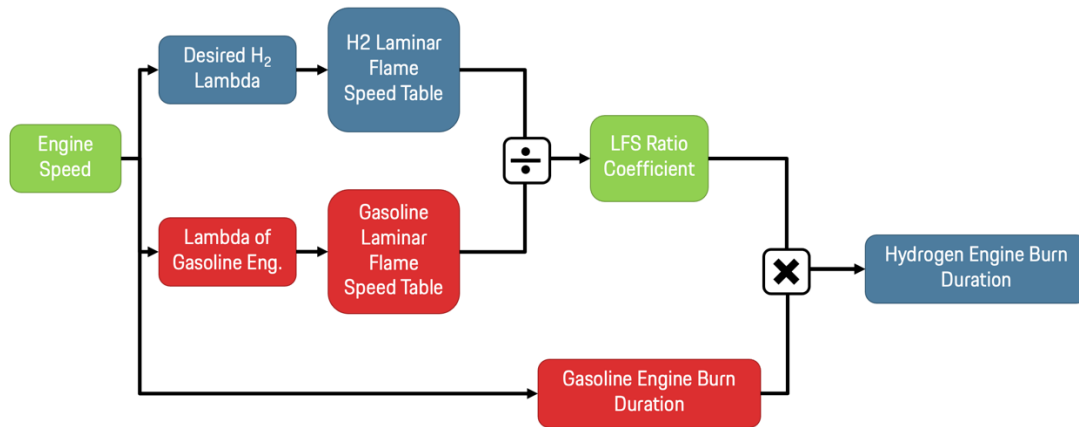


Figure 26 – Burn Duration Estimation Methodology

Of course the hypothesis that has been made is that the effect of turbulence on the laminar flame speed was comparable for both the Hydrogen Engine and the Gasoline one. This hypothesis could not be so distant from what really happens because the increased air flow of the hydrogen engine can be compensated to the high level of boost that will be used.

## 7. Turbocharger solution

One of the main changes that has been done to the gasoline engine to be converted into an Hydrogen version is the turbo system layout. The main challenge in this case is related to the high Air flow Rate that must be provided to have a value of  $\lambda > 2.3/2.4$ , as reported in the chapter 4, thus reducing the temperatures in the combustion chamber and so avoiding NOx emissions. A comparison between the Air Flow of the gasoline engine and the final hydrogen version is reported in Figure 27:

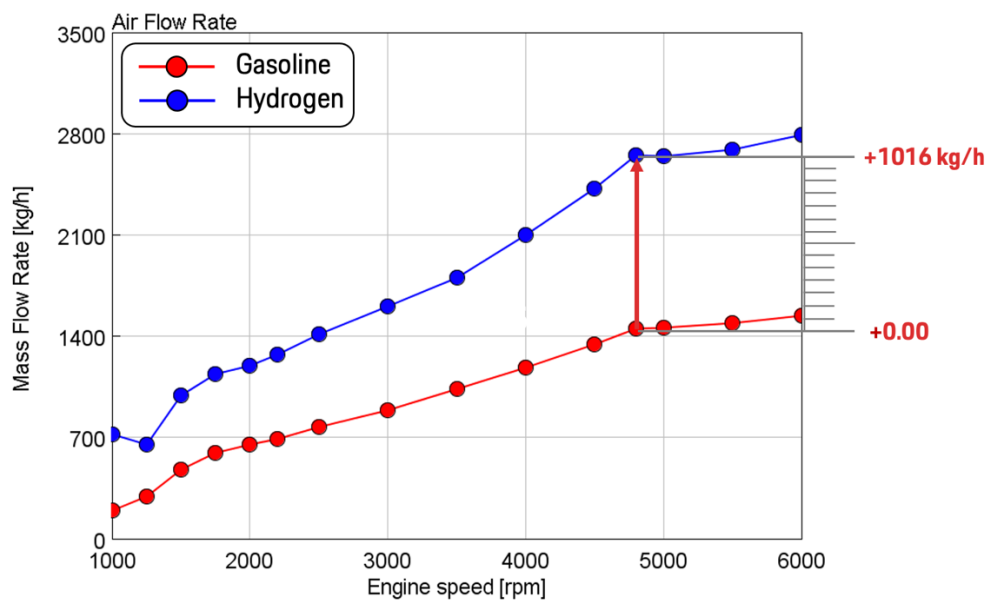


Figure 27 - Air Flow Rate Comparison

To guarantee this high Air flow rate a high compressor pressure ratio both in low end torque and peak power must be adopted like reported in the Figure 28:

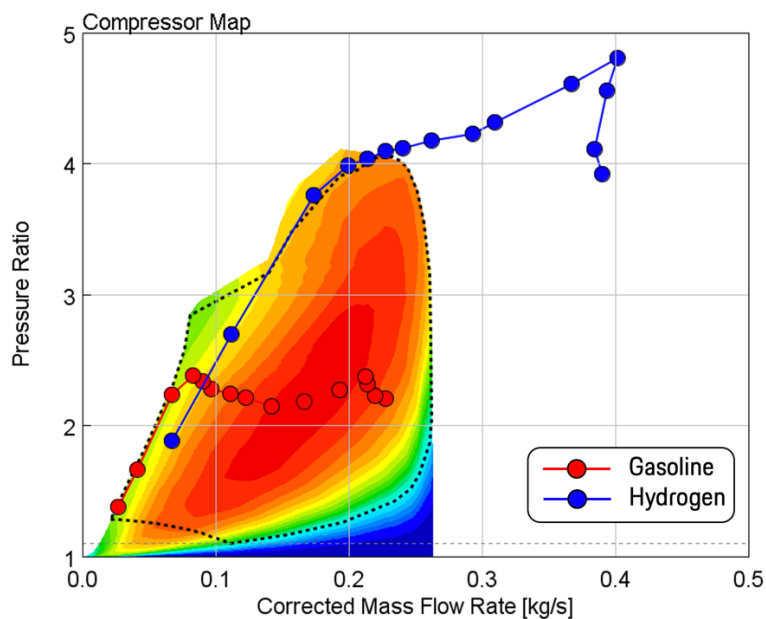


Figure 28 - Compressor Pressure Ratio Comparison

Moreover this High Compressor pressure ratio must be realized considering a low turbine inlet energy available in the hydrogen engine caused by the hydrogen fast combustion and High knock resistance as previously discussed. In Figure 29 a comparison between the turbine inlet temperature of the gasoline and hydrogen engines is reported. At peak power the turbine inlet temperature of the hydrogen engine is about 400°C lower than the gasoline one, resulting in a low energy available to extract useful power with the turbine to move the compressor.

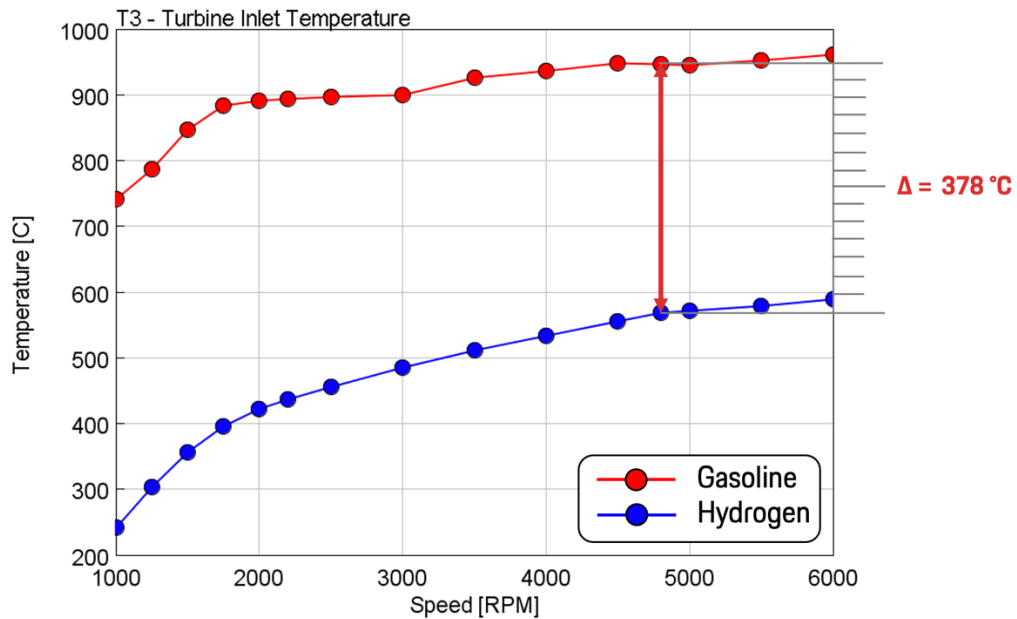


Figure 29 - Turbine Inlet Temperature Comparison

From this analysis is clear how an advanced turbo system layout is required. Different solutions have been tested with 1D simulations on GT power. In the following parts each solution will be briefly discussed and only the selected one will be analyzed in detail.

## 7.1 Single Stage Compression : Bi-Turbo and Inlet Guided Vanes

The first solution that has been tested has the lambda one version has a base but it has no after-treatment system (that is one of the goals of the work), bigger compressors (Figure 32) and Inlet Guided Vanes. The engine scheme is reported in the Figure 30:

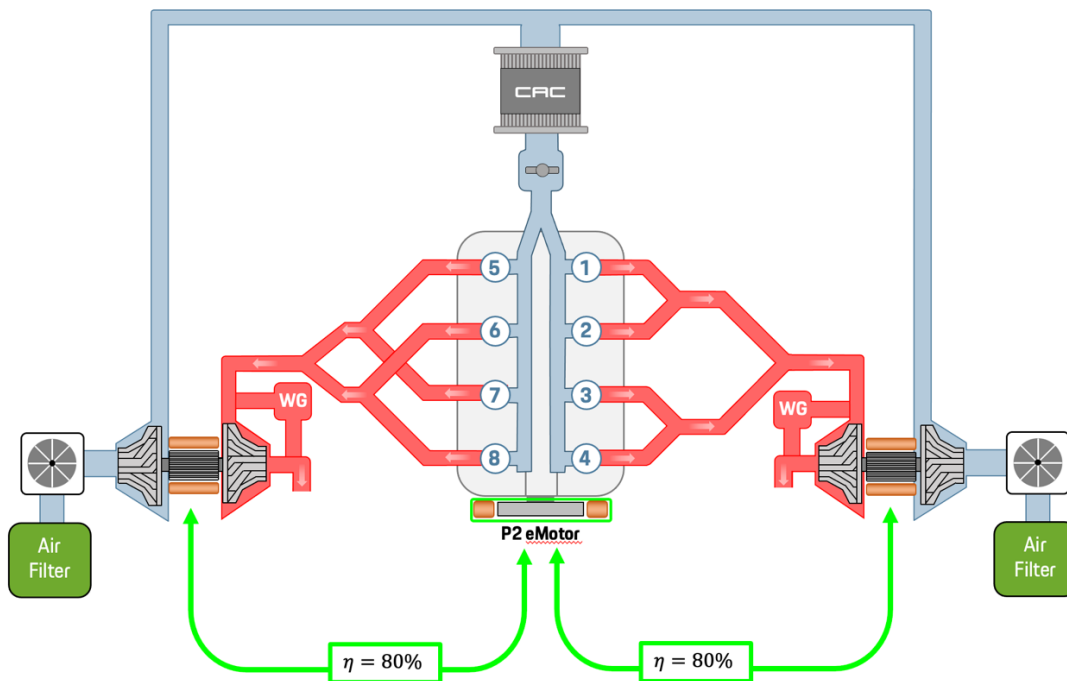


Figure 30 – Bi-Turbo and IGV Engine Scheme

The Inlet Guided Vanes (IGV) are a technology currently used in Formula 1 and consist in different moving blades mounted at the compressor inlet as shown in the Figure 31.



Figure 31 - Inlet Guided Vanes - IGV

These blades are used to scale the compressor map, as shown in Figure 32, and to gain some performances in the low end torque zone of the engine.

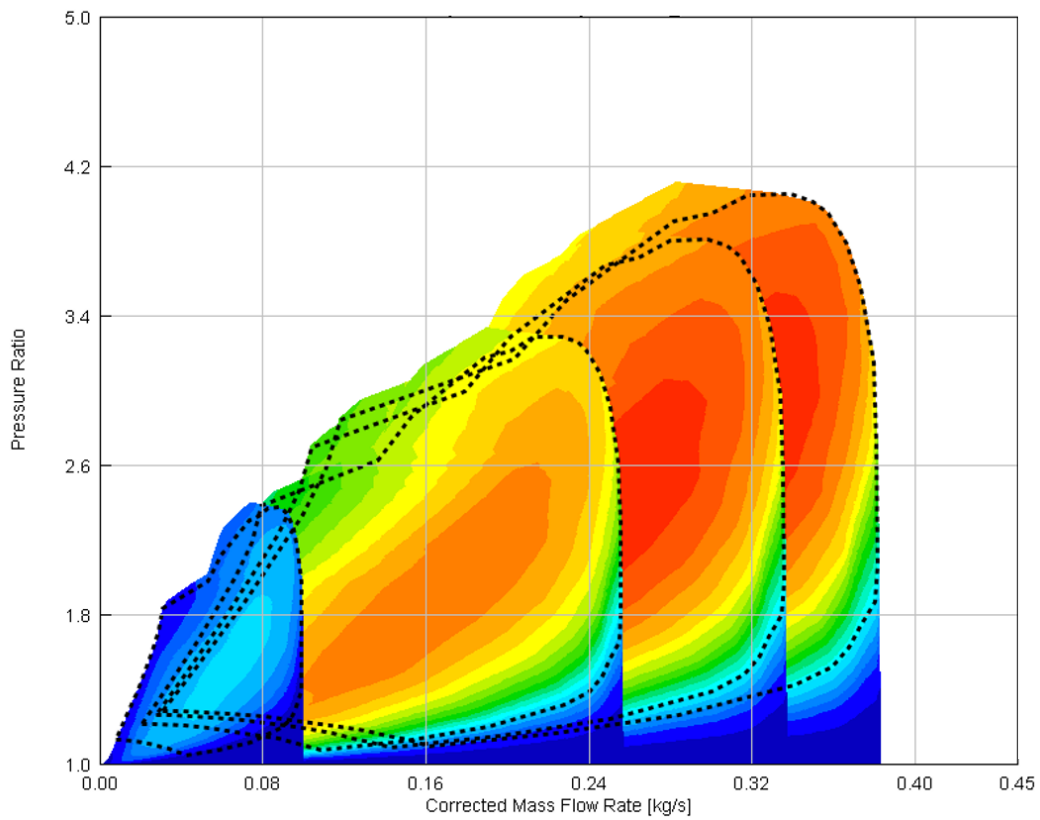


Figure 32 - IGV Compressor Map Scaling

However this solution was feasible until a lambda value of 2.2/2.3 and to further increase the air flow a two stage of compression solution is required.

## 7.2 Two Stage Compression : Lancia Delta S4 Twincharger Inspired

The first twin stage solution that has been tested is inspired to the famous Lancia Delta S4 Twincharger engine (Figure 33) where an additional supercharger is used to further compress the air.

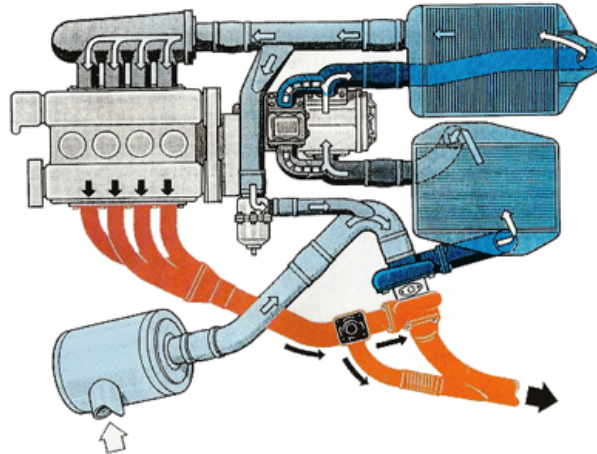


Figure 33- Lancia Delta S4 Engine Scheme

In this case the supercharger is moved from an additional eMachine and a valve system is present to exclude it when it is not needed. The engine scheme is reported in Figure 34:

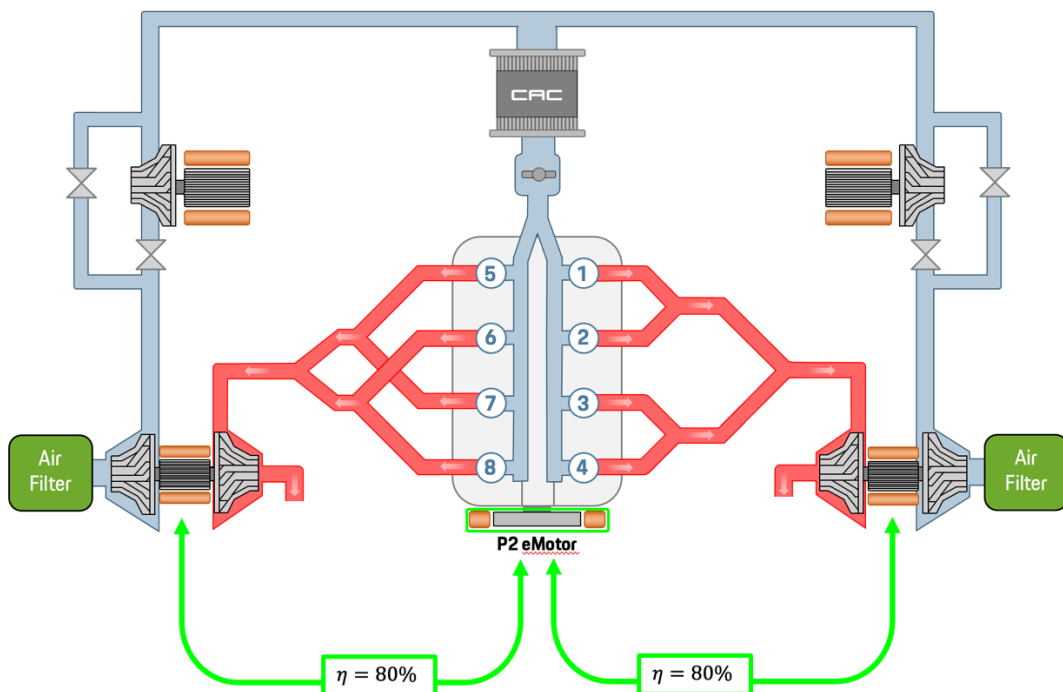


Figure 34 - Lancia Delta S4 Inspired Engine Scheme

This solution showed good results but it implies not a good packaging and two additional eMachines with a complex energy management strategy. The valve system must be also added and finely controlled. For these reasons this solution was not further investigated.

### 7.3 Parallel Compression : Bugatti Chiron Inspired

A parallel compression configuration has been also investigated and the turbo layout is inspired to the Bugatti Chiron Quad-Turbo Engine that is reported in Figure 35.



Figure 35 - Bugatti Chiron Turbo Engine

In this case two compressors work in parallel, the first is linked to the turbine by a turboshaft connected to a first eTurbo, the second one is moved from an additional eMachine. A complex valve system has been used to manage the transition between the Bi-Turbo configuration (low regimes) and the Quad-turbo one (High Regimes). The engine scheme is reported in Figure 36:

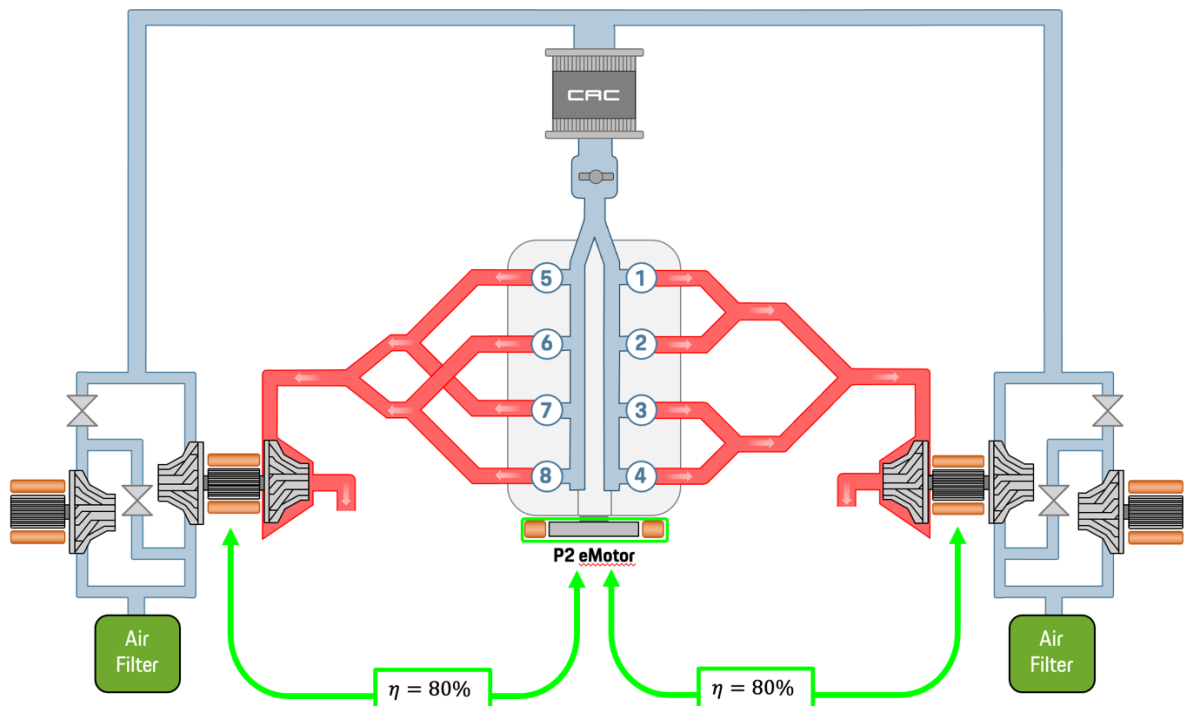


Figure 36 - Bugatti Chiron Inspired Engine Scheme

This solution presents the same critical aspect and disadvantages of the two-stage solution discussed in the paragraph before. The packaging is complex and two additional eMachines are needed with a complex energy management strategy. Furthermore, a complex valve system must be used and the transition strategy must be carefully managed. Also this solution was not be selected because the selected one is reported in the next chapter.

## 7.4 Two Stage Intercooled Compression with Back-to-Back Compressors

This solution is inspired to the SC-VNT Garrett Turbo (Patent number EP 3 249 234 B1) whose scheme is reported in Figure 37.

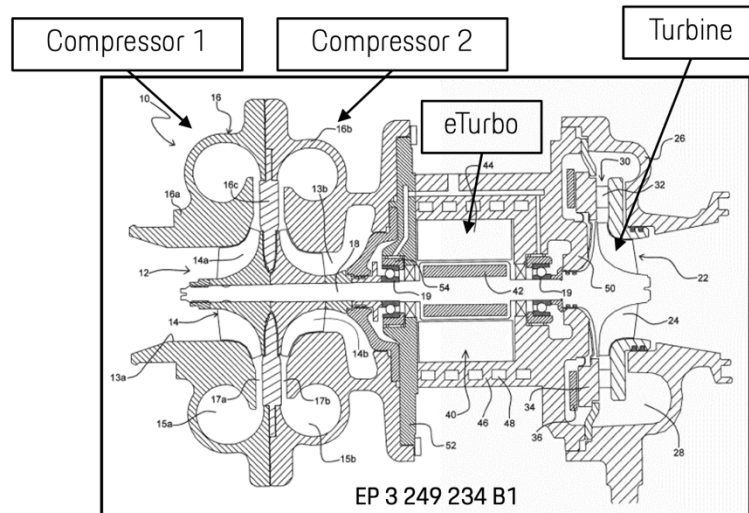


Figure 37 - SC-VNT Garrett Turbo

In this case there are two stage of intercooled compression realized by two compressors mounted back to back on the same shaft of the turbine and the eTurbo. In between the two compressors there is an intercooler used to cool down the charge after the first compression thus minimizing the overall compressor work and reducing the maximum temperature reached during the compression. The engine scheme is reported in Figure 38. (The engine that features this layout will be called the **H64 Engine** from now on.)

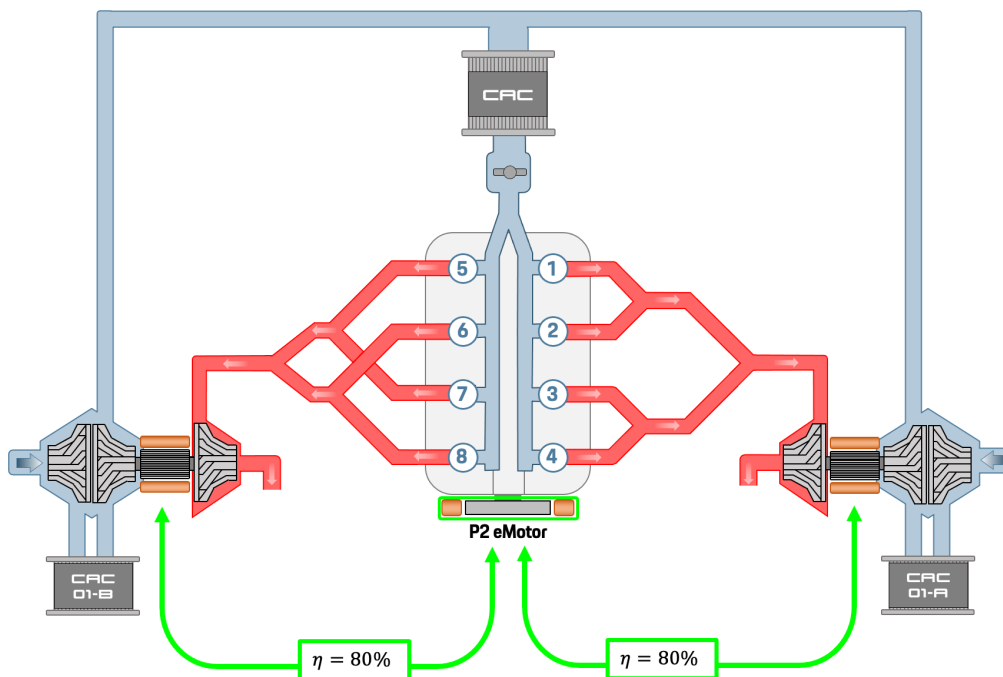


Figure 38 - Back-To-Back Turbo Engine Scheme

In this case the advantages are different. First, this solution has a good packaging and the intercooler gives many advantages like:

- An High level of boost can be realized using just one eTurbo each bank. This is related to the lower compression work required for an intercooled compression compared to a non-intercooled one, like it is shown in Figure 39, below.

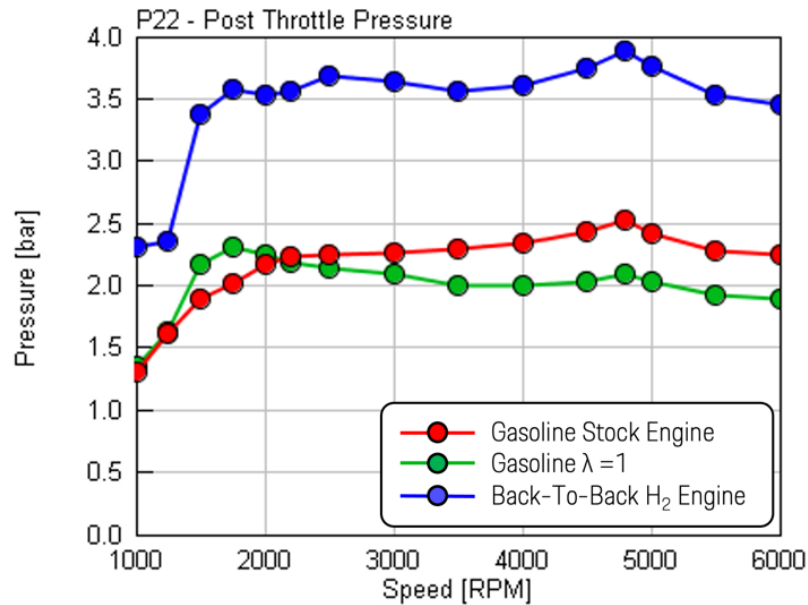


Figure 39 - Boost Pressure Comparison

- A maximum temperature reached during the compressions and in the intake manifold that is comparable with the gasoline engine as shown in Figure 40. This, for example, make possible to avoid to use a Titanium Alloy for the compressor wheels.

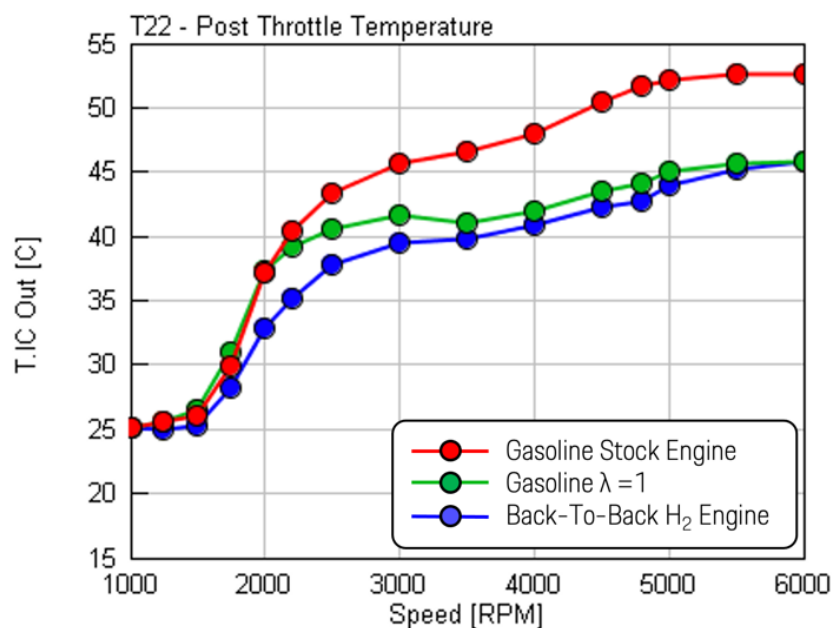


Figure 40 - Intake Manifold Temperature Comparison

It is possible to minimize the compressor work in an intercooled compressor by selecting the right compressor pressure ratio  $\beta$  realized by each compressors, or, in other words, by carefully dividing the total pressure ratio beta in a smart way. From the equation [7.4.1] of the compression work :

$$l_c = l^I + l^II = \frac{\gamma}{\gamma - 1} \cdot R \cdot \left[ T_1 \cdot \left( \beta_1^{\frac{\gamma-1}{\gamma}} - 1 \right) + T_{2'} \cdot \left( \beta_2^{\frac{\gamma-1}{\gamma}} - 1 \right) \right] \quad [7.4.1]$$

The compressor pressure ratio that minimize the compressor work can be calculated by :

$$\frac{\partial(l_c)}{\partial\beta_1} = 0 \rightarrow \beta_1 = \left( \frac{T_{2'}}{T_1} \right)^{\frac{\gamma}{2(\gamma-1)}} \cdot \sqrt{\beta} = SF \cdot \sqrt{\beta} \quad [7.4.2]$$

With :  $\beta_1 = \frac{p_2}{p_1}$ ;  $\beta_2 = \frac{p_3}{p_2}$ ;  $\beta = \frac{p_3}{p_1}$ .

In an intercooled compression where the temperature after the intercooler is the same of the one at the inlet of the first compressor the relation becomes:

$$SF = 1 \rightarrow \beta_1 = \beta_2 = \sqrt{\beta} \quad [7.4.3]$$

The compressor pressure ratio is linked to the compressor's tip speed that is proportional to the compressor diameter. To minimize the compression work at Full Load, so to minimize the power provided from the eTurbo in the worst case, the two compressor must be dimensioned considering the optimal ratio between B1 and B2 from 7.4.2. Of course a perfect dimensioning in each condition is impossible but in this way it is possible to have an indication of the possible best dimensioning and then, using a DoE approach, find the perfect trade off. This is what has been done in this case and the resulting dimensions are reported in Table 5 with a comparison with the stock and lambda one version specifications.

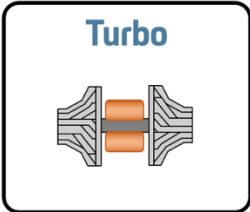
	Stock	$\lambda = 1$	H64	
 <p><b>Turbo</b></p>	Compressor	56 mm	58 mm	76 /60 mm
	Turbine	50 mm	60 mm	62mm
	WG	Control	Closed	Closed
	E-Turbo	-	10kW	16kW
 <p><b>Engine</b></p>	Ignition	Standard	TJI	Standard
	CR	9.5	10.5	11
	Lim. Press	-	-	210 bar

Table 5 - Stock Engine, Lambda 1 Version and H64 Specs

## 8. Performances

In this chapter, Full Load and Part Load Performances of the H64 Engine will be investigated.

### 8.1 Full Load Performances

In Figure 41 are reported the full load performances of the hydrogen version. The H64 engine concept has the same full load performances of the gasoline versions with about 5% more efficiency at peak power and a maximum efficiency of 42%. The energy from the P2 machine to the eTurbo is entirely used for boosting, no energy recover is possible.

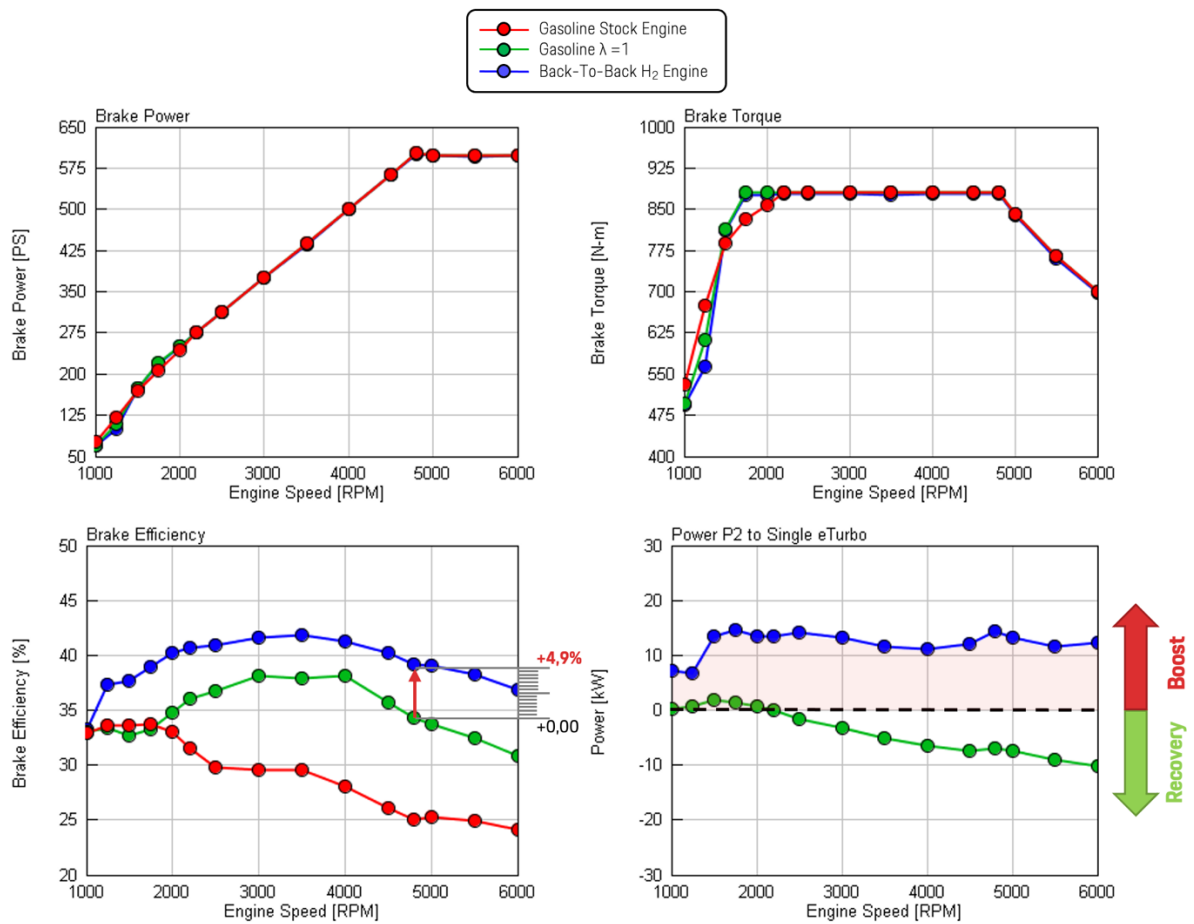


Figure 41 - Full Load Performances Comparison - Power, Torque, Efficiency and P2 Power

From Figure 42 it can be noticed that energy recovery cannot be done at full load because the boost pressure to be reached is really high (compared to gasoline) and the turbine cannot provide much power to the compressors because of the low temperature, and so energy, available at its inlet. It can be also noticed how the intake manifold temperature (top right) is comparable with the one of the gasoline engine and how the maximum In-Cylinder pressure is limited under 210 bar at full load (bottom left).

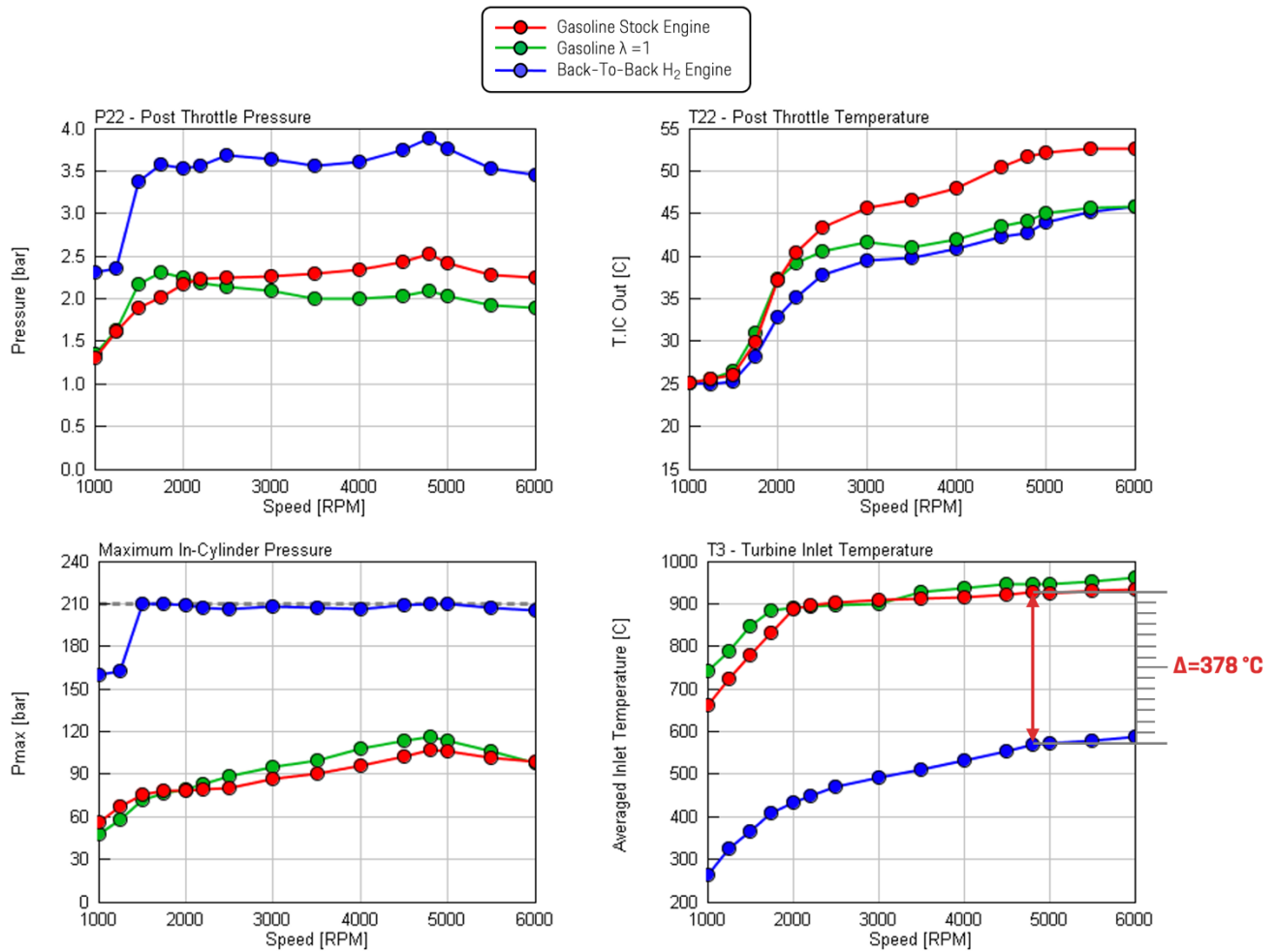


Figure 42 - Full Load Performances Comparison - P22, T22, PMax and T3

In Figure 43 the Engine-Out Emissions are reported. Although the hydrogen version has no aftertreatment system it has no HC and CO emissions, and Ultra Low NOx Emissions. As a reference the Euro 6 limit for Heavy Duty Engines tested on stationary tests is reported.

The H64 as a NOx emission level under that limit for the whole full load without an After-Treatment System.

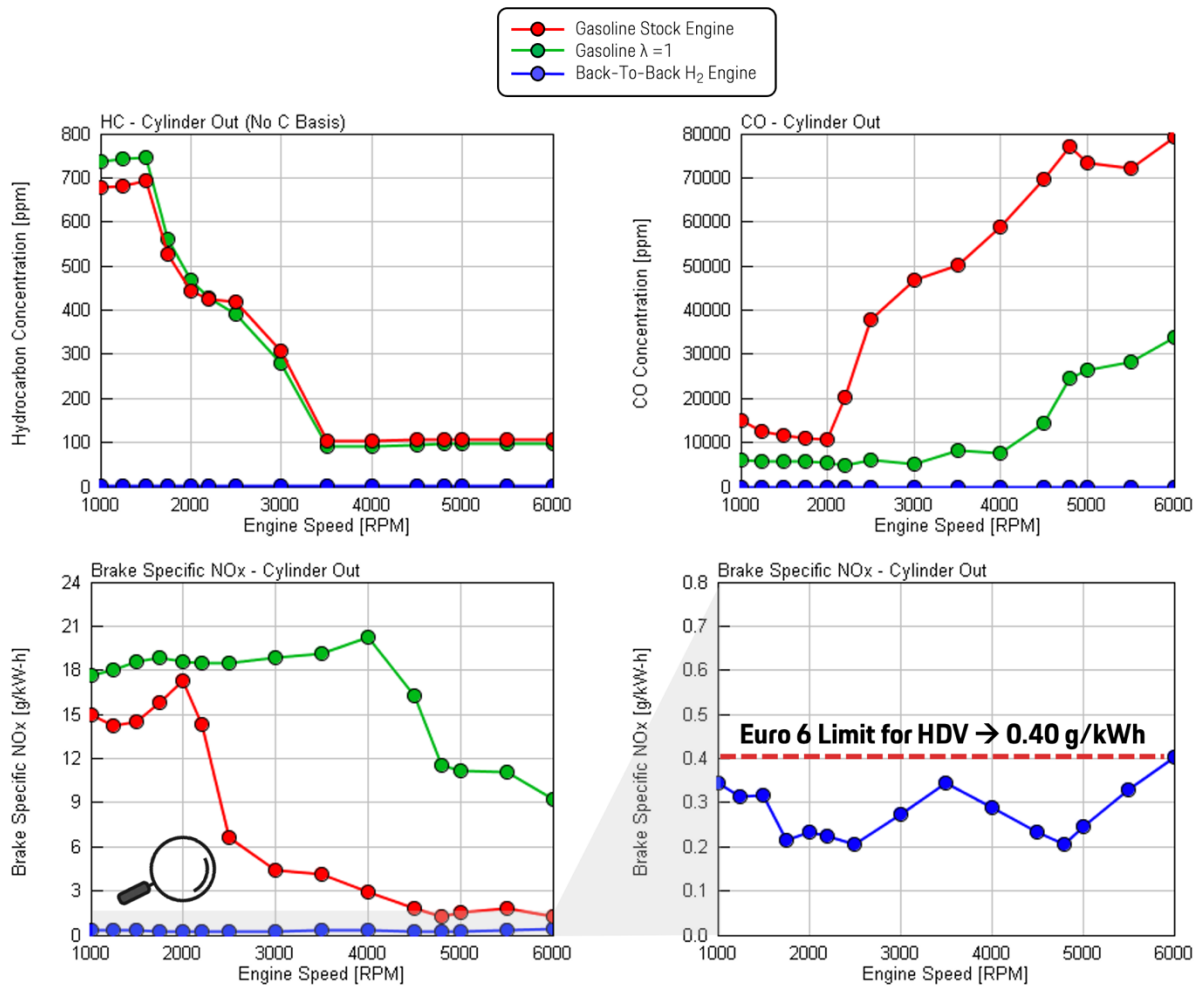


Figure 43 - Full Load Performances - Engine-Out Emission Comparison

## 8.2 Part Load Performances

Part load has been also investigated and it has been realized by reducing the power provided from the P2 electric machine to the eTurbo, thus reducing the boost. The power provided from the P2 machine to the eTurbo for the whole engine map is reported in Figure 44:

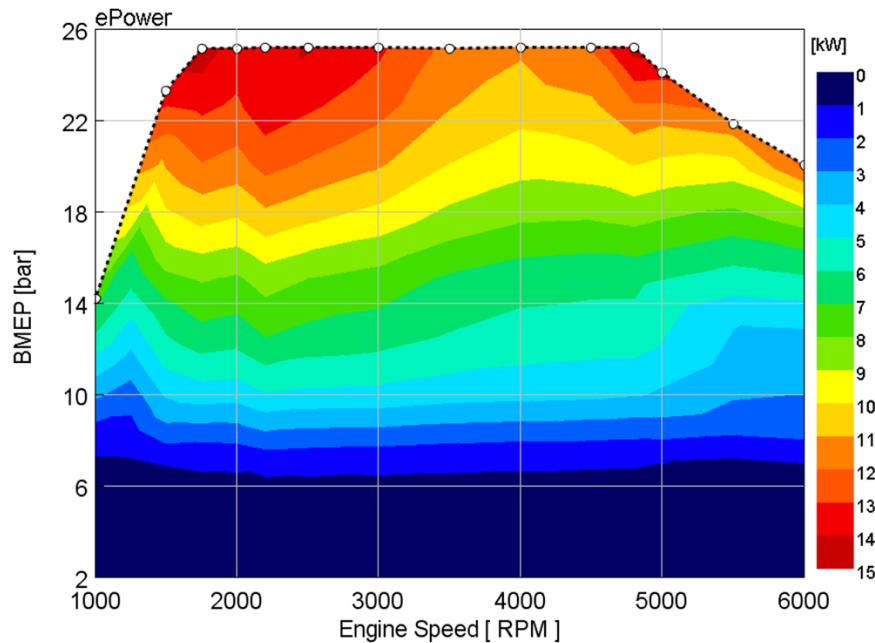


Figure 44 - Power from P2 eMachine to eTurbo

From Figure 45 it can be also noticed how, as soon as the power to help the turbine to move the compressor is zero, to further reduce the load the Throttle Valve has been used. There is a wide zone of the engine map where the Throttle Valve is wide open, and only for really low loads it starts to be used.

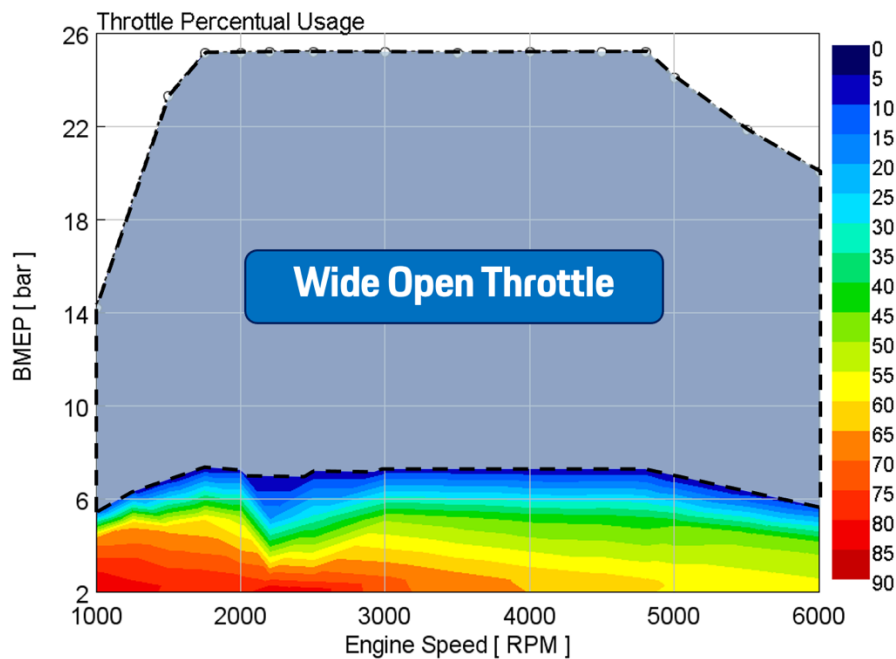


Figure 45 - Throttle Position

At the same time, lambda value has been increased to further reduce the maximum temperature in the combustion chamber and so the NOx production. This is possible thanks to the wide flammability limits of hydrogen, as shown in Figure 46.

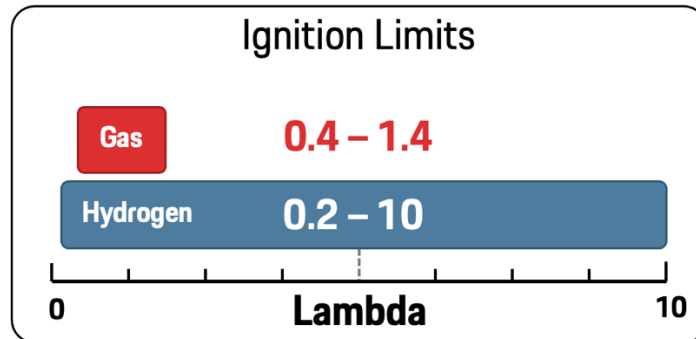


Figure 46 - Ignition Limits: Hydrogen vs Gasoline

However, according from literature data regarding hydrogen engines, a value of lambda between 2.2 at full load and 3.1 at part load has been used, as shown in Figure 47.

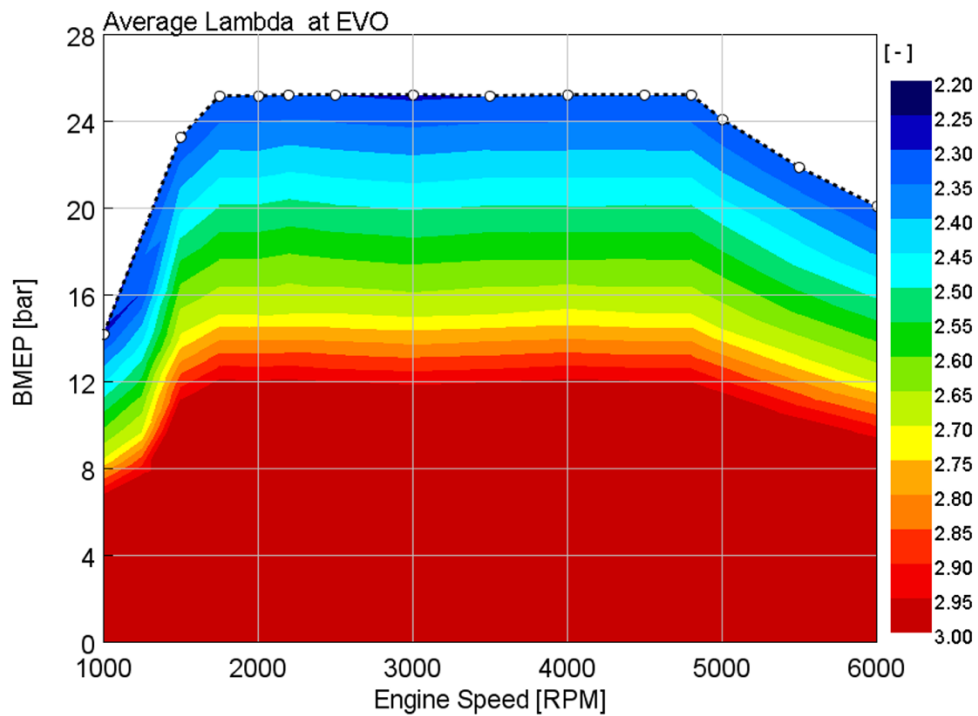


Figure 47 - Full Engine Map Average Lambda

Full Map data are reported in the Figure 48 and Figure 49.

Close to zero NOx emission for most of the engine map can be observed from the top left diagram in figure 48, this thanks to the lean combustion and so the lower temperatures reached in the combustion chamber. Moreover from the brake efficiency diagram (bottom left) it can be noticed a wide high efficiency zone, with an average value of about 42%. This is related to the limited usage of the throttle valve, as shown in the Part Load Strategy, that leads to reduced pumping losses and so higher efficiencies.

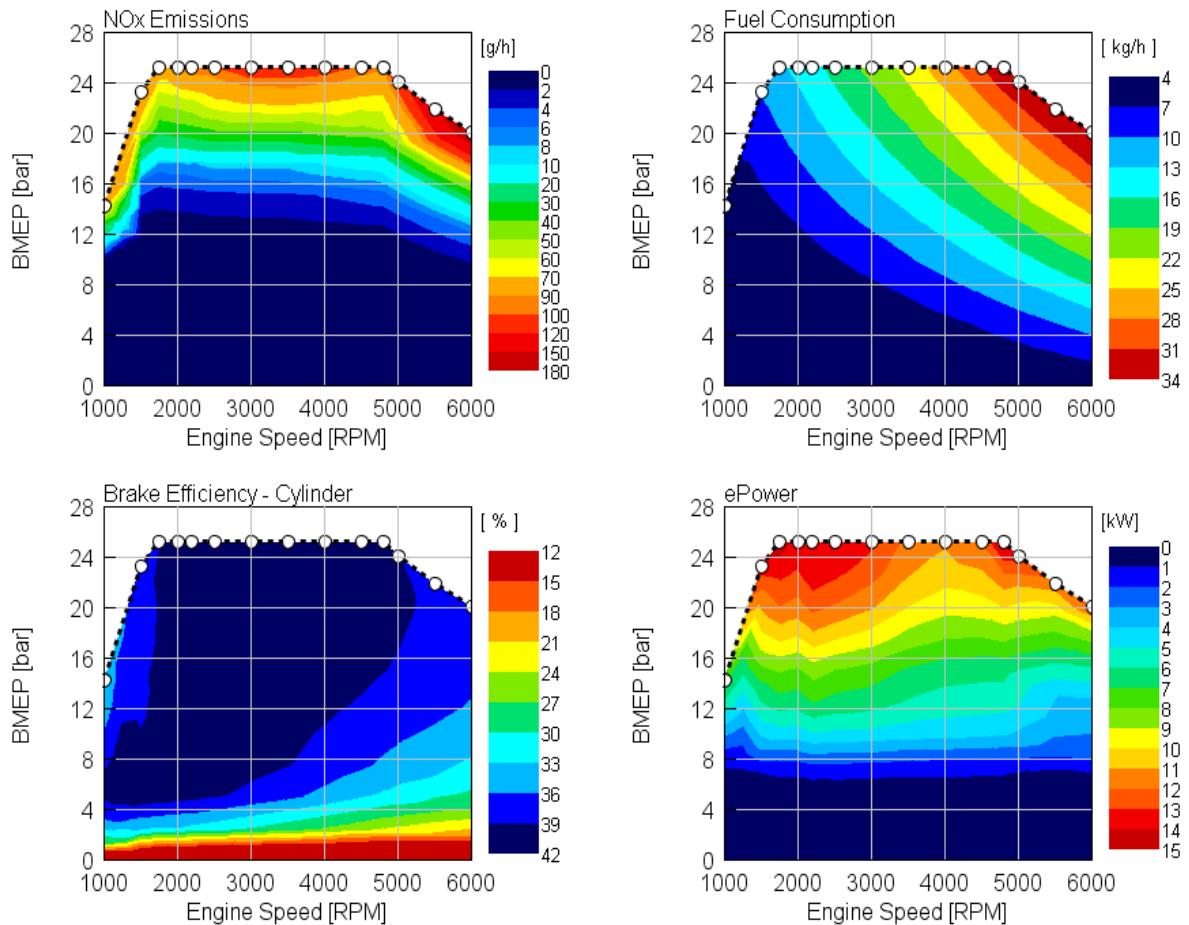


Figure 48 - H64 Engine - Full Map Data: NOx, Fuel Consumption, Efficiency and Power from P2

In the bottom right diagram the power provided from the P2 eMachine to the eTurbo is reported, in the top right, instead, it is reported the fuel consumption map that will be used for the driving cycle simulation in chapter 9.

In Figure 49, other interesting Full Map Data are reported.

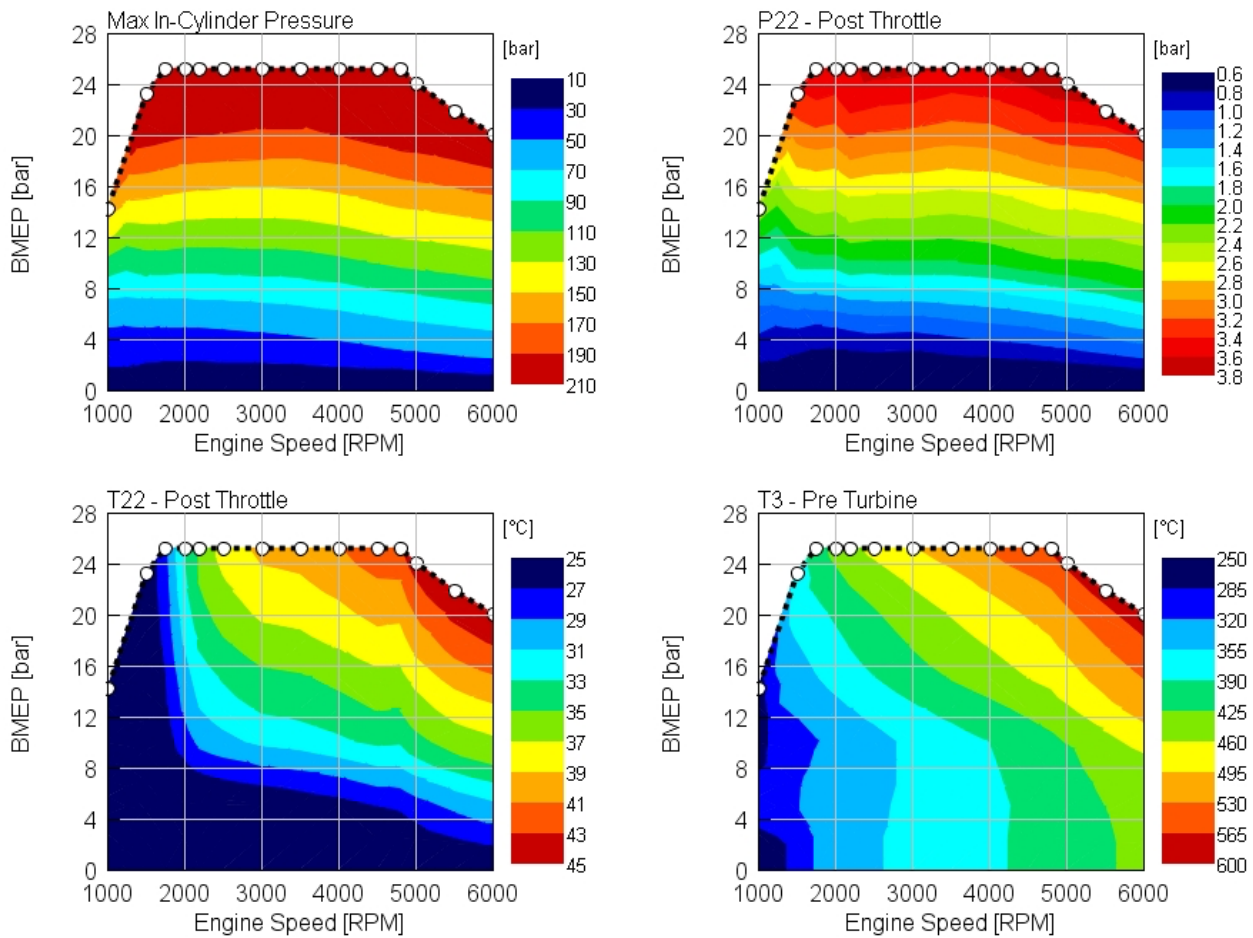


Figure 49 - H64 Engine - Full Map Data: Max In-Cylinder Pressure, P22, T22 and T3

In the top left diagram the maximum In-Cylinder pressure is reported, again it can be noticed how its value has been limited under 210 bar at full load to avoid possible damages. The maximum boost pressure is 3.8, much higher than a traditional high performance turbocharged gasoline engine and it must be reached considering a very poor turbine inlet temperature (and so energy), as shown in the picture bottom right.

In conclusion, in the bottom left diagram is reported the temperature inside the intake manifold and it is clear how the intercooled compression allows to reach high levels of boost pressure keeping the maximum temperature in a range comparable with a traditional high performance turbocharged gasoline engine (considering that the same intercooler has been used).

## 9. Driving Cycles

With the full engine map available from the stationary simulation, it is possible to build up a methodology to test the engine, mounted on a vehicle, performing driving cycle simulations. The selected driving cycle for emissions and fuel consumption calculation is the WLTC : Worldwide Harmonized Light-Duty Vehicles Test Cycle.

The Worldwide harmonized Light-Duty Vehicles Test Cycles (WLTC) are chassis dynamometer tests for the determination of emissions and fuel consumption from light-duty vehicles. The tests have been developed by the UN ECE GRPE (Working Party on Pollution and Energy) group. The WLTP replaces the European NEDC based procedure for type approval testing of light-duty vehicles with the transition from NEDC to WLTP occurring over 2017-2019. The WLTP procedures includes several WLTC test cycles applicable to vehicle categories of different power-to-mass (PMR) ratio as reported in Table 6. The PMR parameter is defined as the ratio of:

$$PMR = \frac{\text{Rated Power [W]}}{\text{Curb Mass [kg]}} \quad [9.1]$$

The curb mass (or kerb mass) means the “unladen mass”, not including the driver, as defined in ECE R83. However, EU regulations appear inconsistent with GTR 15 and replace the curb mass with “mass in running order”, which includes the driver and is 75 kg higher [18]. The cycle definitions may also depend on the maximum speed ( $v_{max}$ ), which is the maximum speed of the vehicle as declared by the manufacturer and not any use restriction or safety based limitation. Cycle modifications are allowed to accommodate drivability problems for vehicles with power to mass ratios close to the borderlines or with maximum speeds limited to values below the maximum speed required by the cycle.

WLTC Test Cycles			
Category	PMR [W/kg]	Vmax	Speed Phase Sequence
Class 3b	> 34	≥ 120	Low 3 + Medium 3-2 + High 3-2 + Extra High 3
Class 3a		< 120	Low 3 + Medium 3-1 + High 3-1 + Extra High 3
Class 2	34 ≥ PMR > 22	-	Low 2 + Medium 2 + High 2 + Extra High 2
Class 1	≤ 22	-	Low 1 + Medium 1 + Low 1

Table 6 - WLTC Test Cycles



## 9.1 Driving Cycle simulation methodology

The simulation of the driving cycles is performed using a numerical model based on a simplified kinematic approach thanks to which it is possible to obtain, instant by instant, the operating conditions in terms of average effective pressure (bmep) and engine revolutions. Once the engine operating points have been obtained, it is possible to refer to a consumption map, valid in stationary operating conditions, to calculate both emissions and specific fuel consumption.

The selected vehicle to test on the driving cycle with the H64 engine is the **Aurus Senat**. In the Tables 7-8-9 the main data regarding the vehicle are reported. It can be noticed how heavy the vehicle is and how much power it absorbs at 100 km/h considering that, as a reference value, the Porsche 911 absorbs 16kW-17kW depending on the rear wing position.



Figure 52 - Aurus Senat

<b>Aurus Senat - Vehicle Data for WLTC</b>		
Mass	[kg]	2650
Absorbed Power @ 100 km/h	[kW]	26.0

Table 7 - Aurus Senat Vehicle Data

<b>Transmission Data</b>	
Transmission Efficiency (Constant)	0.944
Final Ratio	4.083

Table 8 - Aurus Senat Transmission Parameters

<b>Engine and Wheels Data</b>		
Displacement	[dm <sup>3</sup> ]	4.4
Wheels Inertia	[kg · m <sup>2</sup> ]	2.7794
Wheel Radius	[mm]	397.25
Engine Inertia	[kg · m <sup>2</sup> ]	0.183
Idle Engine Speed	[rpm]	1000
Idle Fuel Consumption	[kg/h]	0.438
Fuel Density @700bar	[g/l]	42

Table 9 - Aurus Senat - Engine and Wheels Data

## 9.2 Kinematic Model

The kinematic approach to obtain the operating characteristics of an internal combustion engine is based on a 'backwards method'. It consists in tracing the kinematic chain that links the movement of the wheels to the one of the engine in order to calculate the angular speed and the operating conditions at each instant during the homologation cycle. It is assumed that the vehicle is able to exactly follow the target speed profile of the driving cycle, eliminating the possible source of variability introduced by the driver.

The relationship that allows to link the vehicle speed to the engine rotational speed is the following:

$$n \text{ [rpm]} = \frac{V \cdot 30}{\pi \cdot R_0} \cdot \tau_p \cdot \tau_{\text{gear}} \quad [9.2.1]$$

where:

- $V$  is the vehicle speed in  $[m/s]$ ;
- $R_0$   $[m]$  the tyre rolling radius ;
- $\tau_p$  &  $\tau_{\text{gear}}$  the final ratio and the gear ratio respectively;

Starting from the driving cycle, characterized by its own speed profile, it is therefore possible to obtain through the eq. [9.2.1] the instantaneous engine speed.

At this point it is possible to calculate the power delivered by the engine for different operating points of the cycle. From the energy balance as the car progresses, it is possible to derive the following relationship:

$$P_m \cdot \eta_t = F_{res} \cdot v + m_{\text{trasl}} \cdot \frac{dv}{dt} \cdot v \quad [9.2.2]$$

where:

- $P_m$  is the Power;
- $\eta_t$  the transmission efficiency;
- $F_{res}$  is the force necessary for the vehicle to advance at constant speed, including rolling resistance, aerodynamic and related to any slope of the road you are traveling on. It is possible to express this value as a function of the vehicle speed through coefficients called coast down coefficients obtained through a regression of specific experimental tests;
- $m_{\text{trasl}} \cdot \frac{dv}{dt} \cdot v$  represents the contribution of power necessary for the acceleration of the vehicle where  $m_{\text{trasl}}$  is the apparent moving mass of the car which differs from the total mass when the vehicle is stationary as it includes the inertia of all the components in rotation during motion.

The value of  $m_{trasl}$  can be obtained through a kinetic energy balance of the vehicle:

$$\frac{1}{2} \cdot m_{trasl} \cdot v^2 = \frac{1}{2} \cdot m_{vehicle} \cdot v^2 + \frac{1}{2} \cdot J_{wheel} \cdot w_{wheel}^2 + \frac{1}{2} \cdot J_{trans} \cdot w_{trans}^2 + \frac{1}{2} \cdot J_{engine} \cdot w_{engine}^2 \quad [9.2.3]$$

The contribution of the inertia of the transmission  $J_{trans}$  is usually negligible compared to that of the engine and wheels, therefore the following expression can be used:

$$m_{trasl} \cong m_{vehicle} + \frac{J_{wheel}}{R_0^2} + J_{engine} \cdot \frac{\tau_p^2 \cdot \tau_{gear}^2}{R_0^2} \quad [9.2.4]$$

For the sake of completeness, it is necessary to observe how the translating apparent mass is dependent on the gear engaged due to the term  $\tau_{gear}^2$ , therefore it will vary with the transmission ratio used during the various instants of the test.

Once the engine power output value has been obtained, it is possible to calculate the brake mean effective pressure (bmep) as:

$$bmep \text{ [bar]} = 1200 \cdot \frac{P_m \text{ [kW]}}{n[\text{rpm}] \cdot V \text{ [dm}^3\text{]}} \quad [9.2.5]$$

It is evident that the engine operating points in terms of rpm and bmep are easily obtained for each simulation's instant. However during the simulation it has been necessary to set any negative bmep equal to the value in idle operating conditions, and any bmep values higher than the maximum allowed by the motor full load curve, equal to the value indicated by the curve itself.

### 9.3 Emissions and Fuel Consumption Calculation

Consumption maps obtained experimentally in stationary conditions, as shown in Figure 53 and 54, are used to calculate the consumption and emissions of the car under analysis.

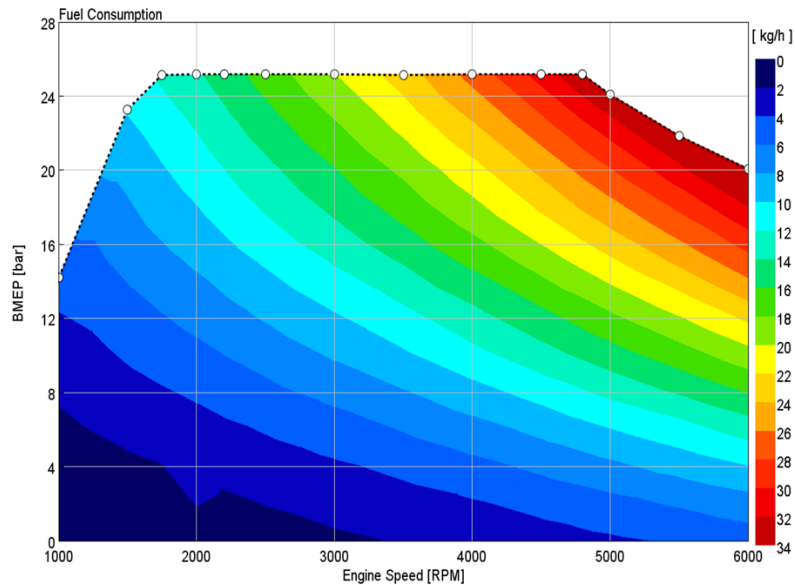


Figure 53 - Fuel Consumption Map from Stationary Simulations

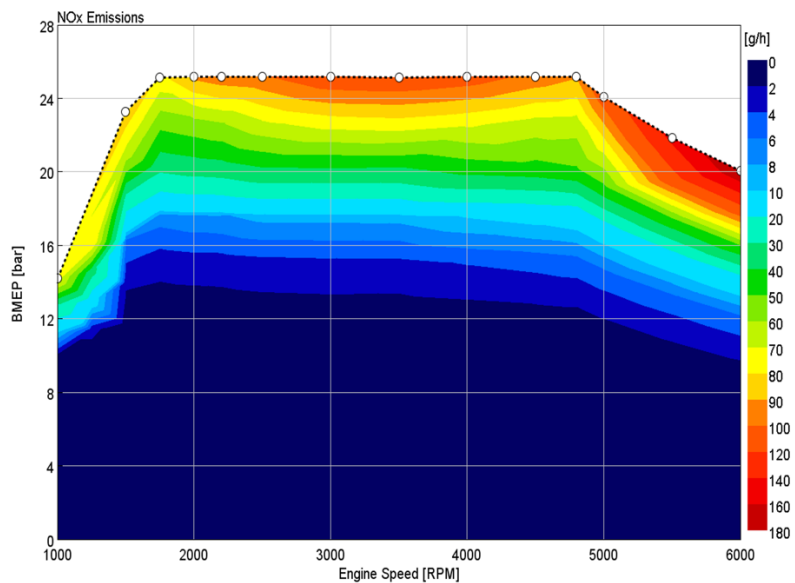


Figure 54 - NOx Emission Map from Stationary Simulations

These maps are provided as double entry tables which show the hourly fuel consumption values or the hourly emission values of NOx as a function of the number of engine revolutions (rpm) and brake mean effective pressure (bmep).

The consumption maps provide data on emissions and discrete consumption, i.e. relative to fixed values of rpm and bmep, therefore a double linear interpolation is necessary to assign a fuel consumption ( $f_c$ [kg/h]) and emissions value ( $NO_x$ [g/h]) at each simulation's instant.

In particular, the fuel consumption map is defined for a number of engine revolutions between 1000 rpm and 6000 rpm and for bmep values between 0.5 bar and 25.25 bar, while the NOx map is defined by number of revolutions motor between 1000 rpm and 6000 rpm and for bmep values between 0 bar and 25.25 bar. The following minimum values of NOx emissions and fuel consumption will correspond to each operating condition below the limits shown in the maps:

- Minimum NOx emissions = **0.00 g/h**
- Minimum Fuel Consumption = **0.438 kg/h**

Once the consumption and the instantaneous emissions are known, it is possible to carry out the integrations numerically:

$$f_{c,tot} = \int_0^t f_c \cdot dt; \quad [9.3.1]$$

$$NO_{x,tot} = \int_0^t NO_x \cdot dt; \quad [9.3.2]$$

to obtain the cumulative values for a certain instant t.

Considering the total distance traveled in the cycle, the final values of fuel consumption and NOx emissions are obtained in terms of liters of fuel consumed every 100 km and milligrams of NOx emitted each kilometer:

$$C_{spec} \left[ \frac{l}{100km} \right] = \frac{f_{c,tot} [g]}{\rho_{fuel} \left[ \frac{g}{l} \right] \cdot d [km]} \cdot 100; \quad [9.3.3]$$

$$NO_{x,spec} \left[ \frac{mg}{km} \right] = \frac{NO_{x,tot} [g]}{d [km]} \cdot 1000 \quad [9.3.4]$$

Where  $d$  is the distance, in kilometers, covered by the vehicle during the homologation cycle.

## 9.4 Calculation of the mechanical energy required and recoverable

The energy demand represents an important comparison parameter between different types of driving cycles. Once the trend of the power delivered by the engine is known, it is possible to calculate the value of 'positive power', i.e. power intended for traction, and of 'negative power', generated during the braking phases, through numerical integration . While the positive power is indicative of the energy demand of the specific driving cycle, the negative power represents the amount of energy that could be recovered through a 'regenerative braking' mechanism during the vehicle deceleration phases. Starting from these definitions it is possible to estimate what are the values of mechanical energy required and recoverable mechanical energy in the event that the vehicle is equipped with regenerative braking; the values of specific mechanical energy and specific recoverable energy are then calculated.

$$\text{Mechanical Energy} = \int_0^{t_{fin}} P_{m,positive} \cdot dt ; \quad [9.4.1]$$

$$\text{Specific Mechanical Energy} = \frac{\text{Mechanical Energy}}{km_{Tot}^{WLTP}} ; \quad [9.4.2]$$

$$\text{Recoverable Energy} = \int_0^{t_{fin}} P_{m,negative} \cdot dt ; \quad [9.4.3]$$

$$\text{Specific Recoverable Energy} = \frac{\text{Recoverable Energy}}{km_{Tot}^{WLTP}} ; \quad [9.4.4]$$

## 9.5 Start & Stop and Cut-Off Technologies Implementation

The always more stringent regulations regarding emissions are pushing the cars manufacturer to find smart solutions to minimize fuel consumption and emissions. Technologies like Cut-Off and Stop-Start are a perfect example and they have a direct influence on the driving cycles results. The developed simulation code allows to consider the possibility that the car being analysed may be equipped with these technologies, taking into account their effects technologies on fuel consumption and emissions. In particular, Cut-Off and Stop-Start act differently on engine operation and can both be present on the same car.

The 'Cut-Off' is a particular control strategy, which can be implemented in electronic injection systems, which provides the ability to stop fuel injection when the accelerator pedal is not pressed. This system, however, is only active when the engine is above a certain minimum number of revolutions in order to avoid unwanted shutdown. In this case, it was taken into account that the system is enabled if the engine speed is greater than 1000 rpm and the power delivered is negative, or in the case of running with the accelerator pedal raised. In the implementation of the code, therefore, has been added the possibility to contemplate the use of the Cut-Off by not considering the fuel consumptions and emissions when negative engine power is recorded in the cycle and, at the same time,  $n > 1000$  rpm.

The 'Stop-Start', on the other hand, is a system that allows the engine to be switched off automatically when the clutch is disengaged and the gearbox is in neutral. In this way, emissions and fuel consumption are reduced when the engine is idling, stationary and with the gearbox in neutral. The system is enabled only after the combustion gas after-treatment systems have reached the thermal regime, such as the Cat-Heating phase in a three-way catalysts, but in this particular case no aftertreatment system is present so that possibility has not been taken into account. The implementation in the code is similar to what has been done for the Cut-Off, in particular fuel consumptions and emissions have been not considered when the gearbox is in neutral (Ratio = 0) and vehicle speed is zero.

Moreover, it is possible to simulate the entire driving cycle even if both the Cut-Off and Stop-Start systems are present and active in the vehicle.

It is important to note that the model used for the analysis of the influence of these technologies on the data obtained from the guide cycles admits various simplifying hypotheses. In particular, the internal combustion engine is considered to be operating in the thermal regime conditions, i.e. when the initial transients are completed and therefore the temperatures suitable for correct operation have been reached. This simplification is not trivial since generally the first phases of the homologation cycle are carried out without having yet reached the thermal regime conditions with important penalties as regards consumption and emissions.

## 10. Results

The results of the analysis are reported below. In Figure 55 the cumulative value of NO<sub>x</sub> and Hydrogen consumed during WLTC are reported, both in Conventional and Start & Stop + Fuel Cut-Off mode.

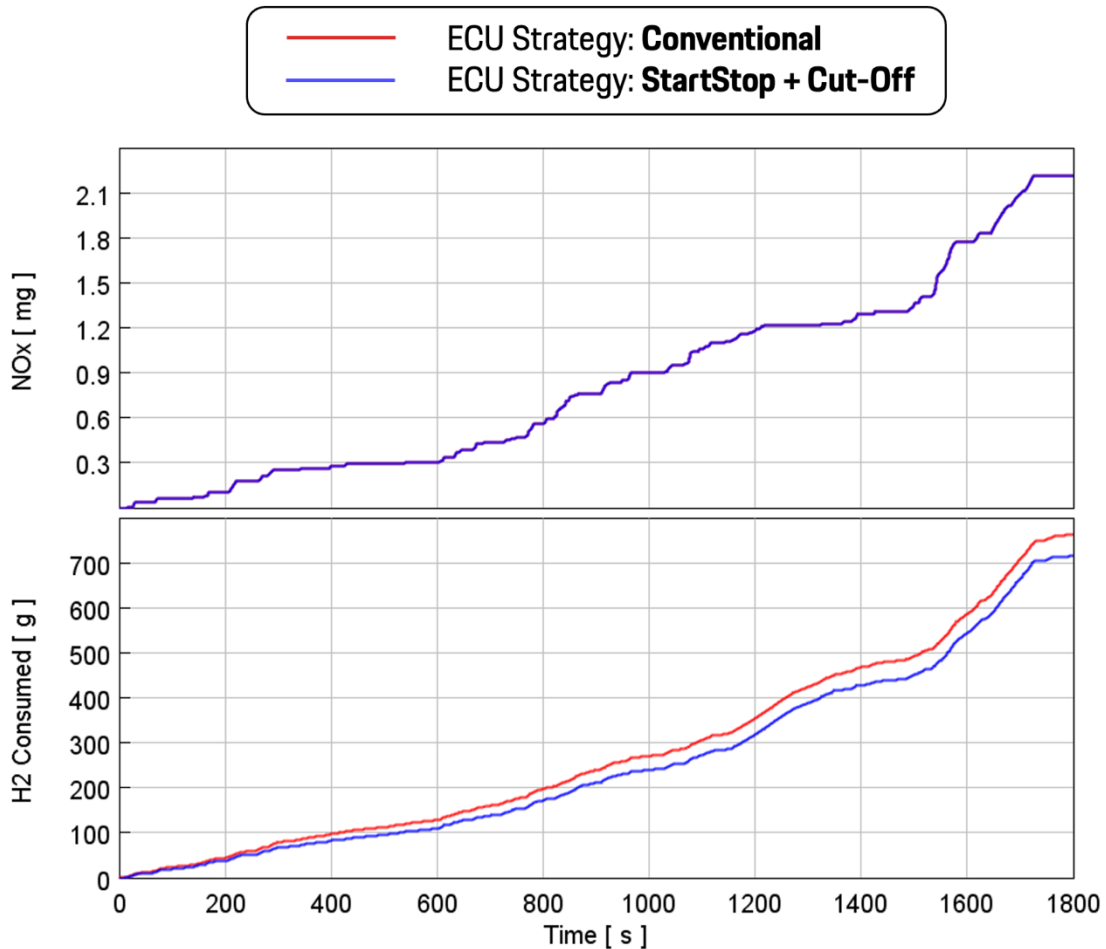


Figure 55 - Cumulative NO<sub>x</sub> Emissions and H<sub>2</sub> Consumption

It can be noticed the difference between the two ECU strategies. Start & Stop + Cut-Off strategy allows to reduce the hydrogen consumption of about the 7% but it does not affect the NO<sub>x</sub> production. This is related to the close to zero NO<sub>x</sub> production during idling (where Start & Stops act) and for the relatively low BMEP for the most of the cycle.

In the Table 10 the results of the WLTC simulation are summarized. It shows the total hydrogen consumed during the cycle, the specific Hydrogen consumption and NOx emissions and an estimated range are reported. For this analysis a 6 kg Hydrogen tank has been considered like most of the current hydrogen vehicles on the market.

WLTC Driving Cycle					
ECU Strategy	H <sub>2</sub> Consumed	H <sub>2</sub> Consumption	NOx Spec.	H <sub>2</sub> Tank	Range
	[ kg ]	[kg/100km]	[ mg/km ]	[ kg ]	[km]
Conventional	0.763	3.279	0.095	6	182.98
Start & Stop + Cut-Off	0.715	3.071	0.095	6	195.38
DELTA			<b>- 0 %</b>		<b>+ 6.29%</b>

Table 10 - WLTC Simulation Results

For the best strategy, Start&Stop+CutOff, the total hydrogen consumed during the WLTC is **0.715 kg** resulting in **3.071 kg/100km**, that considering an Hydrogen tank of **6 kg** results in an estimated range of **195.38 km**.

Specific NOx emissions are **0.095 mg/km** and it is also possible to calculate the NOx concentration in the exhaust gasses (considered made by only Air at 25°C) which is **30 µg/m<sup>3</sup>**.

## 10.1 Comparison With European Union Limits

WLTC results can be compared with the European union limits that have been continuously reduced year by year. In the Figure 56 the Specific NO<sub>x</sub> limits for Gasoline and Diesel engines are reported.

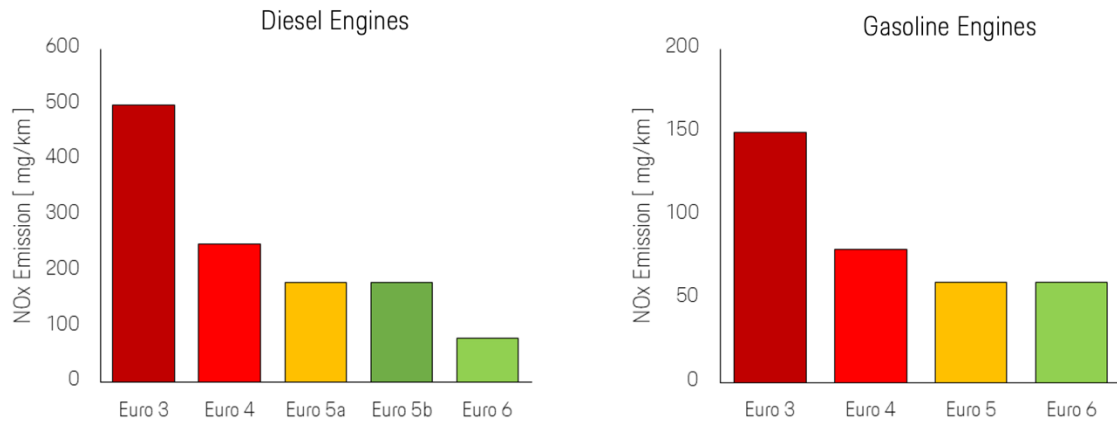


Figure 56 - NO<sub>x</sub> European Union's Limits between Euro3 and Euro 6

The future Euro 7 standard will be fuel neutral (same limits for gasoline and diesel) and the predicted NO<sub>x</sub> limit is 30 mg/km [19], as shown in Figure 57, below.

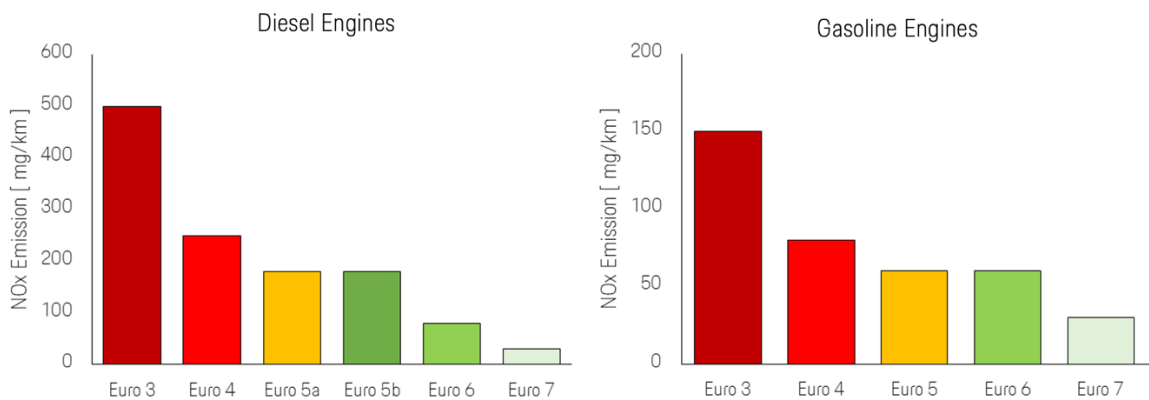


Figure 57 - NO<sub>x</sub> European Union's Limits between Euro3 and Euro 7

According to the Driving Cycle simulation results, the H64 Hydrogen Engine mounted on the Aurus Senat, emits **0.095 mg/km** of NO<sub>x</sub> that **represents a 99.6% Emission compared to the future Euro 7 standards reduction without an After-Treatment system!**

## 10.2 Emissions vs Air Quality

Another interesting analysis can be performed by considering the NO<sub>x</sub> concentration in the exhaust gasses, that as previously reported is **30 µg/m<sup>3</sup>**.

In Europe the Air Quality is estimated using an Index called **AQI (Air Quality Index)**.

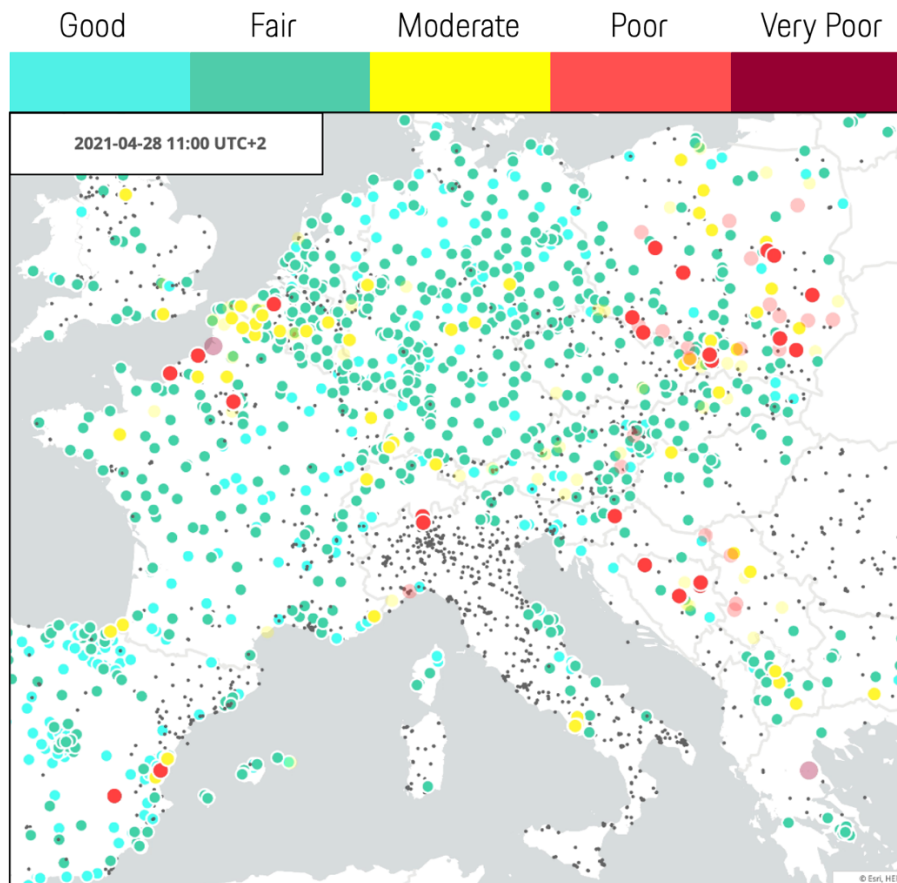


Figure 58 – Example of Air Quality Index for NO<sub>x</sub> in Europe

Considering the maximum hourly NO<sub>x</sub> concentration in the Air measured by one of the sensors in the map (Figure 58), it is possible to evaluate the air quality on a scale between GOOD and VERY POOR (and of course even worse).



Figure 59 - European Air Quality Index Scale based on NO<sub>x</sub> Concentration

Assuming the **30 µg/m<sup>3</sup>** of NO<sub>x</sub> emitted by the H64 as the maximum hourly concentration measured by one of the sensors, **it can be noticed that the engine-out air quality can be considered as GOOD, without an After-Treatment System!**

## 11. Nürburgring Nordschleife Lap Time Simulation

Motorsport is facing a challenging era. The challenge against the climate changes is influencing also its future, Formula 1 must become Carbon-Free before 2030 and electric powertrains are currently started to be used in different series, like Formula E and Extreme E, resulting in a lack of appealing and a reduction of fans. More that 5.5 millions of people are currently working in this sector and to find a way to convert motorsport in a sustainable and carbon-free sector will be crucial.

Hydrogen Engines can be an interesting solution and source of innovation in this sense, Toyota has tested for the first time a 3-Cylinder Turbocharged Hydrogen Engine in a 24 hours race, the Fuji Super TEC 24 Hours, and its president, Akio Toyoda, is convinced that the road is still tough, but hydrogen can represent a valuable and promising solution for the races of tomorrow. For this reason it has been decided to test the H64 Engine mounted on the Aurus Senat in a motorsport application, and, as German tradition wants, the car has been tested with an Hot-Lap in the famous "Green Hell", the iconic Nordschleife Circuit of Nürburgring. The circuit map is reported in Figure 60, below:

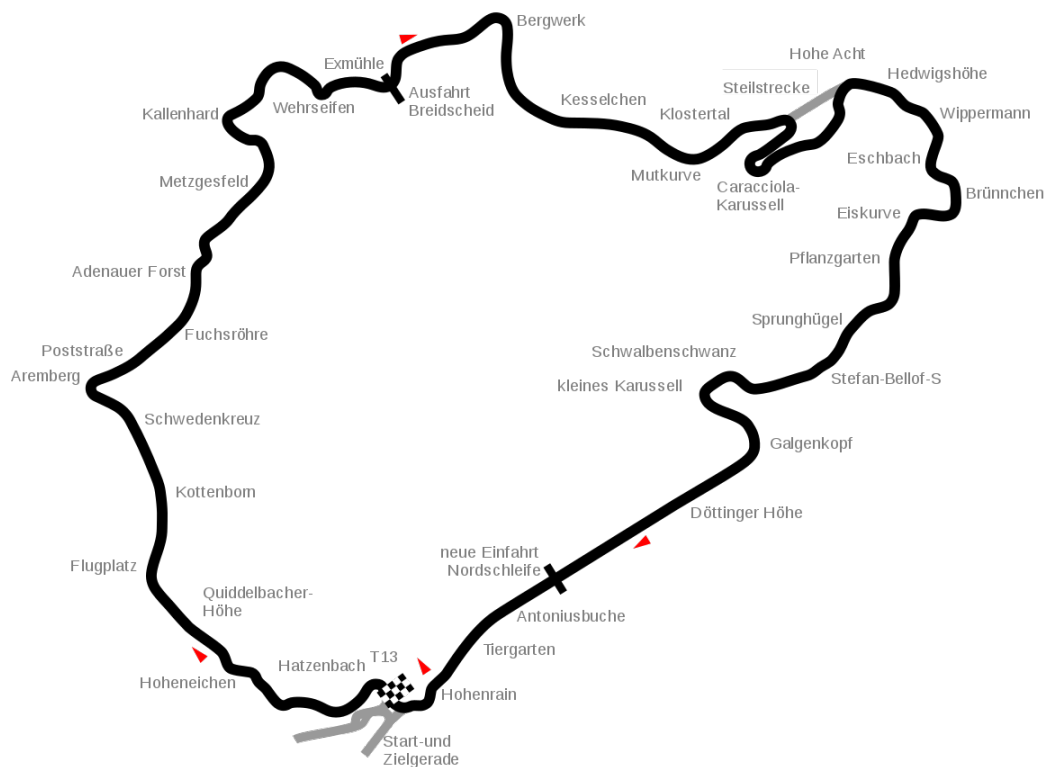


Figure 60 - Nürburgring Nordschleife Circuit Map

The Lap has been done using the engine and the vehicle data on the simulator and to have a close dynamic and aerodynamic behavior a similar vehicle model has been used.



Figure 61 - Aurus Senat on the HotLap at Nordschleife

The circuit has been divided in 5 sectors, listed between A and E as reported in Figure 62, below:

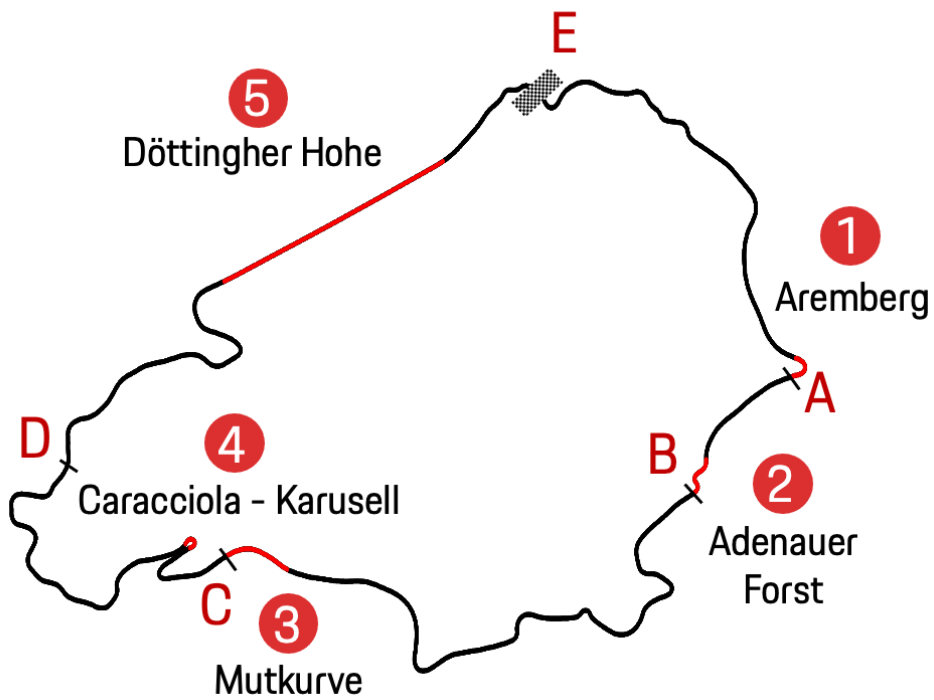


Figure 62 - Nordschleife Selected Sectors

In Table 1, for each sector the Time (end of the sector), the maximum and minimum speed within the sector, the cumulative NOx emissions and Hydrogen Consumption have been reported.

It can be noticed how, in one flying lap, assuming 6 kg of hydrogen tank, more than one third of the tank has been consumed (**2.215 kg**) but NOx emissions about **8,8 mg** for the entire lap. The minimum speed in the lap has been reached at the Caracciola-Karusell with about **69 km/h** and the maximum one has been reached after the Antoniusbuche corner, that is at the end of the Döttinger Hohe straight, with about **261 km/h**.

Nurburgring Nordschleife – Lap Data Analysis						
Sector		Time [ m.ss.00 ]	Max Speed [ km/h ]	Min Speed [ km/h ]	Cumulative	
					H <sub>2</sub> Consumption [ kg ]	NOx Emissions [ mg ]
A	Start - Aremberg	1:36.55	243	72	0.452	2.0
B	Aremberg - Adenauer Forst	2:06.95	240	70	0.597	2.5
C	Adenauer Forst -Mutkurve	4:25.95	213	71	1.214	4.6
D	Mutkurve - Pflanzgarten	6:18.30	186	69	1.620	6.0
E	Pflanzgarten - Finish	8:20.00	261	75	2.215	8.8

Table 11 - Nordschleife Sectors Data Summary

Always from the Table 11 it can be noticed that the lap time is : **8'20"**.

As a reference, this time is the same performed from the Chevrolet Camaro SS (2010) with a 430 HP 6.2 liters V8 gasoline engine.

## 12. Conclusions

The energy supply sector will be, sooner or later, 100% Renewable. In that scenario the problem of intermittent energy production, due to the behaviour of the natural phenomena, must be taken into account.

This means that reliable energy storages will be needed to store, for example, an eventual excess of energy to have it available when the generated power it is not enough to fulfill the energy request.

Hydrogen is a valuable and promising solution for the energy storage and can be also employed by the automotive sector, both in fuel cell and internal combustion engines.

Based on our 1D-CFD simulations, with an hydrogen internal combustion engine it is possible to achieve:

- Almost no emissions without after treatment systems: up to 99.6% of emissions reduction compared to the future Euro 7 Standards
- High Efficiencies – up to 42% and a wide high efficiency zone due to the limited throttle valve usage
- High Specific Power – 136 HP/L : delivering high performances keeping the sound attractiveness
- Good Packaging

This technology also enhances 150 years of European Engine Development Heritage being fast, green, sustainable and, most important, *roaring*.

## BIBLIOGRAPHY

1. MILLINGTON, BEN; DU, SHANGFENG; POLLET, BRUNO G. - "The Effect of Materials on Proton Exchange Membrane Fuel Cell Electrode Performance". Journal of Power Sources, 2011.
2. ALINE LEON - "Hydrogen technology, Mobile and portable application", Springer-Verlag Berlin Heidelberg, 2008.
3. DESANTES FERNÁNDEZ, JM.; LÓPEZ SÁNCHEZ, JJ.; MOLINA ALCAIDE, SA.; LÓPEZ PINTOR, D. - "Validity of the Livengood & Wu correlation and theoretical development of an alternative procedure to predict ignition delays under variable thermodynamic conditions. Energy Conversion and Management", 2015.
4. JOHN B. HEYWOOD - Internal Combustion Engine Fundamentals. Second Edition, McGraw-Hill series in mechanical engineering, McGraw-Hill, New York, 2018.
5. DELOITTE CHINA - "Fueling the future of mobility, Hydrogen and Fuel Cell Solutions for Transportation", Volume 1, Financial advisory, 2020.
6. HYDROGEN COUNCIL, MC KYNSEY & COMPANY - "A perspective on Hydrogen Investment, market development and cost competitiveness", 2021.
7. DR. CEDRIC ROUAUD, TREVOR DOWNES, ANDREA TREVISAN - "Developing heavy-duty hydrogen powertrains for 2025 and beyond". RICARDO Technology Webinar, 2020
8. A.WIMMER, T.WALLNER, J.RINGLER, F. GERBIG - "H<sub>2</sub>-Direct Injection – An highly promising combustion concept", BMW Research Group and Technology, 2005.
9. J.C. LIVENGOOD AND P.C. WU - "Correlation of autoignition phenomena in internal combustion engines and rapid compression machines.", Symposium (International) on Combustion, 1955.
10. ALESSANDRO GALLO - "Development of a methodology for the knock prediction in highly charged SI engines by the use of 3D-CFD simulation", Master Thesis, Politecnico di Torino, 2017
11. K. GROTE E J. FELDHUSEN, DUBBEL - Taschenbuch für den Maschinenbau, Springer-Verlag Berlin Heidelberg, 2007.

12. GIOVANNI CORVAGLIA - "Optimization of the gas exchange of a cross-plane V8 engine", Master Thesis, Politecnico di Torino, 2015.
13. GIACOMO AUGUSTO PIGNONE, UGO ROMOLO VERCELLI - "Motori ad alta potenza specifica: Le basi concettuali della tecnica da competizione", Giorgio Nada, Vimodrone (Mi), ed. riveduta e corretta, 2016.
14. GIANCARLO FERRARI - "Motori a combustione interna", Il Capitello, Torino, 4. ed. aggiornata, 2008.
15. HANNAH RITCHIE AND MAX ROSER - "CO<sub>2</sub> and Greenhouse Gas Emissions". Published online at OurWorldInData.org. Retrieved from: 'https://ourworldindata.org/co2-and-other-greenhouse-gas-emissions', 2020
16. NASA, GLOBAL CLIMATE CHANGE - "Global Temperature". Published online at Climate.Nasa.gov, Retrieved from: ' https://climate.nasa.gov/vital-signs/global-temperature/', 2020
17. EUROPEAN COMMISSION – " A Hydrogen strategy for a climate-neutral Europe ". Retrieved from [https://ec.europa.eu/energy/sites/ener/files/hydrogen\\_strategy.pdf](https://ec.europa.eu/energy/sites/ener/files/hydrogen_strategy.pdf), 2020
18. DIESELNET – " Worldwide Harmonized Light Vehicles Test Cycle (WLTC) ". Retrieved from <https://dieselnet.com/standards/cycles/wltp.php> , 2020.
19. QUATTORUOTE MAGAZINE - [https://www.quattroruote.it/news/industria-finanza/2021/04/15/emissioni\\_da\\_bruelles\\_proposte\\_meno\\_restrittive\\_per\\_l\\_euro\\_7\\_scongiurato\\_l\\_addio\\_all\\_endotermico\\_.html](https://www.quattroruote.it/news/industria-finanza/2021/04/15/emissioni_da_bruelles_proposte_meno_restrittive_per_l_euro_7_scongiurato_l_addio_all_endotermico_.html)-Suite
20. GT-Suite: GT-Power Manual. Gamma Technologies, 2016.
21. Converge CFD: Converge CFD 3.1 Manual. Convergent Science, 2016.